INFORMATION TO USERS

This manuscript has been reproduced from the microfilm master. UMI films the text directly from the original or copy submitted. Thus, some thesis and dissertation copies are in typewriter face, while others may be from any type of computer printer.

The quality of this reproduction is dependent upon the quality of the copy submitted. Broken or indistinct print, colored or poor quality illustrations and photographs, print bleedthrough, substandard margins, and improper alignment can adversely affect reproduction.

In the unlikely event that the author did not send UMI a complete manuscript and there are missing pages, these will be noted. Also, if unauthorized copyright material had to be removed, a note will indicate the deletion.

Oversize materials (e.g., maps, drawings, charts) are reproduced by sectioning the original, beginning at the upper left-hand corner and continuing from left to right in equal sections with small overlaps.

University of Alberta

THE ELASTICITY OF INTRINSICALLY ANISOTROPIC ROCKS

by

Pavlo Y. Cholach   (C)

A thesis submitted to the Faculty of Graduate Studies and Research in partial fulfillment
of the requirements for the degree of **Doctor of Philosophy.**

in

Geophysics

Department of Physics

Edmonton, Alberta
Spring 2005

"These thoughts did not come in any verbal formulation. I rarely think in words at all.
A thought comes, and I may try to express it in words afterward."

Einstein, Albert (1879-1955)

Моїм батькам, Галині і Ярославу.

Abstract

In this dissertation the elasticity of intrinsically anisotropic rocks is investigated by both the analysis of experimental measurements on rock samples and forward modelling of elasticity through specially derived averaging techniques. Three different types of rocks that display intrinsic anisotropy of elastic waves are considered separately in each Chapter.

In Chapter 2 the results of extensive laboratory measurements of P- and S-wave velocities and shear-wave splitting of metasediments, metavolcanics and plutonic rocks from the Flin Flon Belt (FFB) of Trans-Hudson Orogen (THO) are analyzed. Metamorphosed rocks exhibit strong P-wave anisotropy (up to 24%) and shear-wave splitting. The effect of sample scale heterogeneities is estimated and compared to anisotropy. Despite three distinctive elastic symmetries present in the investigated rocks, the overall symmetry of the collection appeared to be transversely isotropic.

In Chapter 3 intrinsic elastic properties of upper mantle olivine aggregates are investigated by developing an averaging technique that incorporates the orientation distribution function (ODF) of orthotropic-orthorhombic symmetry. In addition to conventional Voigt and the Reuss averages, the Geometric Mean Average (GMA) is derived for this symmetry to provide a unique solution that is independent of the averaging domain. Even though textural properties significantly affect the elasticity of the olivine aggregate, all three averages (derived on the basis of different assumptions) provide comparable results for the olivine aggregate.

In Chapter 4 intrinsic elasticity of a muscovite aggregate is investigated as a function of its texture, from a single crystal to an isotropic aggregate. Main implementation

of this study is to explain intrinsic anisotropy of sedimentary shales. Limits of seismic anisotropy of muscovite aggregates are estimated by calculating anisotropic parameters as a function of texture. Despite the strong dependence of the values of elastic constants on the averaging technique used, anisotropic elastic parameters, especially anellipticity, are practically independent of the averaging assumptions.

The averaging techniques aimed to determine the elasticity of an aggregate as a function of its texture are derived in the thesis for specific symmetries that are displayed by naturally deformed rocks. The effect of their application to different types of intrinsically anisotropic rocks differs and discussed in detail in the thesis.

Acknowledgements

First of all, I would like to acknowledge Dr. Douglas Schmitt for supervision, continuous support and interest throughout my Ph.D. project.

Thorough reviews and useful suggestions of Examination Committee members that undoubtedly improved manuscript are greatly appreciated.

I also would like to thank academic staff, former and current graduate students in Geophysics (especially Dr. Ulrich Theune) for numerous challenging discussions on various geophysical (and unrelated!) topics during my five years in the UofA.

I would like to acknowledge Department of Physics staff for providing administrative support, especially Lynn Chandler and Sarah Derr, and technical assistance (many thanks to Len Tober) during my studies and research in the Department.

Special thanks to number of individuals whose data and laboratory measurements were used in the thesis, particularly in the Chapter 2 on the elasticity of Flin Flon rocks.

Finally, I would like to acknowledge Christine Bilak for her vision and inspiration that encouraged me to undertake this study.

Contents

List of Tables

List of Figures

Preface

In the discipline of Geophysics, researchers deal with a wide spectrum of physical properties of Earth materials that includes elasticity, magnetism, density, and electrical conductivity, to name a few. Elasticity holds a prominent place among these mainly because of the level of sophistication in our understanding of this property and because of the wealth of information it carries via seismic observations of the Earth. Methods employing elastic wave propagation are most frequently used to investigate the elastic properties of rocks. The methodologies of elastic wave propagation are considerably developed in geophysics as they are flexible and directly applicable to solving a wide range of geophysical problems.

In general, *elasticity* is introduced through the relationship between an applied stress and the subsequently acquired strain in the deformation of a body. If the body returns to its original shape after the stress is removed the deformation is said to be elastic. Elastic deformation within the elastic limit consists of two regions: linear - where strain is linearly proportional to applied stress, also known as Hooke's Law, and non-linear one. This thesis is concerned with the elasticity that is defined in the region of small deformations where a linear form of Hooke's Law applies. This thesis narrows the topic of investigation to the scope of elasticity of 'intrinsically anisotropic rocks, a terms to be defined here first:

- the term *intrinsic* implies that only constituent mineral phases and their spatial orientations contribute to the elastic properties of investigated material;

- the term *anisotropy* stands for directional dependence of the physical property of an investigated material or medium. Commonly, in geophysics, the dependence of elastic wave velocity on the direction of wave propagation is defined as elastic

anisotropy. More generally, the term *anisotropy* can be defined as the dependence of elastic wave velocity on direction of wave polarization. Anisotropy [1] incorporates effects such as shear wave splitting (the elastic analogy to optical birefringence) and a general discrepancy of phase (plane wave) and group (ray) velocities.

In the thesis the definition of the term *texture* is adopted from the field of textural analysis and means *lattice preferred orientation* (LPO) of constituent minerals of aggregate. This definition narrows the meaning of the term *texture* as it's normally used in geological investigations.

---

[1] In this work, the term anisotropy is to be taken to mean elastic anisotropy for convenience. Other physical properties such as electrical conductivity, magnetic susceptibility, and permeability also can be highly anisotropic.

Chapter 1

Introduction

Seismic observations of the dependency of compressional (P) and shear (S) wave velocities on the direction of propagation and of shear-wave splitting in the Earth has made the study of anisotropy one of the most exciting and challenging research themes in Solid Earth Geophysics. Anisotropy carries a wealth of information about the structural and textural elastic properties of the medium it propagates through. In Geophysics this may be the only means to access information on the elastic properties of the Earth's interior to the increasingly demanding level of resolution. In this introduction to the thesis, the various evidence for the presence of seismic anisotropy in the Earth is briefly reviewed. The main sources of elastic anisotropy in rocks and in Earth's interior are discussed. The theoretical background describing elasticity of anisotropic materials is outlined. Finally, the major challenges of the determination of intrinsic elastic properties of anisotropic rocks that have been addressed in the thesis are defined.

1.1 Geophysical observations of elastic anisotropy

During the past half century considerable geophysical evidence for seismic anisotropy has accumulated. This wealth of observations has made anisotropy a widely accepted characteristic of the Earth's interior (e.g. *Babuska and Cara*, 1991). All rock-forming minerals are elastically anisotropic and anisotropy is an inherent property of most rocks. Anisotropy has been detected at various scales with different geophysical techniques. Anisotropy is manifested in rock samples several millimeters in size by high frequency ultrasonic laboratory measurements (e.g. *Migliori and Fisk*, 1993), in sedimentary layers

1

and metamorphic rock formations at scales up to hundreds of meters in thickness in exploration seismic surveys (e.g. *Jolly*, 1956; *Winterstein and Paulsson*, 1990; *Miller et al.*, 1994; *Kebaili and Schmitt*, 1996; *Leslie and Lawton*, 1999), and in massive blocks (up to tens of kilometers) of the continental lithosphere during the seismological observations of surface and teleseismic body waves (e.g. *Silver*, 1996; *Montagner*, 1998). This Section briefly overviews the evidence for elastic anisotropy in rocks and in the Earth's interior.

1.1.1 Ultrasonic measurements of anisotropy on rock samples

The importance of the laboratory anisotropy measurements in Rock Physics investigations cannot be overemphasized. The results of ultrasonic experiments are essential for the proper understanding of elastic wave behaviour in rocks. The knowledge of elastic behaviour of rocks gained from laboratory experiments is also of critical importance in other areas of geophysics. For example, exploration seismology benefits from the proper design of surveys that take into account the elastic behaviour of subsurface geology and although it has been ignored in most seismological studies, consideration of anisotropy is becoming more of a necessity in the processing and interpretation of applied seismic and global seismological observations (e.g. *Vestrum et al.*, 1999).

By analogy to the determination of elastic constants in rock-forming minerals (e.g. *Aleksandrov and Ryzhova*, 1961; *Babuška*, 1981; *Bass*, 1995) various ultrasonic techniques have also been developed for determination of the elastic properties of rocks (e.g. *Schreiber et al.*, 1973; see also Appendix A for brief review of experimental techniques). The relative simplicity of the experimental configuration and the close relationship of the observed elastic anisotropy to the physical properties of materials makes the laboratory ultrasonic measurements of elastic wave velocities a basic technique for the fine-scale investigation of anisotropy in rocks.

Despite initial simplified assumptions in considering rocks as isotropic polycrystalline aggregates (e.g. *Simmons and Wang*, 1971), laboratory measurements consistently revealed a directional dependence of the elastic velocities in nearly all types of rocks. Since the 1950's, elastic anisotropy has been of constant interest to experimental geophysicists. *P*- and *S*-wave velocities have been measured on almost all naturally occurring rocks (e.g. *Guéguen and Palciauskas*, 1994; *Ahrens*, 1995). Elastic anisotropy has been reported in a

2

variety of sedimentary rocks, including shales (*Jones and Wang*, 1981; *Banik*, 1984; *Vernik*, 1993; *Johnston and Christensen*, 1995; *Vernik and Liu*, 1997; *Hornby*, 1998; *Wang*, 2002), sandstones (*Mavko et al.*, 1995), calcite rocks (*Khazanehdari et al.*, 1998) and reservoir carbonate rocks (*Dey-Barsukov et al.*, 2000), as well as metamorphic and igneous rocks (*Kern*, 1978; *Babuška*, 1984; *Ji et al.*, 1997; *Takanashi et al.*, 2001). Ultrasonic laboratory measurements have detected seismic anisotropy in mylonites (*Ji et al.*, 1993; *Burlini and Kunze*, 2000), metapelites (*Burlini and Fountain*, 1993), schists (*Godfrey et al.*, 2000), granites (*Sano et al.*, 1992; *Pros et al.*, 1998b), granodiorites and quartzites (*Babuška and Pros*, 1984), anorthosites (*Seront et al.*, 1993), and gneisses (*Ji and Mainprice*, 1988; *Aleksandrov and Prodayvoda*, 1994; *Brosch et al.*, 2000; *Meltzer and Christensen*, 2001). With predominant frequencies near 1 MHz and compressional wave velocities in the range of 2 to 8 km/sec, the wavelength in a typical ultrasonic experiment is 2-8 mm, allowing elastic wave to detect causes of anisotropy of few millimeters in dimension.

1.1.2 Observations of seismic anisotropy in the uppermost crust

In addition to laboratory ultrasonic measurements, seismic anisotropy has also been observed on several orders of magnitude larger scales during exploration seismic surveys (*Helbig*, 1994). Seismic anisotropy of geological strata can be sampled with a typical frequency range of 10-120 Hz and a wavelength of seismic wave in the range of 25-400 m. A directional dependence of P-wave velocities was reported for seismic surveys of different geometries, including reflection (e.g. *Thomsen*, 1988; *Lynn and Thomsen*, 1990; *Grechka and Tsvankin*, 1999; *Thomsen et al.*, 1999), refraction surveys (*Helbig*, 1964; *Leslie and Lawton*, 1999), and vertical seismic profiling (VSP) (e.g. *Jolly*, 1956; *Gaiser*, 1990; *Winterstein and Paulsson*, 1990; *Yardley and Crampin*, 1991; *Liu et al.*, 1993; *Miller et al.*, 1994; *Kebaili and Schmitt*, 1996; *Leaney et al.*, 1999). The main objective of the above mentioned exploration surveys was to determine the orientation of the predominant fracture set form anisotropy.

Recently, *Holmes et al.* (2000) reported an unconventional experiment to measure seismic anisotropy in a mine environment. The unique possibility of making multidirectional measurements allowed not only the seismic anisotropy of granite masses to be detected, but also allowed prediction of the orientation of cracks and gneissic layering within the granodiorites investigated.

3

1.1.3 Seismological observations of anisotropy in the lower crust and upper mantle

Seismological records of surface *Rayleigh* and *Love* waves and P_n, P, S, SKS, $SKKS$ phases of body waves (e.g. *Lay and Wallace*, 1995) reveal anisotropy on a global scale.

Since the original work of *Smith and Dahlen* (1973) on the azimuthal velocity dependence of Love and Rayleigh waves in an anisotropic medium, surface waves have been extensively used for investigations of anisotropy in the Earth's interior. Inversion of dispersion curves of Rayleigh and Love waves is one of the manifestations of seismic anisotropy (*Montagner*, 1986). *Montagner and Nataf* (1986) followed *Smith and Dahlen* (1973) method of inverting azimuthal variations of surface velocities to provide functional dependence of anisotropy with depth. Since then, large sets of Love and Rayleigh dispersion curves have been inverted to better reconstruct the 3-D variations of anisotropic parameters in the upper mantle. Present day models of the Earth's interior account for anisotropy in the upper mantle (e.g. *Babuška et al.*, 1998; *Montagner*, 1998).

Azimuthal and lateral anisotropy in the lower crust and upper mantle has been widely reported from observations of variations in P_n phase body wave. Azimuthal variations of P_n velocity provide information about subhorizontal properties of the mantle just beneath the *Moho* discontinuity. *Hess* (1964) first reported azimuthal dependence in seismic velocity of P_n phase that propagates subhorizontally beneath the oceanic *Moho* discontinuity. *Bamford* (1977) analyzed large sets of P_n traveltimes from deep continental refraction profiles. His analysis suggested a 6 to 7 % anisotropy of P_n in the continental lithosphere beneath western Germany. Tomographic analysis of *Hearn* (1999) required 5% of P-wave anisotropy to properly image the uppermost mantle from P_n wave observations.

More complete information about the 3-D structure of the Earth's interior may be obtained from observations of teleseismic P- and S-waves seismic anisotropy. Mapping the lateral changes of P-wave anisotropy within the subcrustal lithosphere on teleseismic P-residual spheres allows detection of direction of the symmetry axis of the observed anisotropy (*Babuška et al.*, 1993). Joint interpretation of P-wave delay times with polarization analysis of shear wave splitting of SKS phase (see review by *Silver* (1996) for more details) resolved the ambiguity in the interpretation of vertical velocity anomalies in the

4

mantle (*Plomerova et al.*, 1996, 1998; *Babuška et al.*, 1998; *Babuška and Plomerova*, 2001).

The relationship between the shear wave splitting of *SKS* teleseismic wave and seismic anisotropy has been extensively studied (e.g. *Crampin and Yedlin*, 1981; *Crampin*, 1985b; *Crampin and Lovell*, 1991; *Mainprice and Silver*, 1993; *Ji et al.*, 1994; *Vauchez and Barruol*, 1996; *Savage*, 1999). Estimation of contributions of crustal anisotropy (*Barruol and Mainprice*, 1993; *Weiss et al.*, 1999b) and upper mantle anisotropy (e.g. *Barruol and Kern*, 1996) to shear-wave splitting of almost vertical *SKS* arrivals improve interpretation of observed anisotropic effects for more accurate delineation of discontinuities in the Earth's interior.

1.2 Sources of anisotropy in the Earth's interior

It has been shown in the previous Section that anisotropy of the Earth's interior is observed on various scales. This implies that different sources of elastic anisotropy can be sampled and can contribute to overall observed anisotropic effect. Indeed, the origin of elastic anisotropy is non-unique. The physical properties of rock are superposed upon geological structure with preferential symmetries that are further enhanced by the subsurface distribution of stresses to produce the overall *in situ* anisotropy (such cumulative effects of different sources on observed anisotropy have been discussed, for instance, by *Hood*, 1991; *Werner and Shapiro*, 1998, 1999; *Rasolofosaon et al.*, 2000). Elastic wave propagating in an anisotropic medium senses the integral effect of the different causes of anisotropy. Elastic constants obtained from velocity inversion are affected by the superposition of the various sources of anisotropy and may, in general, have complicated and non-linear behaviour as a function of pressure and temperature (*Kumazawa*, 1969; *Kern*, 1978).

The non-uniqueness of the origin of anisotropy imposes ambiguity on geological interpretation of observed variations in *P*- and *S*-wave velocities. By selecting specific geological settings, the origin of observed seismic anisotropy is most commonly attributed to three mechanisms:

- horizontal or inclined layering of rock units;

- extensive networks of oriented cracks and microfractures (also incorporates oriented pore space), that usually further complicated by *in situ* stress state, and

- textured rocks with a *lattice preferred orientation* (LPO) of the constituent minerals.

In many cases, all three sources are superposed and contribute simultaneously to the anisotropy. On a global scale the correlation of the source of the seismic anisotropy observed on the Earth's surface as a function of the depth is complex (e.g. *Montagner*, 1998). Anisotropy may be attributed to the combined effect of layering, fracturing and LPO in the sedimentary formations and upper crust (*Crampin*, 1991; *Crampin and Lovell*, 1991; *Miller et al.*, 1994; *Leaney et al.*, 1999), fracturing and LPO in the lower crust (e.g. *Crampin*, 1985a; *Crampin and Atkinson*, 1985; *Mainprice and Nicolas*, 1989), and predominantly to the LPO of constituent minerals in the upper mantle (e.g. *Christensen*, 1984). In this Section all three sources of anisotropy are discussed.

1.2.1 Anisotropy produced by horizontally layered (stratified) medium

In many geological settings, but especially in sedimentary basins with characteristic sub-horizontal layering, seismic P-wave propagates substantially faster in the horizontal than in the vertical direction reflecting their so-called *transverse isotropy* (TI). Seismic waves in a TI medium behave similarly to elastic waves in the single crystals of hexagonal symmetry. This property of a TI medium allows a better understanding of the dependencies of velocities on the elastic properties. Early theoretical work on the wave propagation in a TI medium were based on a model of the solid composed by thin isotropic horizontal layers (*Riznichenko*, 1949; *Postma*, 1955; *Krey and Helbig*, 1956; *Rytov*, 1956; *Backus*, 1962). Since then, the anisotropy of TI media have been extensively investigated by numerous authors (*Daley and Hron*, 1977; *Levin*, 1979; *Berryman*, 1979; *Helbig*, 1981, 1984a,b; *Byun*, 1984; *Hake et al.*, 1984; *Thomsen*, 1986; *Helbig and Schoenberg*, 1987). These studies lead to more systematic characterization of TI media, and parameterizations of P- and S-wave behaviour that significantly simplifies the description of elastic wave velocities in a TI media. An additional, but poorly studied aspects of elastic wave behaviour in TI media is scale-dependent frequency dispersion (e.g. *Werner and Shapiro*, 1999; *Liu and Schmitt*, 2003)

6

Evidence for TI anisotropy produced by thin layers has been reported in laboratory ultrasonic experiments on synthetic materials with well-controlled properties (e.g. *Melia and Carlson*, 1984; *Cheadle et al.*, 1991; *Kebaili and Schmitt*, 1997; *Mah and Schmitt*, 2003) as well as in numerical experiments (e.g. *Schoenberg and Costa*, 1991; *Hovem*, 1995).

1.2.2 Fracture-induced anisotropy

Anisotropy can also be produced if directionally aligned discontinuities, e.g. cracks, microfractures, and mineral grain boundaries are present in an isotropic or anisotropic *quasi*-continuous solid. For example, *Babuška and Pros* (1984) attributed experimentally observed anisotropy of granodiorites and quartzites to a pervasive set of oriented micro-cracks. Several approaches have been taken to develop the theoretical background for the elasticity of cracked solid materials (see, for instance, *O'Connell and Budiansky* (1974); *Watt et al.* (1976); *Hudson* (1980); *Crampin* (1981); *Berryman* (1995) for extensive reviews).

Crampin (1978) developed a technique to model the elastic constants of cracked mate-rials. Calculations of the complex effective elastic constants (*Crampin*, 1981) and further development of Hudson's theory (*Hudson*, 1980, 1981) for a wide variety of crack config-urations and crack geometries allowed *Crampin* (1984) to predict the attenuation of solids filled with a dilute system of cracks. *Schoenberg and Sayers* (1995) suggested the effective compliance tensor of a fractured rock could be rewritten as the sum of the compliance tensors of the non-fractured background rock and of the sets of aligned fractures. Their approach allows the orientation of the dominant fracture system to be obtained from seismic data.

The evidence from seismic anisotropy for the presence of systems of aligned cracks in the crust was discussed by *Crampin* (1985a), *Crampin and Atkinson* (1985). *Crampin* (1985b) evaluated the possibility of using the shear-wave splitting of seismic reflections for estimation of crack orientations. *Leary et al.* (1990) provided a general overview on feasibility of employing shear waves to explore the anisotropic properties of fractured crust. Mechanisms causing shear-wave splitting within the crust were discussed in de-tails by *Crampin and Lovell* (1991).

7

1.2.3 Lattice preferred orientation as a source of intrinsic anisotropy

Hess (1964) suggested that the azimuthal variations in seismic velocities observed during refraction surveys of P_n phase is due to the preferred orientation of olivine crystals in the upper mantle. Since then, considerable attention has been paid to the investigation of the relationship between elastic properties of upper mantle rocks and observed seismic anisotropy (*Christensen and Crosson*, 1968; *Peselnick et al.*, 1974; *Peselnick and Nicolas*, 1978; *Christensen and Salisbury*, 1979; *Christensen*, 1984; *Barruol and Kern*, 1996; *Nicolas and Christensen*, 1987; *Soedjatmiko and Christensen*, 2000; *Christensen et al.*, 2001). These studies suggest that the observed upper mantle seismic anisotropy is closely related to the lattice preferred orientation of constituent peridotite minerals, mainly olivine and pyroxenes. The significant contribution of LPO of olivine in peridotites to shear wave splitting of observed teleseismic SKS waves is also well established (e.g. *Mainprice and Silver*, 1993; *Ji et al.*, 1994; *Silver*, 1996; *Vauchez and Barruol*, 1996).

The relation between observed seismic anisotropy and LPO of plastically deformed peridotites leads to the suggestion that the observed seismic anisotropy may be directly interpreted as a manifestation of geodynamic processes in the upper mantle related to plate motion (e.g. *Carter et al.*, 1972; *Fuchs*, 1977; *Karato*, 1987, 1998; *Vauchez et al.*, 2000). Numerous works were devoted to the investigation of olivine lattice preferred orientation development in polycrystalline aggregate and numerical modelling of LPO produced seismic anisotropy of the upper mantle (*Wenk et al.*, 1991; *Chastel et al.*, 1993; *Tommasi*, 1998; *Vauchez et al.*, 1998; *Tommasi et al.*, 1999, 2000) and will be discussed in more details in Chapter 3.

1.3 Elasticity and anisotropic wave propagation

"We are like dwarfs standing [or sitting] upon the shoulders of giants, and so able to see more and see farther than the ancients."

Bernard of Chartres, circa 1130

The concepts and principals of the theory of elasticity are based on original publications of Galileo, Newton, Euler, Laplace, Cauchy, Hooke, Snell and other famous scientists and philosophers. Contributions to the theory of waves in anisotropic media may

8

be traced to the original works of Hamilton and Kelvin in the first half of the XIX century (see *Helbig*, 1994, for detailed historical sketch). An extensive work on the mathematical aspects of the theory of elasticity was published by *Love* in 1882. The basic principals of continuum mechanics and the physics of crystals were reviewed and systemized in the excellent book by *Nye*, 1957 (here the reprint *Nye* (1990) is typically cited). Since then, several books serve as comprehensive references on the theory of elastic wave propagation in crystals and solids, including those by *Fedorov* (1968), *Musgrave* (1970) and *Auld* (1990). The texts of *Aki and Richards* (2002) and *White* (1983) describe different applications of the theory of elasticity to seismic wave propagation in the Earth's interior and incorporate some aspects of elastic anisotropy. Most recently, books by *Babuška and Cara* (1991), *Helbig* (1994) and *Tsvankin* (2001) deal with the topic of elastic anisotropy in variety of geophysical applications. A brief overview on the theory of elastic wave propagation in anisotropic media is presented in Appendix B. This Section concentrates on current techniques of modelling elasticity in rocks, and on the major problems of the investigation of intrinsic elasticity of polycrystalline aggregates addressed in the thesis.

1.3.1 Modelling elasticity of multiphase polycrystalline rocks

Rocks naturally occur as textured multiphase mixtures of anisotropic minerals. To further complicate matters, discontinuities in the form of fractures, microcracks and pore space, usually saturated with fluid phases, are prevalent. Not surprisingly, modelling the elastic properties of such complex systems are still particularly challenging and remains an actively developing topic in Rock Physics and continuum mechanics research.

Several attempts have been made to take the most general approaches to modelling rocks as multiphase composite materials (e.g. *Hashin and Shtrikman*, 1963; *Hill*, 1965; *Budiansky*, 1965; *Kröner*, 1967). Extensive reviews on the elasticity of composite materials are available by *Watt et al.* (1976); *Willis* (1981) and *Berryman* (1995). *Eshelby* (1957) treated heterogeneous material as an effective medium consist of a region (the inclusion) with the properties different from the homogeneous surrounding (the matrix), and derived analytical solutions for inclusions of ellipsoidal shape. Since then, *O'Connell and Budiansky* (see 1974); *Budiansky and O'Connell* and others extended this technique to spherical, disc- and needle-shape aligned or disordered inclusion geometries (*Watt et al.*, 1976). Ef-

9

fective medium theory is widely used to model elasticity of porous and cracked solids as well as textured polycrystalline aggregates.

The scope of the review presented here is restricted to the investigation of the elasticity of polycrystalline aggregates. Furthermore, with this restriction, isotropic monomineralic polycrystalline aggregates composed of anisotropic crystals are first considered. It may be assumed that only the physical properties of the volume weighted constituent minerals contribute to the overall elastic constants of the material. Further assumptions of uniformly distributed strain or stress throughout the aggregate allow definition of the Voigt and the Reuss bounds, respectively (*Voigt*, 1928; *Reuss*, 1929, see also Appendix D for details on the Voigt and the Reuss averaging). Hill's average (*Hill*, 1952) is taken as an arithmetical mean of the Voigt and Reuss widely separated bounds to provide unique solution consistent with experimental measurements in some cases (e.g. *Chung and Buessem*, 1967b). Effective medium theory has been applied to the polycrystalline aggregate composed of weakly anisotropic crystals by *Lifshitz and Rozenzweig* (1946). A more general formulation of the effective medium theory in application to polycrystals is based on the standard methods to solve the *Lippmann-Schwinger* equation of quantum mechanics scattering theory was given by *Zeller and Dederichs* (1973). Although restricted by several assumptions, these authors presented a solution for an isotropic polycrystalline aggregate composed of weakly anisotropic crystals of cubic symmetry; they also mentioned the difficulties of obtaining analytical solutions for suitable practical cases.

Application of variational approach by *Hashin and Shtrikman* (1962a,b) narrowed the upper and lower bounds of the elastic constants compared to the Voigt-Reuss (VR) bounds. This method was initially developed by authors for the case of isotropic polycrystalline mixtures of crystals of cubic symmetries and extended to incorporate crystals of other symmetries as low as monoclinic by *Watt* (1979, 1980); *Watt and Peselnick* (1980) and *Watt* (1986, 1987, 1988).

A more general approach developed by *Kröner* (1977) incorporates these previous results into a recursive procedure that is a modification and extension of *Zeller and Dederichs* (1973) work. The bounds of effective medium are established through the n-point correlation functions ($n = 1, 2, 3, ..., \infty$). Restrictions of statistical homogeneity, isotropy, and disorder are imposed on correlation functions. First order upper and lower bounds

10

coincide with the Voigt and the Reuss bounds. For the statistically homogeneous and isotropic material of grade $n = \infty$, and disorder of grade $n = 2$ bounds coincide with the Hashin-Shtrikman bounds. For the material of statistical properties of homogeneity, isotropy, and disorder of overall grade $n \to \infty$ upper $C^{(+n)}$ and lower $C^{(-n)}$ bounds converge to the self-consistent solution C^{SC} (*Hershey and Dahlgren*, 1954; *Kröner*, 1958). The recursion formula must be applied to calculate the effective elastic constants of higher-grade polycrystalline aggregates (*Kröner*, 1978). 'Seeds' are required to initiate this recursive procedure. For the odd-order bounds the first order ($n = 1$) Voigt-Reuss bounds are needed. For the even-order bounds (e.g. the Hashin-Shtrikman bounds) the zero-order bounds are required (*Nadeau and Ferrari*, 2001). The application and accuracy of different averaging techniques to model the elasticity of rocks has been discussed by numerous authors (e.g. *Kumazawa*, 1969; *Crosson and Lin*, 1971; *Christensen*, 1971; *Babuška*, 1972; *Thomsen*, 1972) and *Bunge* (1974).

One serious defect of many averaging procedures is they are not properly invertible. In elasticity, invertibility means that the stiffnesses may be obtained from the inverse of compliances, and vice versa. More precisely, the set of elastic stiffnesses determined using the averaging procedure should be the same as the corresponding set of elastic stiffnesses obtained from inversion of elastic compliances also calculated using the same averaging procedure ($[C] = [S]^{-1}$). This is physically necessary condition for real materials. However, many averaging methods fail this physical reality. *Aleksandrov and Aizenberg* (1966) proposed a novel approach to averaging elastic constants of polycrystalline materials. Specifically, they suggested that the averaging technique must be modified by defining new averaging function that accommodates property of invertibility of elastic stiffnesses of the aggregate into its elastic compliances. In other words, averaging can be performed on either stiffnesses or compliances, and produces identical result as it properly should. In this sense, *Aleksandrov and Aizenberg*'s solution is "self-consistent". *Morawiec* (1989) further developed this method for averaging the elastic properties of anisotropic aggregates, i.e. not only scalar properties (e.g. bulk modulus, shear modulus), but also tensorial quantities (e.g. elasticity) can be averaged. *Matthies and Humbert* (1993) named this method the 'Geometric mean' and reported its applicability in the calculation of the Young's modulus of a hypothetical Zn sample. For this case, the geometric

11

mean results were almost identical to those obtained by the self-consistent approxima-
tion. The term geometric mean is slightly misleading as the result produced is not an
exact geometric mean average in a strict mathematical sense. Instead, the *geometric mean
averaging* (GMA) resembles geometric mean averaging but has different properties. The
GMA technique is discussed in detail in this thesis and the method is further devel-
oped here to solve particular problems of hexagonal minerals in TI specimen and an or-
thorhombic minerals in orthotropic specimen. These problems have not been solved pre-
viously to my knowledge but they have important implications for seismological studies.

The averaging procedure is further complicated if the textural properties of an aniso-
tropic aggregate must be taken into account. The textural properties of the aggregate
and of the constituent minerals are quantitatively described by an *orientation distribution
function* (ODF) (*Viglin*, 1960) incorporated into the averaging. Briefly, an ODF statistically
describes the distribution of the orientation of the crystal symmetry axes within the carte-
sian coordinate frame of the specimen. Detailed descriptions of the ODF developed for
the orthorhombic-orthotropic case is derived in Appendix D. Independently, *Roe* (1965,
1966) and *Bunge* (1982) introduced a method of calculating the intrinsic elastic properties
of polycrystalline aggregates based on its texture as described by the ODFs. Since these
original publications, the ODF technique has been extensively applied in metallurgical
studies mainly to determine the elastic constants of *bcc* metals (e.g. *Morris and Heckler*,
1967; *Van Houtte et al.*, 1981). *Sayers* (1986, 1987) used this technique to model elastic con-
stants of a hexagonal zirconium composite and *Thompson et al.* (1994) applied ODF's to
describe the anisotropy of an orthorhombic titanium sheet.

It was mentioned above that the elastic constants of a polycrystalline aggregate may
be calculated by the self-consistent approach (*Kröner*, 1958, 1978) assuming an effective
medium with a specific geometry of inclusions. *Morris* (1970, 1971) incorporated aggre-
gate textural properties into a modified *Kneer* (1965) self-consistent averaging procedure
to calculate elastic properties of orthorhombic symmetry metal plates composed of dif-
ferent cubic crystals. *Humbert and Diz* (1991) and *Diz and Humbert* (1992) discussed the
practical aspects of applications of the self-consistent model. These authors pointed out
that although the SC technique provides a unique solution within the VR bounds, its ap-
plication to complex models such as textured rocks is nontrivial, and convergence of the

SC solution is sensitive to the initial model assumptions.

Texts by *Wenk* (1985) and *Kocks et al.* (1998) discussed applications of the ODFs; but they exclude the application of the GMA method to geomaterials. They pointed out the difficulties in modelling elastic properties due to the fact that rocks are texturally more complicated polycrystalline aggregates, and are composed of lower symmetry minerals than cubic crystals. Therefore, the application of an ODF to geomaterials is currently limited mainly to textured monomineralic aggregates; as such ODF technique is a basic technique to qualitatively account for the elasticity of textured rocks. *Johnson and Wenk* (1986) and *Wenk et al.* (1988) incorporated the ODF to average the elastic properties of an aggregate with orthorhombic symmetry composed of trigonal calcite. *Sayers* (1994) provided explicit formulae to calculate the elastic constants of hexagonal polycrystalline aggregate composed of hexagonal crystals from the coefficients of expansion of the ODF into a series of generalized spherical harmonics. In both cases Voigt's uniform strain assumption has been used. *Mainprice et al.* (1990) used an ODF to investigate the effect of solid state mineral phase transitions ($\alpha - \beta$ quartz, calcite-aragonite, orthopyroxene-clinopyroxene, olivine-spinel) on compressional wave velocity and anisotropy. In all these studies the GMA method was not used or tested against experimental results.

Most of the studies employing ODF averaging assume the Voigt approximation of uniform strain, usually without any detailed physical justification. The only paper known to the author where the more physically meaningful geometric mean (*Aleksandrov and Aizenberg*, 1966) has been applied to geomaterials is by *Mainprice and Humbert* (1994). The velocities of textured plagioclase feldspar and biotite aggregate have been calculated in this study from elastic constants obtained by different method including the Voigt, the Reuss, the Hill, the GMA and the self-consistent model with specific geometry (i.e. grains of spherical shape). Volumetrically minor mineral phases have been neglected to simplify the model. Results of the plagioclase modelling have been compared to experimentally observed velocities. Discrepancy in observed and calculated data was attributed to the cleavage cracks in plagioclase that were not accounted for in the model. After comparing the GMA to other calculations these authors concluded that *'the geometric mean is the best estimate of the seismic properties of the simple averaging methods'.*

Despite this initial success, however, to the author's knowledge the GMA method has

13

not been further extended to other geoscience related problems. One potential reason for this is that the GMA results might be presumed to be relatively close to Hill's solution and therefore provide little or no additional insights for the increased effort. Based on conclusions of these studies and physically more significant assumptions, the GMA has been chosen here as the technique to study the intrinsic anisotropy of rocks and, more importantly, to investigate the dependence of intrinsic elasticity as a function of texture. Results presented in the thesis provide insights related to averaging procedure in general that are of interest to the community; insights some of which were unanticipated.

Textural information, usually given in terms of pole-figures, is required in calculating the elastic constants of a polycrystalline aggregate. Obtaining this information is time and labor intensive and due to technological limitations is imperfect. Even the latest developments in the field of texture analysis such as *electron back scattering diffraction* (EBSD) in the *scanning electron microscopes* (SEM), high resolution X-ray synchrotrons, and diffractometers based on neutron *time of flight* (TOF) diffraction (*Leiss et al.*, 2000) still require further development in order to fulfill present day textural analysis needs. Information about the orientation distribution of many minerals in rock formations at typical geological conditions is very limited [1]. Undoubtedly, textural information on variety of rocks will be readily available as most of the technical challenges of textural analysis will be overcome in this actively developing area of geosciences. However, the investigation of the dependence of elastic properties of rocks on their textural properties should not be affected by the preset day limitations in textural analysis and may be investigated with available theoretical tools through the forward modelling techniques and meaningful assumptions on textural mineral distributions. Such studies can still provide important insights into the understanding of seismic anisotropy and its relation to the fabric of rocks within the Earth. In this thesis application of averaging techniques to model intrinsic anisotropy of different textured rocks is investigated.

---

[1] Quoting H.-R. Wenk (in *Leiss et al.*, 2000): *"There have been many books and a multitude of scientific papers published on various experimental and theoretical aspects of preferred orientation in rocks, yet many questions remain. While much is known about monomineralic rocks such as quartzite, marble and olivinite, we still know practically nothing about polymineralic rocks and do not understand in any quantitative way such basic questions as to how hornblende aligns in an amphibolite, or mica in a gneiss. While the theoretical framework to deal with such materials is still in its infancy (having the balance growth, deformation, chemical reactions, and recrystallization), it is also difficult to characterize the orientations of crystals and orientation relationships between neighbours."*

1.4 Investigation of intrinsic anisotropy: scope of the thesis and main challenges

Understanding the effects of main sources of anisotropy on elastic properties of the medium allows significant improvement in the interpretation of seismic data to be achieved. By distinguishing different sources of anisotropy effect of each one can be better understood. Calculation of elastic properties of the textured aggregate is treated as forward modelling. An advantage of a forward modelling approach is that geologically meaningful properties of the initial model can be assumed (if not available from experiments), and then the effect of different averaging approximations on modelling elasticity as a function of texture can be investigated. The dependence of each elastic constant of the aggregate on its textural properties can be studied to provide insights on intrinsic elasticity of anisotropic rocks. In the thesis, the intrinsic anisotropy is investigated through the averaging elastic properties of polycrystalline aggregate by the GMA technique, as well as conventional the Voigt and the Reuss approaches, with the texture captured in the ODF and incorporated into the averaging procedure.

The major challenges of this approach are the complex mathematical description of the ODF which requires functions that are *specific* to each case of symmetry of the constituent mineral and the statistical symmetry of the aggregate. In addition, specific care should be taken for proper implementation of the GMA technique for the cases of particular symmetries.

The thesis contains three Chapters that deal with different types of rocks, namely collection of metamorphosed sediments and volcanics from the Flin Flon Belt (FFB), continental lithosphere peridotites composed predominantly of olivine, and rocks composed of phyllosilicates such as shales. Despite the diversity of the rock types selected, all three examples are related through rock's intrinsic elastic behaviour defined by elastic anisotropy. Detailed investigation, described in the thesis, revealed similarities and differences in elasticity of these intrinsically anisotropic rocks.

15

1.4.1 Chapter 2 - Flin Flon Belt Seismic Anisotropy

Chapter 2 deals with the experimental determination of elasticity and anisotropy of meta-sediments and metavolcanics from the Flin Flon metamorphic terrane (Trans-Hudson Orogen). The intrinsic anisotropy of the investigated rocks is revealed through the laboratory measurements of P- and S-wave velocities on core samples in directions corresponding to rocks textural properties. The effect of heterogeneities on ultrasonic velocities is estimated. The textural (intrinsic) origin of anisotropy is inferred from the analysis of velocity measurements as a function of confining pressure (up to 300 MPa corresponding to $\sim$ 11 km depth). Metamorphosed sediments and volcanics rocks show strong P-wave anisotropy (up to 21%) and shear-wave splitting. Analysis of overall elasticity of the collection suggest two types of elastic symmetry (transversely isotropic and orthotropic) to be predominant within the Flin Flon metamorphic terrane. The material presented in this Chapter is accepted for publication in Canadian Journal of Earth Sciences.

1.4.2 Chapter 3 - Elasticity of polycrystalline aggregates of orthotropic symmetry

Chapter 3 discusses the effects of different averaging techniques on the estimation of the intrinsic elasticity of monomineralic rocks of orthotropic textural symmetry composed of orthorhombic minerals. In order to investigate the averaging effect on the elasticity, the ODF with orthotropic-orthorhombic symmetry was developed, for first time to our knowledge, to describe orthotropic aggregate composed of orthorhombic crystals. Further, the GMA was applied for first time to the orthotropic aggregate and results were compared to the conventional Voigt and the Reuss averages. Averaging techniques were applied to investigate the elasticity of olivine aggregate with textural properties similar to olivine texture of orthotropic symmetry in naturally deformed peridotites. A short review of the anisotropy of mantle peridotites is provided, and the modelling results obtained are compared with laboratory measurements available in the literature.

16

1.4.3 Chapter 4 - The intrinsic anisotropy of phyllosilicate rich rocks

Chapter 4 deals with the effect of texture on the elasticity and anisotropy of a phyllosilicate aggregate with specific reference to shale elasticity. Phyllosilicates include mica and clay family minerals; their layered structure makes them highly anisotropic. The dependence of the aggregate elastic constants and anisotropic parameters as a function of texture is modelled by different averaging techniques including the GMA. Modelling covers all stages of texture in such aggregate, i.e. development from randomly oriented isotropic aggregate to strongly aligned textured aggregate with elastic properties of single crystal. The results demonstrated a strong dependence of the phyllosilicate elasticity and anisotropic parameters on both texture and choice of averaging procedure. The elastic constants of isotropic phyllosilicates aggregates in the Voigt approximation are 160% of those in the Reuss. Based on results of this study, it has been suggested that the GMA may most appropriately model phyllosilicate intrinsic elasticity. Some results of the study presented in this Chapter have been published in the CSEG Recorder.

1.4.4 Chapter 5 - Discussion and Conclusions

The analysis of this application of different averaging techniques to model the intrinsic elasticity of rocks is presented in the Discussion and Conclusion Chapter of the thesis that summarizes the findings of the above mentioned studies. The differences in the intrinsic elasticity of the rock types investigated is then discussed. One important conclusion arising from comparison of the results of Chapters 3 and 4 is that the assumption on the choice of averaging techniques may be a major source of error in predicting intrinsic elastic properties of some types of rocks, and not so critically important for others. Limitations of the different averaging techniques and their applicability to model intrinsic elasticity and anisotropy is analyzed. Finally, conclusions on modelling the intrinsic elasticity of rocks and suggestions for future research directions are presented.

Chapter 2

Flin Flon Belt Seismic Anisotropy: Elastic Symmetry, Heterogeneity, and Shear Wave Splitting

[1]

This Chapter deals with experimental measurements of the elasticity of intrinsically anisotropic metamorphic rocks from Flin Flon Belt area, Manitoba-Saskatchewan border.

Laboratory measurements of compressional (P) and shear-wave (S) velocities, and shear-wave splitting have been carried out on a set of upper greenschist - lower amphibolite facies metasediments and metavolcanics and plutonic rocks from two ductile shear zones in the Flin Flon Belt (FFB) of the Trans-Hudson Orogen (THO). Selected metamorphic rocks vary in composition from felsic to mafic. Test sites with outcrops of sheared metamorphic rocks were correlated with a series of inclined seismic reflectors possibly extending from the midcrust and intersecting a well mapped shear zone at the surface. Determination of the lithological and physical properties of highly deformed metamorphic rocks is essential for proper interpretation of the nature of observed seismic reflectors. To investigate the anisotropic properties of the rocks, compressional velocity was measured at a confining pressure up to 300 MPa in three mutually orthogonal directions aligned with respect to visible textural features. In addition, on selected samples, shear-wave velocity was measured at two orthogonal polarizations for each of three propagation directions to determine shear wave splitting. The seismic heterogeneity of

---

[1]A version of this Chapter has been accepted for publication, *Cholach et al.* (2004). Some parts of this Chapter were also presented at CGU 2003 and AGU 2003 annual meetings.

hand specimens was also investigated by measuring P- and S-wave velocities on several cores cut in the same direction. Observed compressional wave anisotropy varied from quasi-isotropic to 24%. Maximum observed shear wave splitting reaches a value of 0.77 km/sec at confining pressure of 300 MPa. The pressure invariance of observed P-wave anisotropy and shear-wave splitting indicates that intrinsic anisotropy due to the lattice preferred orientation (LPO) of highly anisotropic minerals such as mica and hornblende is mainly responsible for the measured seismic anisotropy.

2.1 Introduction

Geophysical capabilities in making seismological observations of the crust and mantle at all scales have improved dramatically over the last decade. Technological advances allow us to acquire, store, and process progressively larger volumes of active and passive seismic records. The analysis of such observations, however, has required increasing levels of sophistication in the consideration of scale, structure, and material properties. Often, these analysis must invoke elastic anisotropy to provide a reasonable geological model, that is they must allow the seismic velocity to depend on the direction of wave propagation through the Earth. For example, *Hearn* (1999) included compressional wave anisotropy greater than 5% in order to properly focus tomographic images of the uppermost mantle derived from P_n wave observations. *Vestrum et al.* (1999) demonstrated that conventional seismic migration algorithms that do not account for anisotropy would produce significant lateral positioning errors in active-source seismic measurements in overthrust belts. Large numbers of workers are mapping the polarization directions and time delays associated with shear wave splitting of SKS teleseismic arrivals (e.g. *Park and Levin*, 2002) that are almost exclusively interpreted as indicators of upper mantle fabric. These studies highlight the existence of seismic anisotropy and there is no doubt that it must be included if we are to better understand seismic observations.

The anisotropy of compressional (P) and shear (S) wave velocities is one manifestation of the overall elastic character of a material at many scales. Any loss of symmetry in a material results in anisotropy; elastic wave anisotropy can be produced by preferential mineral orientations obtained during deposition, or developed during diagenesis or

metamorphism, by cracks and joints, and by layering. In void-free metamorphic rocks, the fabric symmetry is usually assumed to take one of three forms: isotropic for a rock with no detectable texture, transversely isotropic for a foliated rock (Figure 2.1a), or orthorhombic for a rock with a clear lineation within its plane of foliation (Figure 2.1b). More precisely, an isotropic material will appear the same across any arbitrary plane or by rotation about any arbitrary axis. A transversely isotropic material will have one plane of symmetry, the XY foliation plane, and a rotational axis of symmetry perpendicular to the foliation - normal Z axis. Once a clear lineation exists, the symmetry of the sample is further reduced to three planes of symmetry, all oriented with respect to the lineation and foliation (Figure 2.1b). As such, observations of seismic anisotropy are diagnostic of texture; and it is this linkage that makes anisotropy such an active area of study.

However, despite the many observations of elastic anisotropy in rocks since the early part of the last century Zismann (1933), the recognition that it is important to consider both for purposes of proper imaging and as a tool for interpretation and the development of mathematical tools (e.g. Auld, 1990) and theoretical approximations (e.g. Thomsen, 1986); Tsvankin (1997) to make modelling of such anisotropy simpler, our understanding of the anisotropy of real rocks remains limited. Metamorphic rocks, in particular, have complex elastic behavior and exhibit seismic velocity anisotropy that can be attributed to their mineralogical composition and textural properties. The elasticity of rocks of different metamorphic facies from a number of shear zones worldwide has been extensively studied. Most of these studies have attempted to focus on the relationship between the rock velocity anisotropy and texture; these results are often used to make inferences on the source of seismic reflectivity within the crust.

Jones and Nur (1982) reported laboratory measured P-wave anisotropy greenschist facies mylonitic rocks from the Columbia River fault zone, BC. The authors concluded that strong seismic anisotropy of these silicic and intermediate rock samples was controlled by the volumetric abundance and degree of lattice preferred orientation of phyllosilicates.

Wang et al. (1989) report measurements of P-wave velocities on a varied suite of mylonitic gneisses, less deformed crystalline protoliths, plutonic and volcanic samples taken from the Whipple Mountains shear zone, California. Velocities were measured to pressures of 500 MPa in three directions through rectangular samples cut parallel to the meta-

20
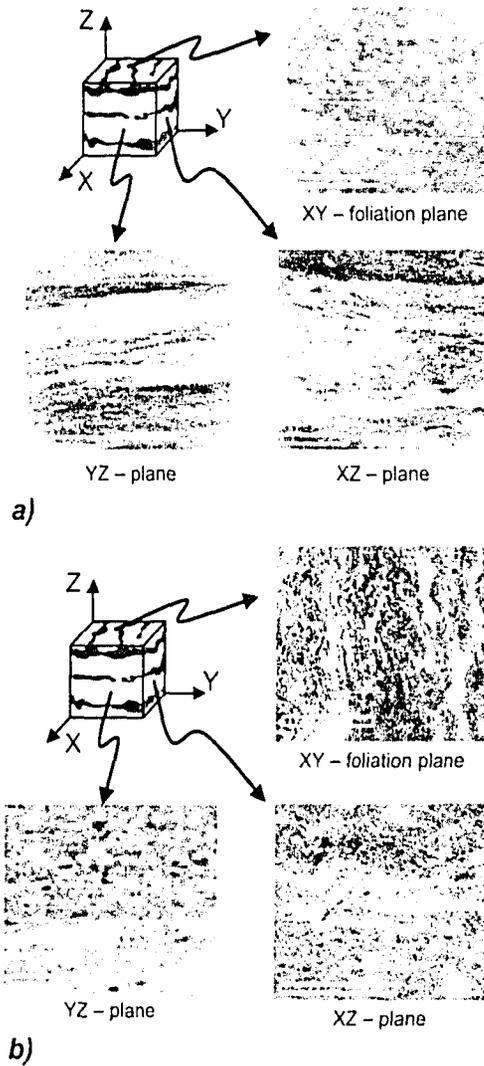
Figure 2.1: Hand specimen coordinate system defined with respect to the visible textural elements of foliation and lineation in metamorphic rocks. The principal axes X and Y both lie within the foliation plane but parallel and perpendicular to the lineation. Principal axis Z is normal to the foliation plane. Scanned thin-sections were cut along the symmetry planes of specimens. a) Strong foliation apparent in the XZ and YZ thin sections but not in the XY thin section in the highly deformed metavolcanic sample 93-1 defines transversely isotropic symmetry; b) presence of the well-developed lineation in the XY foliation plane of metavolcanic sample 93-7 defines orthorhombic symmetry.

morphic fabrics of the samples. In general, the authors observed a high degree of hetero-geneity from sample to sample, in part due to alteration, with P-wave anisotropy values as high as 19.2% being measured.

Kern and Wenk (1990) investigated the pressure and temperature dependence of veloc-ity anisotropy for progressively deformed mylonites from the Santa Rosa Mylonite Zone, southern California. Observed high P-wave velocity anisotropy strongly correlates with the degree of deformation. Measured shear wave splitting was attributed directly to the lattice preferred orientation of biotite. The authors concluded that a 1 km thick layer of the investigated mylonites, which had a velocity variation more than 10%, might be a readily detectable seismic reflector.

Christensen (1989) and *McCaffree and Christensen* (1993) analyzed experimentally mea-sured the compressional and shear wave properties of mylonites from continuous drill core through a major part of the Brevard fault zone, North Carolina. Measured properties of metamorphic rocks of upper amphibolite facies were correlated with the reflectivity of a seismic reflection profile in the vicinity of the drilling site. The observed seismic reflec-tivity was explained by the presence of fine subhorizontal layering of metamorphic rocks that might have originated from lower crustal ductile deformation.

A number of publications have dealt with the elasticity of metamorphic rocks from the Ivrea Zone and adjacent zones of exposed continental crust in northern Italy. *Siegesmund et al.* (1989) reported the pressure and temperature dependence of V_p and V_s aniso-tropy of amphibolites that was mainly related to the texture of constituent hornblende minerals. *Burke and Fountain* (1990) concluded that the preferred orientation of mica con-trols the measured compressional wave anisotropy of investigated schists and gneisses. *Siegesmund and Kern* (1990) reported strong P- and S-wave anisotropy of mylonitic rocks that correlates with both oriented microcracks and LPO of rock-forming minerals. *Burlini and Fountain* (1993) measured P- and S-wave velocities on a set of granulite-facies metape-lites. Two distinctive P-wave velocity patterns of transverse isotropy and orthorhombic symmetry were identified and attributed to the preferred orientation of mica and a com-bination of both mica and sillimanite, respectively.

Ji et al. (1993) and *Ji and Salisbury* (1993) examined the elasticity of mylonites from the Tantato high-grade metamorphic domain in the Snowbird tectonic zone (northern

22

Saskatchewan) and discussed its applications to the interpretation of lower crustal shear-zones reflectivity. On the basis of laboratory P- and S-wave velocity measurements, shear wave splitting measurements and petrophysical studies, the authors concluded that strong anisotropy of amphibolitic mylonites correlates with the volume fraction of aligned hornblende. In contrast, granulite-facies mylonites did not develop significant anisotropy and might be interpreted as quasi-isotropic. *Ji et al.* (1997) obtained similar results for granulite-facies metamorphic rocks from the Morin shear zone in the Grenville Tectonic Province (Québec, Canada).

Zappone et al. (2000) measured compressional wave anisotropy on 12 rock samples from a wide range of metamorphic grades and lithologies taken from the southern Iberian peninsula. Based on measurements to confining pressures of 280 MPa, they reported anisotropies of 1.6% to 17.6% relative to the mean velocities.

Quartz-rich feldspathic gneisses from the Nanga Parbat - Haramosh massif, India, show surprisingly high levels of anisotropy of up to 12.5% and 21% for P-wave and S-wave velocities, respectively (*Meltzer and Christensen*, 2001). These velocities were measured on cylindrical cores cut along the principal metamorphic directions to pressures of 1 GPa. The degree of anisotropy depended on the modal volume of mica mode and the fabric strength. Of particular note was the observation that the maximum velocities in many of the samples were similar to those expected for more mafic rocks. Such anisotropy could influence the velocities of waves propagating along turning rays in seismic refraction studies and could lead to incorrect inferences about the mineralogy at depth.

In the above studies, P- or S-wave speeds were measured along the three presumed principal directions with respect to the lineation and foliation. *Wang et al.* (1989) noted, however, that this does not provide sufficient information to completely characterize the elastic properties, and hence the wave speed anisotropy, at angles different from the symmetry axes. To overcome this limitation, a number of recent studies have included measurements using off-axes cores. Under the assumption that schists are transversely isotropic, *Godfrey et al.* (2000) made high pressure velocity measurements on cylindrical cores cut parallel, at 45°, and perpendicular to foliation. These samples exhibited P-wave anisotropy from 9% to 20% and significant shear wave splitting. The latter values were

23

sufficiently large to account for up to 45% or more of the time delays seen in split SKS teleseismic arrivals over the Haast Schist Terrane in New Zealand. *Okaya and Christensen* (2002) carried out further analysis of these same data to illustrate how crucial off symmetry axis velocity determinations are.

More recently, *Takanashi et al.* (2001) reported results on P- and S-wave velocity measurements for several amphibolites, a biotite gneiss and a biotite schist from the Hidaka Metamorphic Belt, Japan. The observed pattern of seismic anisotropy in this case strongly correlates with the lattice preferred orientation (LPO) of rock-forming hornblende and biotite.

A common conclusion of the above studies is that deformed metamorphic rocks are more likely than not to be elastically anisotropic, with the anisotropy dependent on a variety of factors including mineralogical composition, metamorphic grade, the degree of fabric development, and the extent of brittle deformation. Further, anisotropy has implications for both active source and passive seismology. The main purpose of the study presented in this Chapter is to obtain additional information on the elasticity of metamorphic rocks produced within the Annabel Lake ductile shear zone of the Flin Flon Domain in the Proterozoic Trans-Hudson Orogen. The mapped shear zones correlate well with seismic reflectors that extrapolate to the surface and, indeed, the initial motivation for this work was to explain this strong reflectivity. As will be discussed, this goal was not achieved but the extensive series of high pressure laboratory measurements made on rocks from the shear zone provides considerable insight into the elastic symmetry of the material, its overall elastic properties, the degree of heterogeneity between samples, and the influence of sections of such metamorphosed rock on shear wave splitting observations.

2.2 Elasticity of an anisotropic medium - a review

The literature on the anisotropy of elastic P- and S-waves is rich in physics and only a brief overview of the theory is given here; the reader is referred to *Musgrave* (1970) or *Auld* (1990) for additional details. The main purpose of this section is to demonstrate that the P- and S- wave velocities through a material depend directly on the material's elastic

properties and that quantitative measurements of velocities and density yield the elastic properties directly. Further, while anisotropy in wave velocities can tell us a great deal by themselves, knowledge of the elastic properties are perhaps more useful in that they directly reveal the material's symmetry, and hence metamorphic texture. In the section below, the relationships that allow determination of the elastic properties from measured velocities are developed, *Mah and Schmitt* (2001b) and *Mah and Schmitt* (2003) review this topic more fully.

In any general elastic medium, stress and strain are specified as the second-rank tensors σ_{ij} and ε_{kl}, respectively. The relationship between these two tensorial quantities may be written in the form of the generalized Hooke's Law:

$$\sigma_{ij} = C_{ijkl}\varepsilon_{kl} \tag{2.1}$$

where C_{ijkl} is a fourth rank tensor with 81 components known as elastic constants or stiffnesses and repeated indices summing notations apply (*Auld*, 1990). The elasticity tensor C_{ijkl} fully describes the elastic properties of anisotropic crystals or solids. A number of symmetric and physical arguments reduce this to 21 independent elastic constants for the least symmetric triclinic case. The symmetry of the tensor of elasticity allowed *Voigt* to introduce a simpler matrix notation (*Nye*, 1990) that is commonly used in the geophysical literature where the four indices $ijkl$ are replaced by two indices mn:

$$C_{ijkl} = C_{mn}(i, j, k, l = 1, 2, 3; m, n = 1, \ldots, 6)$$

so that the generalized Hooke's Law may be simplified to a matrix equation:

$$\sigma_I = C_{IJ}\varepsilon_J \tag{2.2}$$

where σ_I and ε_J are 6×1 vectors containing independent components of stress and strain tensors, respectively. In Equation (2.2), the indices I and J are related to the ij in according to the cyclical recipe $I,J = 1, 2, 3, 4, 5, 6$ when ij or $kl = 11, 22, 33, 13$ or $31, 23$ or $32, 12$ or 21, respectively. Each C_{ij} is one of the components of a 6×6 symmetric matrix of 21 independent elastic stiffnesses that may be written in the form:

25

$$C_{ij} = \begin{pmatrix} C_{11} & C_{12} & C_{13} & C_{14} & C_{15} & C_{16} \\ & C_{22} & C_{23} & C_{24} & C_{25} & C_{26} \\ & & C_{33} & C_{34} & C_{35} & C_{36} \\ & & & C_{44} & C_{45} & C_{46} \\ & & & & C_{55} & C_{56} \\ & & & & & C_{66} \end{pmatrix} \tag{2.3}$$

The matrix in Equation (2.3) is symmetric about the diagonal (e.g. $C_{12} = C_{21}$) and for clarity those components below the diagonal are not shown. The number of independent elastic constants in the C_{ij} matrix depends on the elastic symmetry of the investigated medium and may vary between one elastic constant (usually defined as the bulk modulus K) for liquids, two elastic constants (*the Lamé parameters* λ *and* μ) for isotropic solids and up to the twenty one independent elastic constants for the most general case of triclinic symmetry. For this study the most important symmetries are isotropic, transversely isotropic and orthorhombic, which can be described by two, five and nine elastic constants, respectively. For these cases, the matrix of elastic constants will have the form:

$$C_{ij} = \begin{pmatrix} C_{11} & C_{12} & C_{13} & 0 & 0 & 0 \\ & C_{22} & C_{23} & 0 & 0 & 0 \\ & & C_{33} & 0 & 0 & 0 \\ & & & C_{44} & 0 & 0 \\ & & & & C_{55} & 0 \\ & & & & & C_{66} \end{pmatrix} \tag{2.4}$$

In an isotropic medium the coefficients will be $C_{11} = C_{22} = C_{33} = \lambda + 2\mu$, $C_{44} = C_{55} = C_{66} = \mu$, and $C_{12} = C_{21} = C_{13} = C_{31} = C_{23} = C_{32} = \lambda$. The isotropic case is the only one in which the familiar elastic Lamé parameters λ and μ apply. In the transversely isotropic medium only five of the elastic constants from matrix (2.4) are independent ($C_{11} = C_{22}$; C_{33}; $C_{44} = C_{55}$; $C_{66} = 1/2(C_{11} - C_{12})$; C_{12}; $C_{13} = C_{23}$). In the orthorhombic medium all nine non-zero constants from the matrix in Equation (2.4) are independent.

Elastic wave velocities can be calculated from the known elastic constants by solving the so-called *Christoffel equation* (e.g. *Musgrave*, 1970). Under the plane wave assumption the wave equation in an anisotropic medium can be written (see Appendix B for more details):

$$(C_{ijkl}n_j n_l - \rho v^2 \delta_{ik}) u_k = 0 \tag{2.5}$$

where δ_{ij} is the *Kronecker delta* (Nye, 1990), ρ is density, and n_i are the components of the wavefront normal vector. The nonzero values of displacement u_i are obtained as characteristic (*eigen*) vectors corresponding to the characteristic (*eigen*) values of velocities v^2 which are the roots of the standard eigenvector-eigenvalue problem:

$$det \mid C_{ijkl}n_jn_l - \rho v^2\delta_{ik} \mid = 0 \qquad (2.6)$$

The solution of Equation (2.6) represents the velocity surface for an infinite number of plane waves. It is convenient to rewrite (2.5) by introducing the notation

$$\Gamma_{ik} = C_{ijkl}n_jn_l \qquad (2.7)$$

where Γ_{ik} is the symmetric *Christoffel matrix*. Then

$$(\Gamma_{ik} - \rho v^2\delta_{ik})u_k = 0 \qquad (2.8)$$

Equation (2.8) is well known as *the Christoffel equation* and the standard eigenvalue-eigenvector problem may be now rewritten in the form:

$$det \mid \Gamma_{ik} - \rho v^2\delta_{ik} \mid = 0 \qquad (2.9)$$

Solution of the cubic Equation (2.9) for any specific slowness direction n yields three positive values of the squared phase velocity v^2, which correspond to the P-wave and two S-waves. In an isotropic medium the P-wave and S-wave particle motions are purely longitudinal and transverse, respectively. For this case the S-wave polarization (i.e. direction of particle motion) can be in any direction normal to the wave propagation direction; no shear wave splitting is allowed. More generally, the waves are referred to as "*quasi-P*" and "*quasi-S*" waves in an anisotropic medium due to additional complications with regard to the relationships between the polarization and wave propagation directions. Once the material is anisotropic, there will generally be two distinct shear waves in nearly all propagation directions, the polarizations of these two shear waves will be forced into two materially dependent but orthogonal directions and they will travel at different velocities leading to differences in their time of arrival. This phenomena is more

27

commonly known as shear wave splitting. These characteristics are apparent in the examples of velocity surfaces through the three planes of symmetry for isotropic (Figure 2a), transversely isotropic (Figure 2.2b), and orthorhombic (Figure 2.2c) materials.

While the point of the above discussion is to link measured velocities to elastic properties, the mathematics indicates that this is not straightforward in general (*Mah and Schmitt*, 2003). However, within planes of symmetry and along principal axes the wave behaviour, and consequently the formula linking velocities to elastic constants, simplify substantially.

Before going further, it is necessary to place the wave propagation and particle motion directions discussed above in the context of the fabric *XYZ* axes introduced in Figure 2.1 because this is the context within which the laboratory measurements are made (Figure 2.5). In particular, for any *P*- or *S*- wave propagating *along* one of the three axes of symmetry in an isotropic, transversely isotropic, or orthorhombic medium the waves will be purely longitudinal or transverse, respectively and the shear polarizations must lie within the planes of symmetry. Consider, for example, waves propagating only along the lineation direction *X*. The three elastic waves that will exist in such a situation are a *P* mode with polarization in the *X* direction, and two *S*-modes polarized in the *Y* and *Z* directions. In the following discussions we associate these three waves as *XX*, *XY*, and *XZ*, respectively. The *P*-waves along the *Y* and *Z* axes are designated by *YY* and *ZZ*, respectively. The two shear waves propagating in the *Y* direction will similarly be polarized in the *X* and *Z* directions and are assigned *YX* and *YZ*. Similarly, those propagating in the *Z* direction will have polarizations *ZX* and *ZY* (Figure 2.5).

In an isotropic medium the *X*, *Y*, and *Z* axes are arbitrary and the velocities $V_{XX} = V_{YY} = V_{ZZ}$, and $V_{XY} = V_{YX} = V_{XZ} = V_{ZX} = V_{ZY} = V_{YZ}$. With knowledge of the mass density ρ, the complete set of elastic constants is determined via:

$$C_{11} = C_{22} = C_{33} = \rho V_{XX}^2$$
$$C_{44} = C_{55} = C_{66} = \rho V_{XY}^2$$
$$C_{12} = C_{13} = C_{23} = \rho(V_{XX}^2 - V_{XY}^2)$$
(2.10)

Similar symmetries exist in the transversely isotropic case with $V_{XX} = V_{YY} \neq V_{ZZ}$, $V_{ZX} = V_{ZY} \neq V_{XY} = V_{XZ} = V_{YX} = V_{YZ}$. Note that in this case, the selection of the *X* and *Y* axes is arbitrary. The elastic constants that may be obtained from velocity

28
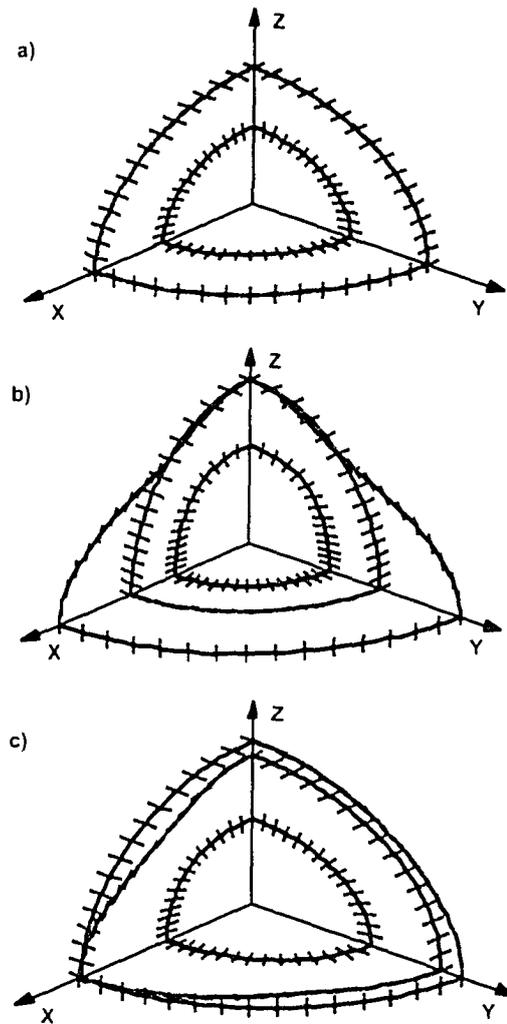
Figure 2.2: Normalized slowness (reciprocal velocity) surfaces and polarization directions of P- and S-waves for different elastic symmetries XYZ directions as in Figure 2.1 Bars indicate directions of particle motion. Note that S modes have lower velocities than the P mode and as such, have larger slownesses and plot further from the origin in the figure. a) P- and S-wave slowness surfaces are perfect spheres in an isotropic medium. b) The most pronounced shear wave splitting is within the symmetry plane for the transversely isotropic medium. c) Complicated P- and S-wave slowness surfaces with shear wave splitting along all three symmetry axes in a medium with orthorhombic symmetry. Note that one shear wave surface displays convexity and concavity in the XZ and YZ planes, respectively.

29

measurements along the symmetry axes are:

$$
\begin{aligned}
C_{11} &= C_{22} = \rho V_{XX}^2 \\
C_{33} &= \rho V_{ZZ}^2 \\
C_{44} &= C_{55} = \rho V_{XZ}^2 \\
C_{66} &= \rho V_{ZX}^2 = \rho V_{ZY}^2 \\
C_{12} &= C_{11} - 2C_{66}
\end{aligned}
\tag{2.11}
$$

For the orthorhombic case, $V_{XX} \neq V_{YY} \neq V_{ZZ}$, $V_{XZ} = V_{ZX} \neq V_{YX} = V_{XY} \neq V_{YZ} = V_{ZY}$. Six of the nine elastic constants may be determined from velocity measurement directions parallel to the symmetry axes:

$$
\begin{aligned}
C_{11} &= \rho V_{XX}^2 \\
C_{22} &= \rho V_{YY}^2 \\
C_{33} &= \rho V_{ZZ}^2 \\
C_{44} &= \rho V_{YZ}^2 \\
C_{55} &= \rho V_{XZ}^2 \\
C_{66} &= \rho V_{XY}^2
\end{aligned}
\tag{2.12}
$$

The independent off-diagonal elastic stiffnesses cannot be determined given only the values of velocity measured along the symmetry axes of Figure 2.2. Despite this, however, one is able to make an assessment of the degree of symmetry of a sample by examination of the diagonal stiffnesses determined in the measurements.

In recent years, many workers (e.g. *Takanashi et al.*, 2001) have used $'\varepsilon - \delta - \gamma'$ parameterizations that allow approximate calculation of the variation in velocity with direction using simpler trigonometric formulas. The original formulas may be found in *Thomsen* (1986) and *Tsvankin* (1997) for transversely isotropic and orthorhombic materials, respectively. For the sake of completeness we have included these parameters in Table 4. However, these parameterizations are not elastic constants, and we would like to reaffirm *Thomsen's* (1986) cautionary remarks about relying on such parameterizations if the true elastic coefficients are known.

2.3 Geological background and sampling

The rock samples for this study were taken from the vicinity of the Annabel Lake Shear zone contained within the Flin Flon Belt (FFB) of the Paleoproterozoic Trans-Hudson Orogen (THO). The orogen, and the FFB in particular has long been studied, due to the

30

existence of large economic mineral deposits. Only a brief overview of the present-day geological models of this complex zone are presented here in order to give a sense of the deformation and metamorphism that these rocks have experienced. Additional details, maps, and references can be found in *Lucas et al.* (1999a, 1999b).

The THO extends from Northern Québec through Saskatchewan and into South Dakota (Figure 2.3a). The Orogen played a major role in the construction of the North American continent by assembling separate Archean cratonic blocks and juvenile Paleoproterozoic terrains (*Hoffman*, 1988; *Lewry and Stauffer*, 1990). The Flin Flon Belt study area (as a part the Canadian Shield) lies in eastern Saskatchewan immediately to the west of the town of Flin Flon, Manitoba. The belt is wedged between the Archean Superior and Hearne cratons to the east and west, respectively.

Recent geological models for the Flin Flon Belt have been developed through the Shield Margin Project and the Trans Hudson Orogen LITHOPROBE Transect. Three main elements of the belt, joined in collisional deformations at 1.84-1.80 Ga, are thought to be an underlying Archean "Sask craton" (3.20 to 2.40 Ga), an intermediate complex of metamorphosed juvenile arc, oceanic, plutonic, volcano-sedimentary, and fluvial-alluvial sandstones ranging in age from 1.92 Ga to 1.85 Ga that make up the Flin Flon Belt, and an uppermost metamorphosed series of marine turbidites (1.85-1.84 Ga) and sandstones in the Kisseynew Domain. Essentially, the Flin Flon Belt consists of a series of 1.92 - 1.87 Ga arc and sea floor assemblages called the "Amisk collage" (*Lucas et al.*, 1996) separated by highly strained zones at 1.88 - 1.87 Ga and crosscutting plutons at 1.87 - 1.84 Ga. These plutons are thought to be superimposed on the collage by later arcs. Uplift ca. 1.85 - 1.84 Ga led to erosion of continental sediments (Missi Group) and marine turbidites (Burntwood Group) coeval with the decaying arc volcanism, events that led to the protoliths of the nonplutonic rocks studied here. Construction of the stack began with the Flin Flon Belt overriding the Sask craton along a décollment with interleaving between the Flin Flon Belt and the Kisseynew Domain from 1.84 - 1.80 Ga. Peak metamorphism and deformation occurred at 1.82 - 1.80 Ga.

As might be imagined, the geological structure in this area is complex. A simplified geological map of the study area (Figure 2.3, b), abstracted from *Ashton et al.* (1988), separates the surficial bedrock geology essentially into plutonic and nonplutonic rocks.

31
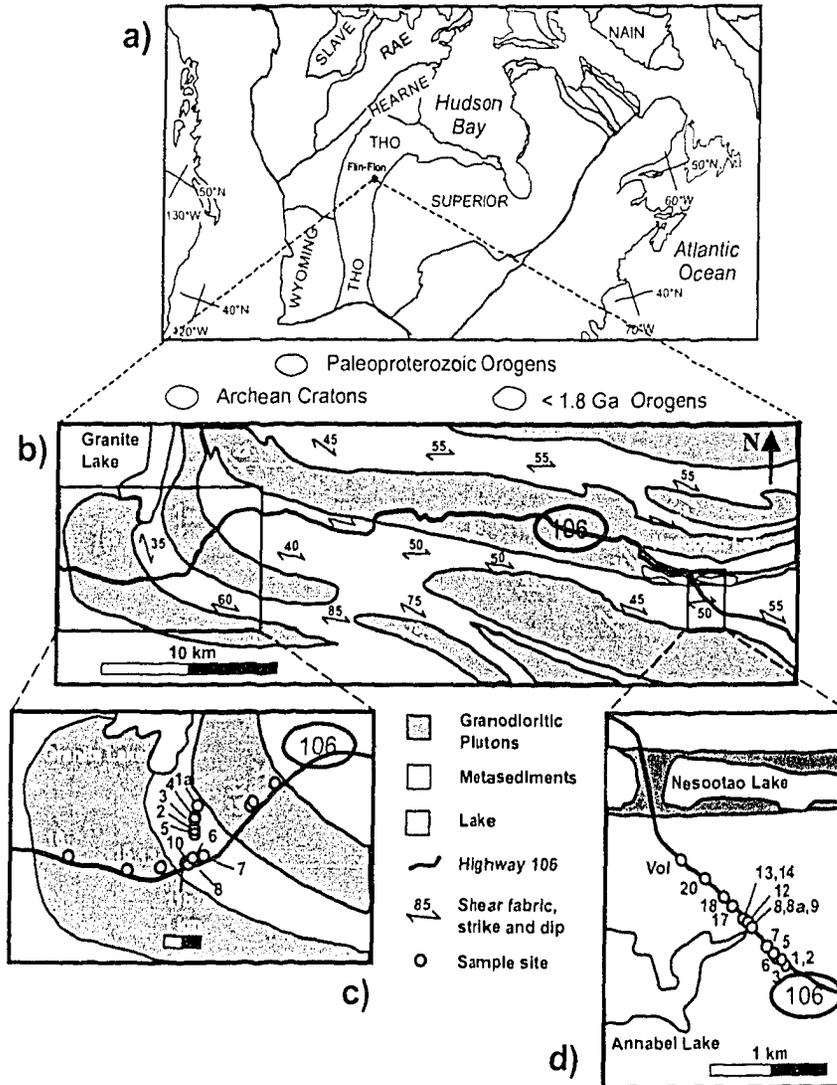
Figure 2.3: *a)* Location of the study area relative to the Archean provinces of continental North America. *b)* Simplified geological map of the Flin Flon Belt section along Saskatchewan highway 106 with location of the Granite Lake and Nesootao Lake sampling areas indicated. The map represents an abstract of the detailed mapping of Ashton et al. (1988). White regions represent zones comprised of metavolcanic/metasedimentary rocks. Dark grey regions are plutons. The strike and dip of the local shear fabric are indicated by the orientation of the arrows and the overriding number, respectfully. *c)* Locations of Granite Lake samples. *d)* Locations of Nesootao Lake samples.

32
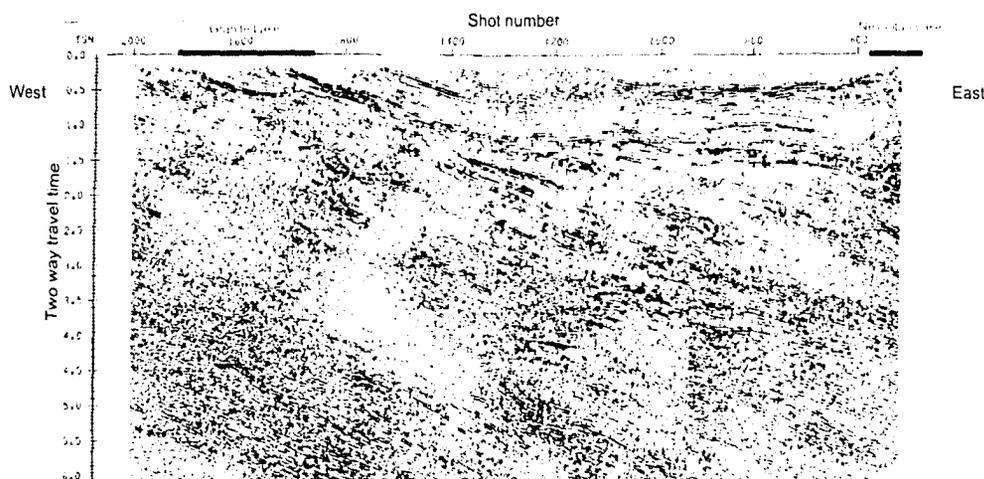
Figure 2.4: Section of the LITHOPROBE THO transect seismic Line 9 east of the Sturgeon weir fault. The lines labelled 'Granite Lake' and 'Nesootao Lake' correspond to the length of the segments of Saskatchewan highway 106 through the expanded segments of Figure 2.3 c and 2.3 d, respectively. The well-identified zone of east-dipping reflectors correlates at the surface with the Flin Flon Belt ductile shear zone test sites.

The LITHOPROBE THO transect Line 9 (Figure 2.4) was acquired along Saskatchewan highway 106 through the area (*Lucas et al.*, 1993). To the west of this image, a series of prominent seismic reflectors with an apparent dip to the east from near the surface in the vicinity of Granite Lake extends possibly to midcrustal levels. To the east of shot number 1200 a second interesting 'canoe' shaped event is seen at ~ 0.5 seconds two-way travel. This event is likely associated with the contact zone between the pluton and underlying metasediments/metavolcanics to the west of Nesootao Lake and could in part be due to out of plane reflections. Together, these reflectors show a great deal of structure between the plutons and the "Amisk collage" rocks (*Lewry et al.*, 1994; *Lucas et al.*, 1996). Our initial objectives was to attempt to explain these strong seismic events using laboratory - derived impedances of candidate rocks outcropping at the surface extensions of the reflectors.

There has been some limited earlier field and laboratory work on rocks from the FFB. *Hajnal et al.* (1983) compared pressure - dependent velocities measured in the laboratory on several Amisk volcanics to borehole and surface observations. While these authors demonstrated the large differences between competent laboratory samples and

fractured near surface materials, the investigation was mainly concentrated on the near-surface fracture distribution in different types of rocks as well as analysis of frequency-dependent attenuation in seismic, borehole and laboratory velocity measurements. The limited number of samples for laboratory measurements and the lack of directional dependencies of velocities in rocks made it difficult to incorporate these data in order to assist the interpretation of the reflectors in Line 9. Thus sampling was carried out at the Granite Lake and Nesootao Lake locations along Saskatchewan highway 106, approximately 40 and 20 km west of Flin Flon, Manitoba (Figure 2.3 c, d). During the first trip in 1991, metamorphic samples of variable composition were collected at the test site in the proximity of Granite Lake and during a trip in 1993 sampling conducted at a second site near Nesootao Lake (Figure 2.3 d). Fresh bedrock exposures were limited by Quaternary cover near Granite Lake. The Nesootao Lake sampling was more continuous with frequent fresh exposures opened by road cuts through the bedrock.

The Granite Lake hand specimens were collected over an 8 km section (Figure 2.3, c) that crosses the shear zone. All specimens from the 1993 trip were collected over a 3 km section covering an exposure of the same ductile shear zone in the vicinity of Nesootao Lake (Figure 2.3, d). Aside from the plutons, the samples collected display strong visible foliation defined by interchangeable layers of deformed quartz and hornblende (Figure 2.1).

To determine modal compositions and estimate mineral grain parameters, 97 thin sections cut parallel to the XY, XZ and YZ planes of each of the hand specimens were analyzed. Digital micrographs of thin sections were taken under plane-polarized light and average grain cross section areas were estimated by tracing each grain on the digital image. The mineralogical composition of each sample was determined by point counting on the thin sections that were oriented normal to the foliation (more then 300 points/slide). Results of the determination of mineralogical composition are summarized in Table 2.1.

The compositions of the metasediments vary from felsic to mafic as can be noted from significant variations in the modal quartz content, especially in the Granite Lake collection.

The peak metamorphic pressure (P) and temperature (T) were estimated on a few of these samples using microprobe-based garnet-biotite Mg/Fe geothermometry (*Ferry and*

Table 2.1: Mineralogical composition of the Granite Lake and the Nesootao Lake samples

Sample	Mineralogy
Granite Lake Metasediments	
1	41.8% QZ, 35.4% PL, 19.9% HBD, 1.8% GT
3	33.3% QZ, 47.3% PL, 13.6% BIO, 3.8% GT
4	41.9% QZ, 32.8% PL, 16.5% BIO, 2.7% GT, 4.2% SIL
5	40.2% QZ, 40.3% PL, 19.1% BIO
7	24.8% QZ, 51.7% PL, 18.3% BIO, 2.5% GT, 2.8% OPQ
10	19.7% QZ, 22.8% PL, 31.9% BIO, 5.3% GT
11b	24.4% QZ, 52.5% PL, 23% BIO
Granite Lake Metavolcanics	
2	25.5% PL, 25.2% BIO, 49.3% HBD
6	7.6% QZ, 56.5% PL, 9.7% BIO, 20.9% HBD, 3.9% ACS
8	4.15% QZ, 66.6% PL, 9.5% BIO, 18.2% HBD
Granite Lake and Nesootao Lake plutons	
13	2.7% QZ, 43.2% PL, 4.7% BIO, 46.9% HBD, 2.2% KF
15a	6.6% QZ, 60% PL, 10.0% BIO, 10% HBD, 10.9% KF
16	6.6% QZ, 60% PL, 10.0% BIO, 10% HBD, 10.9% KF
32	2.5% QZ, 61.8% PL, 27.3% HBD, 5.2% KS, 2.0% ACS
33	47% PL, 35.5% HBD, 15.5% CPX
34	34.9% QZ, 52% PL, 8.2% BIO, 2.3% HBD
93-8a	45.2% QZ, 29.1% PL, 16.3% BIO, 7.2% EPD
VOL-A	27.3% QZ, 64.8% PL, 6.7% BIO
VOL-B	22.5% QZ, 61.2% PL, 8.3% BIO, 1.9% OPQ
Nesootao Lake Metasediments	
93-2	39.5% QZ, 21.3% PL, 17.1% BIO, 3.5% HBD, 16.5% KS
93-3	60.2% QZ, 5.5% PL, 18.2% BIO, 8.3% HBD, 3.9% ALTN, 3% - CTE
93-8	43.2% QZ, 10.5% PL, 24.1% BIO, 6.4% HBD, 13.3% MS
93-9	25.7% QZ, 45% PL, 22.7% BIO, 4.6% OPQ
93-12	39.7% QZ, 23.3% PL, 22.8% BIO, 2.5% HBD, 9.6% EPD
93-13	28.1% QZ, 38.5% PL, 28.1% BIO, 4.2% ALTN
93-14	39.5% QZ, 3.6% PL, 30.8% BIO, 19.7% MS
93-17	33.4% QZ, 17.4% PL, 30.9% BIO, 2% OPQ, 15.1% MS
93-18	51.3% QZ, 38.6% BIO, 8.3% ALTN
93-20	31.6% QZ, 12.2% PL, 34.9% BIO, 2.2% OPQ, 11.6% ST
VOL-I	13.2% QZ, 16.3% PL, 67.1% HBD
VOL-III	10.8% QZ, 1.4% PL, 59.2% HBD, 9.4% CTE, 19.2% EPD
Nesootao Lake Metavolcanics	
93-1	30.8% QZ, 12.7% PL, 49.6% HBD, 4.9% EPD
93-5	21% QZ, 11.7% PL, 66.7% HBD
93-6	10.8% QZ, 21% PL, 41.8% HBD, 21.4% EPD
93-7	17.9% QZ, 23.4% PL, 51.9% HBD, 2.5% CTE, 3.7% EPD

Abbreviations: QZ-quartz, PL-plagioclase, BIO-biotite, MS-muscovite, HBD-hornblende, GT-garnet, KF-K-feldspar, CPX-clinopyroxene, OPX-orthopyroxene, SIL-silimanite, EPD-epidote, CTE-calcite, ST-staurolite, ACS-accessory, OPQ-opaque minerals, ALTN-alterations abbreviations after Oardley, 1989)

35
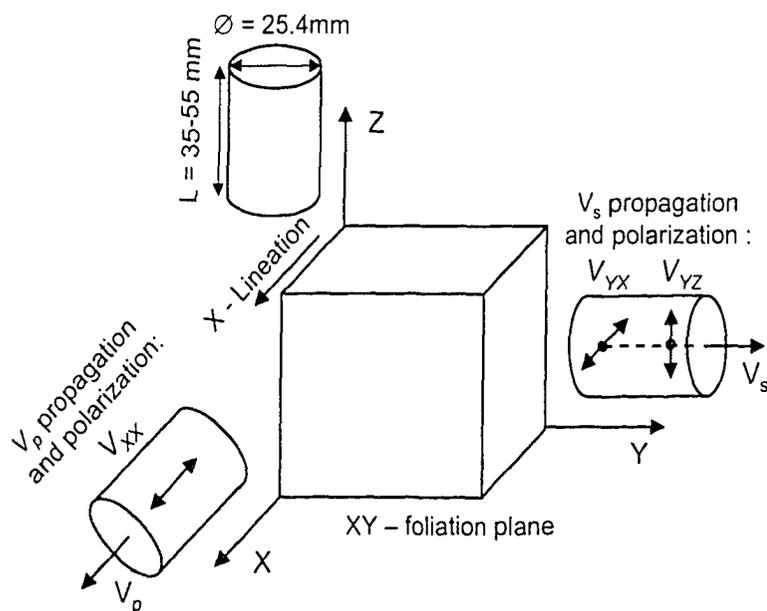
Figure 2.5: Relationship between the fabric-dependent XYZ coordinate system and velocity measurements directions. Velocity measurements along the sample symmetry axes have been identified by both wave propagation (first subscript) and polarization directions (second subscript). For example, V_{XX} refers to the longitudinally polarized wave propagating along the lineation direction X. V_{YX} and V_{YZ} refer to the two shear modes propagating in the foliation plane but perpendicular to the lineation, with transverse polarizations parallel to the lineation and perpendicular to the foliation plane, respectively.

Spear, 1978) and by considering the stability fields of characteristic minerals. The estimated peak temperatures scatter about 500°C and 530°C for the Nesootao and Granite Lake samples, respectively. Grains of sillimanite aligned with foliation in sample 4 are presumably of syntectonic origin and indicate temperatures of more than 500°C and pressure of 400 MPa. Staurolite grains that are not aligned with the foliated texture formed after the main deformation phase and reflect temperatures of 500 – 650°C. Garnet-biotite thermometry combined with the stability conditions for staurolite and sillimanite suggest peak P-T conditions at 510 – 530°C and ~ 400MPa (equivalent to ~ 14 km depth). These P-T conditions and the presence of characteristic minerals suggest the rocks investigated fall at the boundary of the upper greenschist and mid amphibolite metamorphic facies (*Yardley*, 1989).

2.4 Experimental procedure and results

2.4.1 Sample preparation

P-wave and S-wave measurements were made on cylindrical cores (2.54 cm diameter × 3.5 to 5.5 cm length) from 16 Granite Lake and 19 Nesootao Lake specimens (Table 2.1). The cores were cut from specimens aligned with respect to visible textural features. Each Granite Lake specimen has one core cut perpendicular to the foliation plane and at least one core parallel to the foliation plane. If visible lineation was present, two cores were cut within the foliation plane, one parallel and one perpendicular to the lineation direction as shown in Figure 3. More emphasis was placed on the Nesootao Lake cores because of the more frequent sampling possible there; and at least three mutually orthogonal X, Y, and Z samples were cored from each specimen. In addition, several cores were cut in the same direction in some samples (e.g. core sample 93-1-X1 and 93-1-X2), allowing investigation of the heterogeneity within a given specimen. Altogether, 147 cores were cut (Table 2.2). The ends of cores were flattened and made parallel using a surface grinder.

After cutting and flattening, the cores were dried in the vacuum oven for over 6 hours at temperatures near 80°C. Bulk densities were obtained by the immersion method to an uncertainty of better than ± 0.5% (Table 2.2). The variations in density between cores obtained from the same specimen are generally less than 1%, indicating a consistency of the mineral composition within any given sample. The porosities of the samples were not determined experimentally but estimated to be less than 1% at room pressure. The fact that the submerged masses of samples did not appreciably change during the density measurement is indicative of their low permeability and porosity.

P-wave measurements were made on all the cores; S-waves were measured only on a subset from the Nesootao Lake suite. Longitudinal mode, 2.54 cm diameter, 1-MHz frequency, piezoelectric ceramics were placed at both ends of the cores for the P-wave measurements. Similar transverse mode ceramics were used for the S-wave measurements. The S-wave ceramics provide a mechanical pulse polarized parallel to the ends of the samples and care needed to be taken to ensure that the polarization directions of both transverse mode ceramics were properly in line and that they were appropriately oriented with respect to the rock's principal textural X, Y, or Z axes as indicated earlier

37

(Figure 2.5). Note that only one set of ceramics could be used for each run; core samples for which S-wave velocities were determined required 1 P-wave and 2 orthogonally oriented S-wave runs. The piezoelectric ceramics were mechanically damped with an epoxy-tungsten backing mixture in order to broaden the overall transducer bandwidth. The attached ceramic transducers and rock sample were then hermetically sealed in a flexible urethane to exclude the pressure vessel fluid from the rock and this assemblage was placed in the pressure vessel.

2.4.2 Measurement technique

A conventional pulse transmission technique (*Molyneux and Schmitt*, 1999, 2000) was used to obtain P and S wave velocities using longitudinally and transversely polarized piezoelectric ceramics, respectively. Briefly, the transmitting ceramic was activated by fast rise-time, 200 Volt square pulse that generated the appropriate mechanical wave. The response of the receiving ceramic was recorded at rates from 4 to 10 ns per sample depending on the digital oscilloscope used a typical final waveform trace was constructed from 100 to 500 progressively stacked records to reduce random noise. The waveform was then transferred to a computer to be stored for later transit time determination.

In each run, waveforms were acquired in increments of ~10 MPa from room pressure to 300 MPa (equivalent of ~11 km depth) and back. Pressure is applied not so much to mimic in situ conditions but to close as much of the microcrack porosity in the rocks as possible in order that the velocities are representative of the intrinsic mineralogical textures of the samples. The results from one S-wave run consisting of nearly 60 traces (Figure 2.6a) highlight the well-known decrease in pulse transit times with increasing confining pressure. The main S-wave pulse train is clearly distinguished in a section (Figure 2.6b) taken from one of the waveforms of Figure 2.6a. In this study the pulse onset was used to determine the transit time. Figure 2.6b also shows a smaller parasitic P-wave arrival that is likely produced at the edges of the transmitting ceramic when it is pulsed this arrival did not give consistent P-wave transit times and was ignored.

Velocities reported in Tables 2.2 and 2.3 are simply the ratio of the sample length determined by repeated calliper measurements at room pressure to the transit time; the uncertainty of the measurements of length and transit time will depend on the sample

---

38
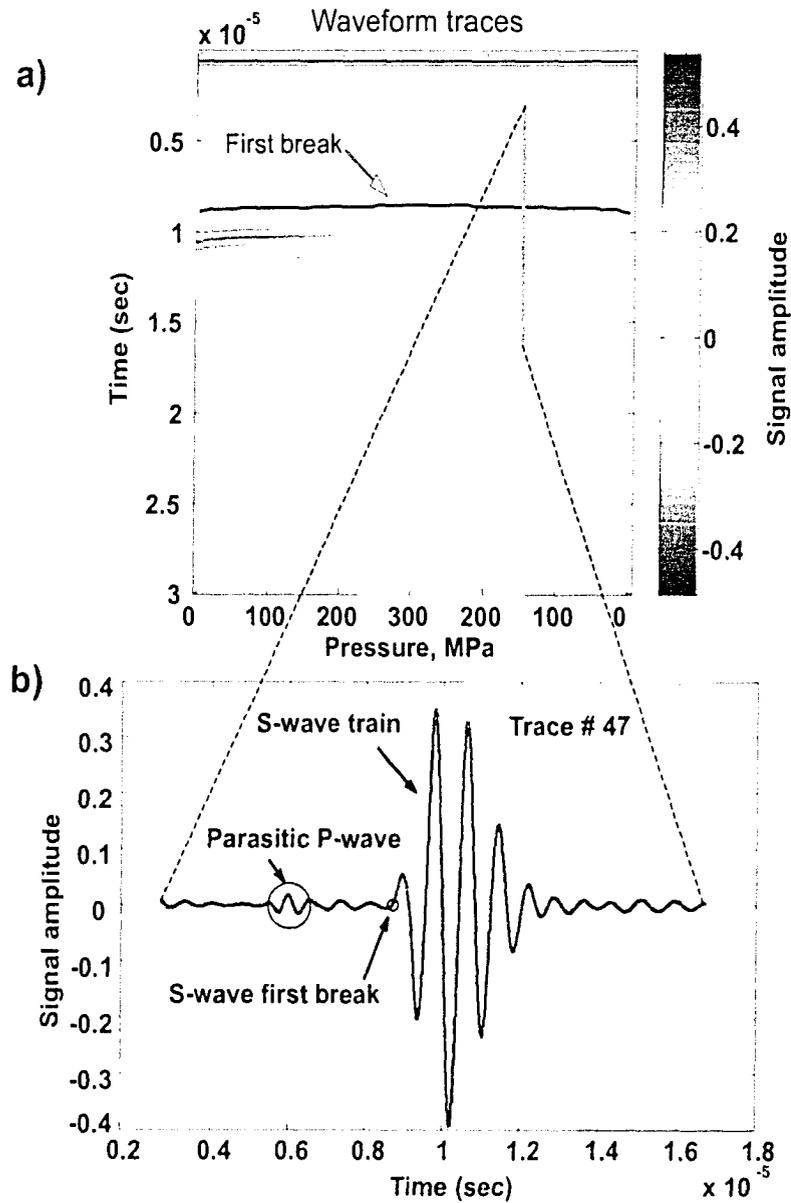
Figure 2.6: a) Representative gather of waveform traces for a shear wave velocity run at different confining pressures. Overlaid black line indicates shear-wave first break. b) Single trace from the gather with identified P- and S-waves and defined shear-wave first break.

39

length but for the worst case was always less than 1%, which is less than the variations in velocity observed for different cores with the same axial orientation from the same specimen. As has been shown by numerous authors, phase (plane-wave) velocities are determined in the short cylindrical geometry of these experiments (e.g., *Dellinger and Vernik*, 1994; *Johnston and Christensen*, 1995). The fact that phase velocities, and not ray (group) velocities are determined is important if elastic constants are to be determined, particularly for directions inclined to the symmetry axes (see *Kebaili and Schmitt*, 1997).

2.5 Results and Discussion

2.5.1 *P*-wave velocities

One example of the pressure dependence of *P*-wave velocities is shown for the entire suite of 6 cores taken from sample 93-1. Cores Z1 and Z2 both have axes normal to foliation and they show a larger increase in velocity at low pressures to approximately 150 MPa, suggesting that the planes of the microcracks within these rocks are primarily parallel to the foliation. The other four cores are cut within the plane of foliation; their compressional velocities increase nearly linearly with pressure and show little hysteresis when the pressure is decreased. This suggests that the microcrack porosity does not significantly influence these axial directions. It is important to note that the two cores cut in the Y direction show similar values of velocity while the two X cut cores do not. This discrepancy between two similarly oriented cores from the same specimen illustrates the effect that heterogeneity at the decimeter scale can have on these rocks.

Table 2.2 gives the *P*-wave velocities measured at confining pressure of 200 MPa and 300 MPa for all 147 cores, pressures considered to be sufficiently high to close most of the microcrack porosity. Note that the core sample ID in the first column in Table 2.2 was an arbitrary name given to the core when it was cut and its name may or may not correspond with the proper core axis direction relative to the sample texture given in the fourth column.

The *P*-wave anisotropy was estimated by calculating the anisotropy coefficient $A_P = (A_{max} - A_{min})/(A_{max} + A_{min}) * 200\%$ and is summarized along with the results of *P*-wave velocity measurements (at 200 MPa and 300 MPa), pressure derivatives dV/dP,

40

Table 2.2: P-wave velocities, densities and average grain cross-section sizes

Sample ID	Density, (g/cm^3)	Grain X - sec., (mm^2)	Pr./Pol. direction	Velocity @ 200MPa	Velocity @ 300MPa	$\sim dV/dP$, T = const	A, (%)
93-1-X1	2.946	0.011	XX	6.90	6.91	0.01	12.1
93-1-X2	2.982		XX	7.18	7.20	0.02	
93-1-Y1	2.930	0.007	ZZ	6.37	6.38	0.01	
93-1-Y2	2.920		ZZ	6.43	6.44	0.01	
93-1-Z1	2.953	0.006	YY	7.09	7.10	0.01	
93-1-Z2	2.941		YY	7.03	7.05	0.02	
93-2-X1	2.721	0.003	XX	6.51	6.53	0.02	10.3
93-2-X2	2.719		XX	6.54	6.55	0.01	
93-2-X3	2.717		XX	6.50	6.52	0.02	
93-2-Y1	2.720	0.007	ZZ	5.99	6.02	0.03	
93-2-Y2	2.724		ZZ	6.03	6.06	0.03	
93-2-Y3	2.718		ZZ	5.88	5.91	0.03	
93-2-Z1	2.718	0.004	YY	6.36	6.38	0.02	
93-2-Z3	2.721		YY	6.38	6.41	0.03	
93-3-X2	2.752	0.060	ZZ	5.96	5.98	0.02	6.0
93-3-Y1	2.743	0.032	XX	6.33	6.35	0.02	
93-3-Y3	2.735		XX	6.29	6.30	0.01	
93-3-Z1	2.741	0.025	YY	6.24	6.25	0.01	
93-5-X	2.994	0.005	XX	7.28	7.30	0.02	9.0
93-5-Y	2.993	0.116	ZZ	6.66	6.67	0.01	
93-5-Z	3.001	0.008	YY	7.07	7.08	0.01	
93-6-X1	2.965	0.025	XX	6.82	6.83	0.01	3.2
93-6-X2	2.978		XX	7.00	7.00	0.00	
93-6-Y1	2.987	0.051	ZZ	6.76	6.78	0.02	
93-6-Y2	2.974		ZZ	6.76	6.78	0.02	
93-6-Y3	3.026		ZZ	6.81	6.84	0.03	
93-6-Z2	2.968	0.010	YY	6.85	6.87	0.02	
93-07-X1	2.919	0.006	ZZ	6.53	6.54	0.01	9.2
93-07-X2	2.912		ZZ	6.51	6.54	0.03	
93-07-Y	2.946	0.004	XX	6.87	6.88	0.01	
93-07-Z1	2.920	0.003	YY	6.98	7.00	0.02	
93-07-Z2	2.897		YY	6.99	7.00	0.01	
93-07-Z3	2.960		YY	7.16	7.17	0.01	

Table continued on next page

41

Table continued from previous page

Sample ID	Density, (g/cm^3)	Grain X - sec., (mm^2)	Pr./Pol. direction	Velocity @ 200MPa	Velocity @ 300MPa	$\sim dV/dP$, T = const	A, (%)
93-8-X1	2.767	0.110	ZZ	5.89	5.92	0.03	8.4
93-8-Y1	2.764	0.080	YY	5.89	5.92	0.03	
93-8-Y2	2.758		YY	6.04	6.08	0.04	
93-8-Y3	2.764		YY	5.98	6.00	0.02	
93-8-Z1	2.766	0.140	XX	6.38	6.39	0.01	
93-8-Z2	2.759		XX	6.42	6.44	0.02	
93-8A-X2	2.744	35.000	-	6.22	6.24	0.02	1.9
93-8A-Y1	2.740	58.000	-	6.28	6.30	0.02	
93-8A-Y2	2.747		-	6.26	6.28	0.02	
93-8A-Y3	2.753		-	6.32	6.34	0.02	
93-9-X1	2.762	0.040	YY	6.25	6.27	0.02	8.4
93-9-X2	2.770		YY	6.52	6.54	0.02	
93-9-X3	2.799		YY	6.22	6.24	0.02	
93-9-Y1	2.788	0.110	ZZ	5.98	6.01	0.03	
93-9-Y2	2.784		ZZ	6.14	6.16	0.02	
93-9-Y3	2.797		ZZ	6.03	6.04	0.01	
93-9-Z1	2.746	0.036	XX	6.31	6.33	0.02	
93-9-Z2	2.797		XX	6.39	6.40	0.01	
93-12-X	2.712	0.190	ZZ	6.15	6.19	0.04	6.0
93-12-Y1	2.853		XX	6.53	6.57	0.04	
93-12-Y2	2.852	0.890	XX	6.22	6.25	0.03	
93-12-Z	2.707	1.510	YY	6.18	6.21	0.03	
93-13-X1	2.706	0.047	YY	6.30	6.32	0.02	9.3
93-13-X2	2.712		YY	6.32	6.34	0.02	
93-13-X3	2.712		YY	6.32	6.34	0.02	
93-13-Y1	2.723	1.730	ZZ	5.86	5.89	0.03	
93-13-Y2	2.713		ZZ	6.05	6.08	0.03	
93-13-Y3	2.714		ZZ	5.83	5.86	0.03	
93-13-Z1	2.712	0.736	XX	6.39	6.41	0.02	
93-13-Z2	2.714		XX	6.41	6.43	0.02	
93-14-X1	2.757	0.050	ZZ	5.39	5.44	0.05	24.0
93-14-X2	2.754		ZZ	5.39	5.43	0.04	
93-14-Y1	2.758	0.030	YY	6.89	6.91	0.02	
93-14-Z	2.755	0.070	XX	6.27	6.30	0.03	

Table continued on next page

42

Table continued from previous page

Sample ID	Density, (g/cm^3)	Grain X - sec., (mm^2)	Pr./Pol. direction	Velocity @ 200MPa	Velocity @ 300MPa	$\sim dV/dP$. T = const	A, (%)
93-17-X1	2.752	0.190	XX	6.36	6.39	0.03	12.2
93-17-X2	2.745		XX	6.39	6.41	0.02	
93-17-X3	2.746		XX	6.42	6.44	0.02	
93-17-Y1	2.754	0.210	YY	6.41	6.42	0.01	
93-17-Y2	2.752		YY	6.41	6.43	0.03	
93-17-Y3	2.758		YY	6.47	6.50	0.03	
93-17-Z1	2.757	0.170	ZZ	5.74	5.77	0.03	
93-17-Z2	2.757		ZZ	5.71	5.75	0.04	
93-17-Z3	2.760		ZZ	5.75	5.78	0.03	
93-18-X1	2.709	0.084	XX	5.67	5.74	0.07	6.1
93-18-X2	2.723		XX	5.77	5.80	0.03	
93-18-Y	2.722	0.037	ZZ	5.90	5.94	0.04	
93-18-Z1	2.712	0.050	YY	6.07	6.10	0.03	
93-20-X1	2.799	0.028	XX	6.11	6.15	0.04	13.2
93-20-Y1	2.869	0.069	ZZ	5.68	5.74	0.06	
93-20-Z1	2.821	0.013	YY	6.50	6.55	0.05	
VOL-I-X1	2.911	0.013	XX	7.36	7.38	0.02	15.8
VOL-I-X2	2.869		XX	7.07	7.09	0.02	
VOL-I-Y1	2.945	0.004	ZZ	6.33	6.35	0.02	
VOL-I-Y2	2.939		ZZ	6.27	6.30	0.03	
VOL-I-Z	2.889	0.060	YY	7.03	7.04	0.01	
VOL-III-X1	3.027	0.105	ZZ	6.56	6.58	0.02	14.6
VOL-III-X2	3.021		ZZ	6.51	6.55	0.04	
VOL-III-Y1	3.028	0.015	XX	7.42	7.44	0.02	
VOL-III-Y2	3.035		XX	7.50	7.51	0.01	
VOL-III-Y3	3.032		XX	7.57	7.58	0.01	
VOL-III-Z1	3.067	0.190	YY	7.26	7.27	0.01	
VOL-III-Z2	3.069		YY	7.19	7.20	0.01	
VOLC-A-X	2.618	0.280	ZZ	5.58	5.62	0.04	6.9
VOLC-A-Y	2.625	0.320	YY	5.77	5.79	0.02	
VOLC-A-Z1	2.624	0.220	XX	6.00	6.02	0.02	
VOLC-A-Z2	2.627		XX	5.81	5.84	0.03	

Table continued from previous page

Sample ID	Density, (g/cm^3)	Grain X - sec., (mm^2)	Pr./Pol. direction	Velocity @ 200MPa	Velocity @ 300MPa	$\sim dV/dP$, T = const	A, (%)
VOLC-B-X1	2.632	0.230	XX	5.84	5.88	0.04	1.7
VOLC-B-X2	2.635		XX	5.83	5.86	0.03	
VOLC-B-Y	2.631	1.680	YY	5.81	5.84	0.03	
VOLZ-B-Z	2.635	1.170	ZZ	5.74	5.78	0.04	
1a-a1	2.742	0.410	ZZ	5.88	5.90	0.02	6.2
1a-c2	2.760	0.390	XX	6.26	6.28	0.02	
2-1B	2.937	0.220	ZZ	5.75	5.80	0.05	19.6
2-2b	2.946	0.460	YY	6.71	6.74	0.03	
2-3b	2.936	0.150	XX	7.02	7.06	0.04	
3-//lin	2.773	0.120	XX	6.48	6.49	0.01	7.5
3-Llin	2.789	0.210	YY	6.39	6.41	0.02	
3-c2	2.755	0.640	ZZ	5.99	6.02	0.03	
4-c1	2.777	0.280	ZZ	5.93	5.95	0.02	9.1
4-c2	2.767	0.160	XX	6.50	6.52	0.02	
5-c1	2.746	0.370	XX	6.39	6.41	0.02	7.6
5-c2	2.745	0.350	ZZ	5.92	5.94	0.02	
6-L lin	2.796	0.090	YY	6.57	6.59	0.02	9.2
6-//lin	2.807	0.077	XX	6.54	6.55	0.01	
6-c2	2.806	0.100	ZZ	5.98	6.01	0.03	
7-//lin	2.824	0.320	XX	6.59	6.60	0.01	5.3
7-Lfoln	2.841	0.240	ZZ	6.25	6.26	0.01	
7b-Llin	2.855	0.260	YY	6.58	6.60	0.02	
8 Llin	2.814	0.170	YY	7.05	7.06	0.01	2.7
8//lin	2.800	0.180	XX	6.86	6.87	0.01	
8-c3	2.830	0.400	ZZ	6.86	6.87	0.01	
10-c2	2.831	0.140	ZZ	6.10	6.23	0.13	4.7
10//foln	2.864	0.160	XX	6.50	6.53	0.03	
11b//foln	2.705	0.029	XX	6.38	6.41	0.03	10.3
11b-c Lfoln	2.700	0.033	YY	5.83	5.90	0.07	
11b-c1 Lfoln	2.696	-	ZZ	5.70	5.78	0.08	

Table continued on next page

Table continued from previous page

Sample ID	Density, (g/cm^3)	Grain X - sec., (mm^2)	Pr./Pol. direction	Velocity @ 200MPa	Velocity @ 300MPa	$\sim dV/dP$, T = const	A, (%)
13-Llin	2.654	0.200	YY	6.38	6.39	0.01	0.2
13a-//lin	2.658	0.140	XX	6.41	6.44	0.03	
13-c2	2.653	0.130	ZZ	6.38	6.40	0.02	
15a	2.667	0.320	XX	6.33	6.35	0.02	4.2
15a-c1	2.681	0.620	ZZ	6.02	6.09	0.07	
15a-c2	2.687	0.190	YY	6.17	6.21	0.04	
16-c1	2.694	0.440	ZZ	6.44	6.47	0.03	1.4
16-c3	2.700	0.570	XX	6.55	6.56	0.01	
32-c1	2.833	0.280	ZZ	5.99	6.00	0.01	7.1
32-c2	2.823	0.330	XX	6.40	6.44	0.04	
33	2.775	0.860	YY	7.08	7.10	0.02	7.0
33-a//lin	2.943	0.460	XX	7.05	7.08	0.03	
33-c2	2.844	0.700	ZZ	6.60	6.62	0.02	
34-c2	2.710	0.450	XX	6.52	6.55	0.03	4.4
34-c4	2.692	0.470	ZZ	6.24	6.27	0.03	

where $dP = 300MPa - 200MPa$, density, and average grain size for each core sample in Table 2.1. In both collections, the rocks vary in P-wave anisotropy from quasi-isotropic to highly anisotropic. The average P-wave anisotropy for sixteen specimens from the Granite lake collection is 6.7% and reaches as high as 19.6% in sample 2. Only two plutonic samples, 13 and 16, have anisotropy coefficients less than 2% allowing them to be treated as *quasi-isotropic*. Six hand specimens with foliation but no obvious lineation were treated as having quasi transversely isotropic (TI) symmetry and samples 6, 7 and 32 displayed no anisotropy within the foliation plane and were thus considered as transversely isotropic. Five samples (2, 8, 11, 15 and 33) have significant (~ 0.3 km/sec) variations in velocities within the foliation plane and have been defined as orthorhombic. Regardless of symmetry, all the anisotropic samples except for samples 8 and 11, have a slow P-wave velocity normal to the foliation plane and a faster P velocity within the foliation plane. The average difference between the velocity within the foliation plane and normal to the

foliation plane is 0.45 km/sec.

The average P-wave anisotropy of the Nesootao Lake collection is higher than the Granite Lake samples and equals 9.5%. The variation in P-wave anisotropy, however, is similar as the collection includes both quasi-isotropic samples (e.g. 93-8A and VOLC-B) and highly anisotropic samples (e.g. 93-14 and VOL-I). Only three samples (93-6, 93-8A and VOLC-B) might be considered quasi isotropic, with $A_P < 3\%$. Four samples (93-1, 93-9, 93-13, 93-17) were identified as transversely isotropic, having P velocities normal to the foliation plane substantially lower than those within the foliation plane. The remaining twelve samples show orthorhombic symmetry with a general tendency for the compressional velocity to be lower in the direction perpendicular to the foliation plane. For these samples, velocity variations within the foliation plane are also significant, reaching a value of 0.61 km/sec in sample 93-14.

Heterogeneity within the hand specimens was studied by measuring P-wave velocities on core samples that were cut in the same direction. Most of the Nesootao Lake collection had measurements on at least two samples cut along each axis of symmetry. In several cases, the variation of compressional velocity in the same direction exceeds 4%, as in the case of P-wave propagation along the Y direction in sample 93-9. This suggests that care must be taken when interpreting the results of velocity measurements in such deformed rocks. Ideally it would be prudent to make measurements on as many cores as possible, but in reality high pressure measurements are difficult and time consuming to carry out and an appropriate balance between sampling and statistics needs to be found. In most cases, however, compressional wave velocities in the same direction are consistent and vary within the experimental uncertainty.

2.5.2 Shear wave velocities

Nine metasediments from the Nesootao Lake collection were selected to measure shear wave splitting. In all cases, two successive runs with mutually orthogonal sets of shear wave transducers were performed on core samples used for the P-wave measurements. The results from two such runs on sample 93-5 display a nearly linear increase in the V_{YZ} and V_{YX} velocities with pressure (Figure 2.8a). It is important to note that the increase in these velocities over the entire pressure range is less than 100 m/s or about 2%. The shear
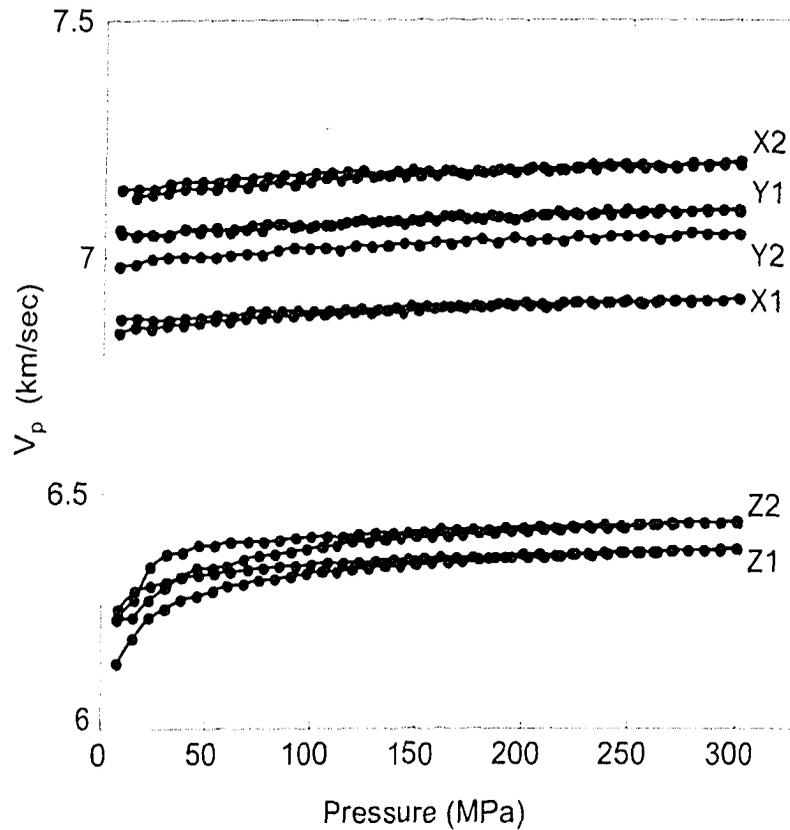
Figure 2.7: Compressional velocities versus confining pressure for sample 93-1.

wave splitting, here taken as the simple difference between the two velocities, displays a small increase with pressure (Figure 2.8b) although no change with pressure would also be allowed by the scatter in the plot together with the expected experimental uncertainty.

Results of the V_S measurements and shear wave splitting are summarized in Table 2.3. In general, the shear wave behaviour correlates with the symmetries inferred on the basis of the compressional wave anisotropy in Table 2.3. Samples 93-3, 93-07 and 93-8 display significant shear wave splitting for propagation within the foliation plane that correlates with the transversely isotropic behaviour of compressional waves (see Figure 2.2b). Samples 93-1, 93-2, 93-5, and 93-12 display substantial variations in shear wave splitting not only within the foliation plane but also normal to the foliation plane. Such shear wave behaviour was interpreted as orthorhombic and correlates well with the as-

sumption of orthorhombic P-wave symmetry for these samples. Shear wave velocities were also measured in two samples (93-6 and 93-8A) with weak compressional wave anisotropy. The measured V_S anisotropy, especially for quasi-isotropic sample 93-8A, approaches the level of experimental uncertainty in determining shear wave splitting, which was estimated to be 0.03-0.06 km/sec. It is also important to note the significant variability of shear wave splitting in the same direction compared to That for compressional waves. Measured shear wave splitting shows no significant variations with pressure.

The seismic section (Figure 2.4) suggests that the deformation structures observed at the surface may extend to depths of 10-km or more. As this is a significant fraction of the overall crustal thickness, it is worthwhile to consider what time delays could be incurred by split shear waves traversing a section of the crust since this value may be significant in certain terrains (*Godfrey et al.*, 2000; *Okaya and Christensen*, 2002). The average shear wave splitting within the foliation plane of the measured metasediments and metavolcanics is 0.27 km/sec. The estimated shear wave splitting of teleseismic SKS waves travelling parallel to the foliation plane though a 10 km thick slab of metasedimentary-metavolcanic rocks in the midcrust section might reach a value of 0.2 sec and significantly contribute to the overall observed shear wave splitting of SKS waves (*Savage*, 1999; *Godfrey et al.*, 2000).

2.5.3 Source of anisotropy

Most of the studied metasediments from both collections show significant P and S velocity anisotropy (Figure 2.9a). Seismic anisotropy in metamorphic rocks is usually attributed to the presence of microcracks and intrinsic anisotropy due to the lattice preferred orientation of constituent anisotropic minerals. We analyze the sources of seismic anisotropy from an analysis of velocity-pressure dependence curves. In our study, neither P- nor S-waves (Figures 2.7 and 2.8) display significantly higher velocity gradients with pressure low confining pressure and both display quasi-linear behaviour at confining pressures higher than 150 MPa, which is lower than the onset of linear behavior usually estimated in literature (200-300 MPa) (*Kern and Fakhimi*, 1975; *Kern*, 1978; *Siegesmund et al.*, 1989; *Burlini and Fountain*, 1993; *Ji et al.*, 1993; *Ji and Salisbury*, 1993). The absence of the high velocity gradients at low confining pressure that are usually attributed to the

48

Table 2.3: Shear-wave velocities and shear-wave splitting at 200MPa and 300MPa and room temperature

Sample ID	Pr./Pl. dir	V_S @ 200MPa	V_S @ 300MPa	Pr./Pl. dir	V_S @ 200MPa	V_S @ 300MPa	δV_S @ 200MPa	δV_S @ 300MPa
93-1-X1	XZ	4.28	4.28	XY	4.40	4.45	0.12	0.17
93-1-X2	XZ	4.26	4.27	XY	4.30	4.32	0.04	0.05
93-1-Y1	ZY	4.19	4.27	ZX	3.81	3.82	0.38	0.45
93-1-Y2	ZY	4.17	4.18	ZX	3.88	3.89	0.29	0.29
93-1-Z1	YZ	4.16	4.16	YX	4.41	4.41	0.25	0.25
93-1-Z2	YZ	3.96	3.97	YX	4.53	4.54	0.57	0.57
93-2-X1	XY	3.77	3.78	XZ	4.15	4.18	0.38	0.40
93-2-X2	XY	3.94	3.95	XZ	3.97	3.97	0.03	0.02
93-2-X3	XY	4.27	4.31	XZ	3.52	3.54	0.75	0.77
93-2-Y1	ZX	3.69	3.76	ZY	3.84	3.88	0.15	0.12
93-2-Y2	ZX	3.50	3.51	ZY	3.66	3.77	0.16	0.26
93-2-Y3	ZX	3.71	3.75	ZY	3.72	3.77	0.01	0.02
93-2-Z1	YX	3.51	3.54	YZ	3.92	3.95	0.41	0.41
93-2-Z3	YX	3.58	3.63	YZ	3.99	4.08	0.41	0.45
93-3-X2	ZX	3.61	3.67	ZY	3.73	3.77	0.12	0.10
93-3-Y1	XZ	3.61	3.62	XY	4.07	4.11	0.46	0.49
93-3-Y3	XZ	3.75	3.76	XY	3.92	3.93	0.17	0.17
93-3-Z1	YZ	3.92	3.93	YX	3.98	4.02	0.06	0.09
93-5-X	XY	4.21	4.22	XZ	4.01	4.02	0.20	0.20
93-5-Y	ZX	4.24	4.29	ZY	4.29	4.29	0.05	0.00
93-5-Z	YX	4.04	4.06	YZ	4.61	4.63	0.57	0.57
93-6-X1	XY	4.20	4.24	XZ	4.66	4.80	0.46	0.56
93-6-X2	XY	4.00	4.02	XZ	4.11	4.15	0.11	0.13
93-6-Y1	ZX	4.16	4.20	ZY	4.23	4.25	0.07	0.05
93-6-Y2	ZX	4.13	4.13	ZY	-	-	-	-
93-6-Y3	ZX	3.99	4.00	ZY	4.06	4.07	0.07	0.07
93-6-Z2	YX	4.15	4.23	YZ	4.01	4.02	0.14	0.21
93-07-X1	ZX	3.94	3.96	ZY	3.86	3.87	0.08	0.09
93-07-X2	ZX	3.87	3.88	ZY	3.87	3.87	0.00	0.01
93-07-Y	XZ	3.77	3.78	XY	4.05	4.08	0.28	0.30
93-07-Z1	YX	3.91	3.91	YZ	4.12	4.13	0.21	0.22
93-07-Z2	YX	4.11	4.12	YZ	-	-	-	-
93-07-Z3	YX	4.10	4.12	YZ	-	-	-	-

Table continued on next page

49

Table continued from previous page

Sample ID	Pr./Pl. dir	V_S @ 200MPa	V_S @ 300MPa	Pr./Pl. dir	V_S @ 200MPa	V_S @ 300MPa	δV_S @ 200MPa	δV_S @ 300MPa
93-8A-Z1	-	3.70	3.73	-	3.75	3.77	0.05	0.04
93-9-X1	YX	3.46	3.48	YZ	3.61	3.61	0.15	0.13
93-9-X2	YX	3.66	3.67	YZ	3.66	3.67	0.00	0.00
93-9-X3	YX	3.32	3.32	YZ	3.40	3.42	0.08	0.10
93-9-Y1	ZX	3.31	3.32	ZY	3.31	3.33	0.00	0.01
93-9-Z1	XY	3.72	3.72	XZ	3.76	3.76	0.04	0.04
93-12-X	ZX	3.33	3.34	ZY	-	-	-	-
93-12-Y2	XY	3.36	3.37	XZ	3.54	3.56	0.18	0.19
93-12-Z	YX	3.37	3.38	YZ	3.49	3.50	0.12	0.12

closure of pores, cracks and microfractures in dry rocks (Birch, 1960; Kern, 1978) suggests that cracks may play only a minor role in our observations. This won't also be consistent with the weak hysteresis in the velocities when the measurements are made in the down pressure cycle.

The stronger velocity gradient for P-waves propagating normal to foliation (Figure 2.7) indicates that whatever microcracks are present in this sample are oriented sub-parallel to the foliation plane. Therefore, preferentially oriented microcracks might contribute to the difference in velocities of seismic waves propagating parallel and perpendicular to the foliation plain at confining pressure less than 100 MPa (equivalent to ~ 3.5 km depth). Anisotropy of P and S velocities at 300 MPa or higher, however, may be attributed solely to the preferred orientation of constituent anisotropic minerals.

The absence of quantitative information on the textural properties of each mineralogical species makes direct correlation of observed seismic anisotropy to the elasticity of polycrystalline aggregates of constituent minerals ambiguous. Some correlations, however, may be suggested on the basis of the mineralogical composition of the metasediments and metavolcanics (Figure 2.9). For example, the presence of highly anisotropic mica minerals significantly contributes to the seismic anisotropy in felsic samples and can be directly identified as a source of seismic anisotropy in sample 93-14, which has the maximum observed compressional wave anisotropy ($A_P = 24\%$)(Figure 2.9a). In the samples of intermediate to basic composition, seismic anisotropy is likely corre-
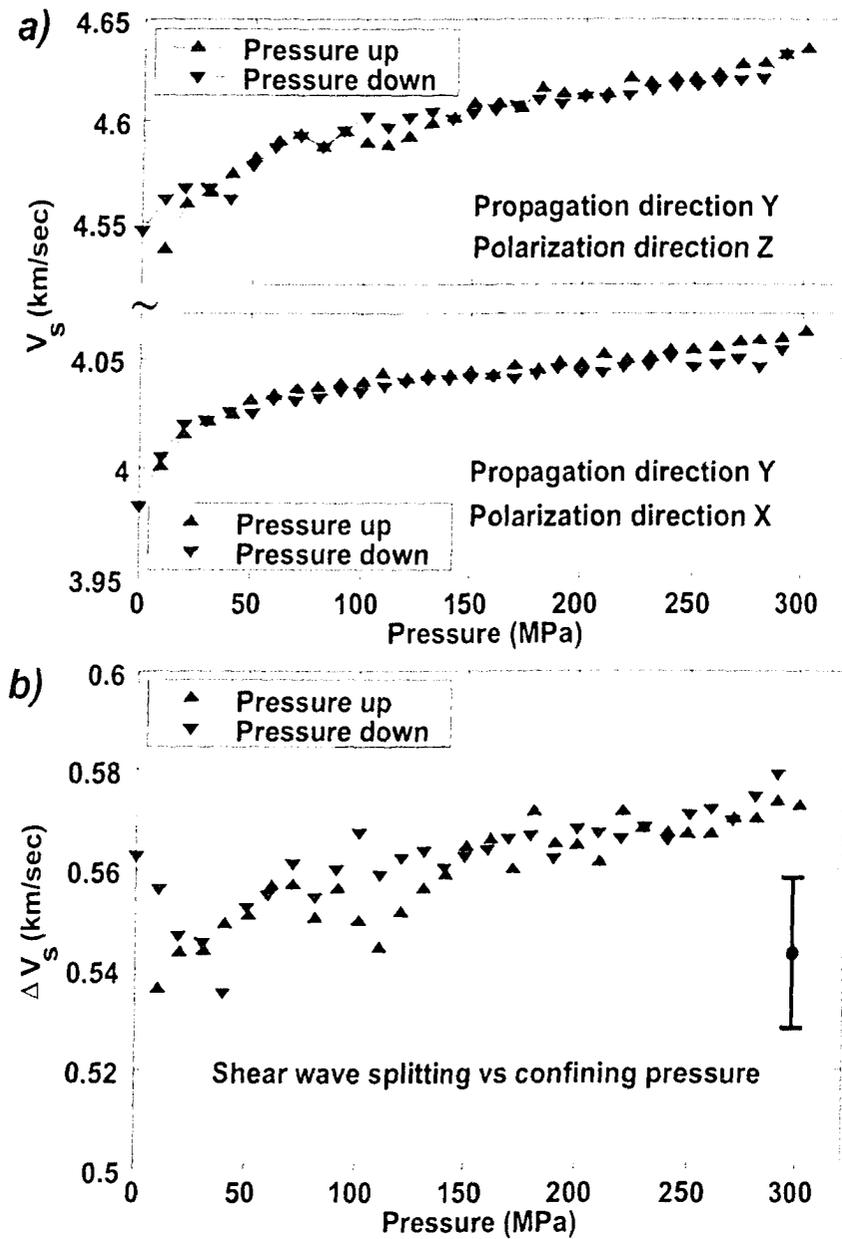
Figure 2.8: *a)* Shear wave velocity versus confining pressure measured along the *Y* direction in metavolcanic sample 93-5. *b)* Shear wave splitting versus confining pressure along the *Y*-axis of sample 93-5. Bar indicates the comparative range of the estimated uncertainty in the shear wave velocity measurements.

51

lated with the abundance of hornblende, which is highly anisotropic (Figure 2.9b). Plagioclase, quartz and pyroxenes do not correlate directly with the observed P- and S-wave anisotropy. The absence of a direct correlation between elastic anisotropy and the modal abundance of these highly anisotropic minerals indicates that the degree of lattice preferred orientation is the most important factor in the development of significant anisotropy. Constructive and destructive interference between different anisotropic minerals might also contribute to the overall observed anisotropy. Detailed quantitative study of the texture of major constituent minerals is needed for proper correlation of the influence of each mineralogical species on the seismic anisotropy of complex multiphase metasedimentary and metavolcanic rocks.

2.5.4 Elastic properties

Elastic stiffnesses C_{ij} were calculated directly from the observed phase velocities (Equations (2.12)) and the average values of the stiffnesses are given in Table 2.4. The utility of expressing the elastic properties in terms of stiffnesses instead of velocities and densities is that the symmetry of the material is more readily apparent. Each of the samples is assigned a symmetry. Samples in which the elastic moduli differ by less than the expected levels of uncertainty are assumed to be quasi-isotropic. Those in which $C_{11} \sim C_{22} \neq C_{33}$ and $C_{44} \sim C_{55} \neq C_{66}$ are considered to have transversely isotropic symmetry, and those with $C_{11} \neq C_{22} \neq C_{33}$ and $C_{44} \neq C_{55} \neq C_{66}$ are orthorhombic.

As can be seen in Table 2.4, elastic moduli vary significantly from sample to sample. One useful exercise is to find the simple average of each of these elastic coefficients. The simple average has some physical significance because it represents the elastic properties of a hypothetical formation composed of equal volumes of each of the samples measured, assumed that the samples are identically aligned with respect to the X, Y and Z axes. Under this assumption the simple average is identical to the Voigt bound (e.g. Watt et al., 1976) and as such, would provide the upper bound to the allowed anisotropy. In reality, the foliations of the rocks in the field are not as well aligned and the real average, if it could be determined, would be more isotropic. However, as indicated in Figure 2.3b, the foliations are regionally consistent.

Simple averages were calculated for both suites individually and are presented to-

52

Table 2.4: Average elastic stiffnesses (GPa) and anisotropic parameters

Polar. ID	XX C_{11}	YY C_{22}	ZZ C_{33}	ZY,YZ C_{44}	ZX,XZ C_{55}	XY,YX C_{66}	Anis. parameters $\varepsilon^{(1)}$	$\varepsilon^{(2)}$	$\gamma^{(1)}$	$\gamma^{(2)}$	ρ_{ave} g/cm^3	Elst. sym
93-1	148	148	120	50	49	58	0.11	0.11	0.09	0.07	2.945	TI
93-2	116	111	98	41	39	40	0.07	0.09	0.02	-0.01	2.720	ORT
93-3	110	107	98	41	37	44	0.04	0.06	0.09	0.04	2.743	ORT
93-5	160	133	150	60	52	51	-0.06	0.03	0.00	-0.07	2.996	ORT
93-6	142	140	139	51	54	52	0.01	0.01	-0.03	0.01	2.983	qISO
93-7	139	146	125	46	44	48	0.08	0.06	0.05	0.03	2.926	ORT
93-8	114	99	97	-	-	-	0.01	0.09	-	-	2.763	ORT
93-8a	107	109	111	39	-	-	-0.01	-0.02	-	-	2.748	qISO
93-9	112	112	103	34	35	35	0.04	0.05	0.00	0.01	2.780	TI
93-12	117	104	104	33	33	32	0.00	0.06	-0.02	-0.02	2.781	ORT
93-13	112	109	96	-	-	-	0.07	0.08	-	-	2.713	TI
93-14	109	132	81	-	-	-	0.31	0.17	-	-	2.756	ORT
93-17	113	115	92	-	-	-	0.12	0.12	-	-	2.753	TI
93-18	90	101	96	-	-	-	0.03	-0.03	-	-	2.716	ORT
93-20	106	121	95	-	-	-	0.14	0.06	-	-	2.830	ORT
VOL-I	151	143	118	-	-	-	0.11	0.14	-	-	2.911	ORT
VOL-III	171	161	130	-	-	-	0.12	0.16	-	-	3.040	ORT
VOLC-A	92	88	83	-	-	-	0.03	0.06	-	-	2.623	ORT
VOLC-B	91	90	88	-	-	-	0.01	0.02	-	-	2.633	qISO
1	109	-	95	-	-	-	-	0.07	-	-	2.751	TI
2	146	134	99	-	-	-	0.18	0.24	-	-	2.940	ORT
3	117	115	100	-	-	-	0.07	0.08	-	-	2.772	TI
4	118	-	98	-	-	-	-	0.10	-	-	2.772	TI
5	113	-	97	-	-	-	-	0.08	-	-	2.745	TI
6	120	121	101	-	-	-	0.10	0.09	-	-	2.803	TI
7	123	124	111	-	-	-	0.06	0.05	-	-	2.840	TI
8	132	140	134	-	-	-	0.03	-0.01	-	-	2.814	ORT
10	122	-	110	-	-	-	-	0.06	-	-	2.847	TI
11b	111	94	90	-	-	-	0.02	0.12	-	-	2.700	ORT
13	110	108	109	-	-	-	0.00	0.01	-	-	2.655	qISO
15a	108	104	99	-	-	-	0.02	0.04	-	-	2.678	ORT
16	116	-	113	-	-	-	-	0.02	-	-	2.697	qISO
32	117	-	102	-	-	-	0.07	-	-	-	2.828	TI
33	148	140	125	-	-	-	0.06	0.09	-	-	2.854	ORT
34	116	-	106	-	-	-	-	0.05	-	-	2.701	TI

Table 2.5: Average elastic stiffnesses with standard deviation, (GPa)

Mean value	C_{11}	STD	C_{22}	STD	C_{33}	STD	C_{44}	STD	C_{55}	STD	C_{66}	STD
Nesootao Lake	121	24	119	21	106	4	44	9	43	8	45	9
Granite Lake	120	12	120	16	106	11	-	-	-	-	-	-

gether with the standard deviations for each elastic constant at the bottom of Table 2.5. A surprising result is that both averages are nearly the same. Furthermore, the overall elastic stiffnesses tends to be transversely isotropic.

The standard deviations, too, are of interest. Heterogeneity within the crust has for the most part been ignored in seismological studies. However, heterogeneity, or more precisely the relative dimensional scale of heterogeneity with respect to the wavelength of interrogating seismic waves can have some important influences on the observed seismic velocities (see *Molyneux and Schmitt*, 1999).

2.6 Conclusions

Two representative collections of textured metamorphic rocks with compositions that vary from felsic to basic have been studied to determine the elastic behaviour of deformed low-grade metamorphic rocks. Measurements of the P- and S-wave velocities and shear wave splitting indicate that samples of the metasediments and metavolcanics vary from the moderately to highly anisotropic with an average P-wave anisotropy of 6.7% for the Granite Lake collection and 9.5% for the Nesootao Lake collection, with individual samples displaying quasi-isotropic, transversely isotropic or orthorhombic elastic symmetry. P-wave symmetry was correlated with V_s measurements and shear wave splitting to reinforces these inferences on the elastic symmetry.

The observed seismic anisotropy is directly related to the visible fabric. The velocities in most samples do not show large increases with pressure above 150 MPa, indicating that most of the cracks are closed at lower pressures. At high confining pressures the observed P- and S-wave anisotropy is caused by lattice preferred orientation of constituent anisotropic minerals. The presence of mica and hornblende influence the level of seismic anisotropy for felsic and basic metasediments, respectively. There is no direct evidence for a correlation of the seismic anisotropy with the volumetric abundance of quartz, pla-

54
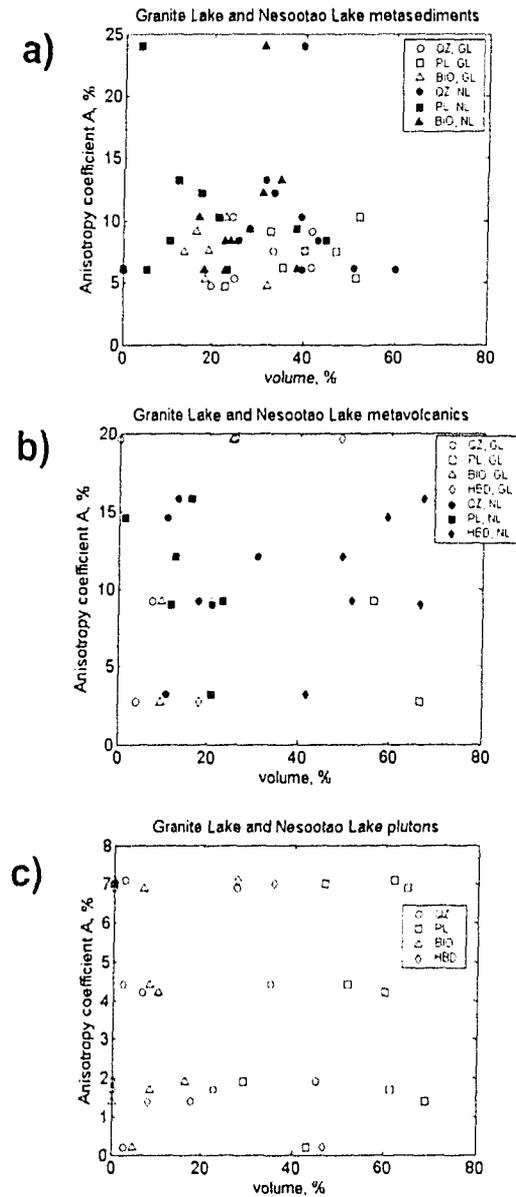
Figure 2.9: Mineral abundance of investigated rocks is plotted versus anisotropic coefficients for *a)* metasediments; *b)* metavolcanics; *c)* plutons (QZ - quartz, PL - plagioclase, BIO - biotite, HBD - hornblende, GL stands for Granite Lake collections, NL for Nesootao Lake).

55

P-wave velocity vs. density
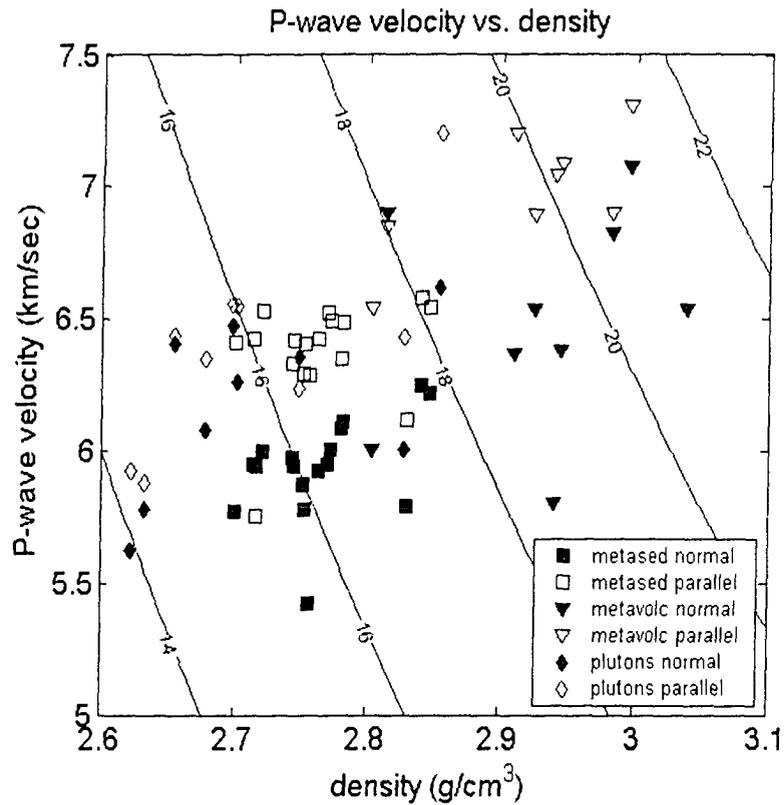
Figure 2.10: Compressional wave velocity versus density for measured samples. Contours of constant acoustic impedance provide mapping of obtained results on acoustic impedance scale. Velocity normal and parallel to foliation plotted to reflect effect of anisotropy.

gioclase or pyroxenes.

The experimentally observed velocity and density contrasts in these anisotropic rocks (more than 10-16% seismic anisotropy) may influence seismic reflectivity (*Jones and Nur*, 1982; *Kern and Wenk*, 1990; *Siegesmund and Kern*, 1990) and should be taken into consideration in seismological studies of the reflectivity of ductile shear zone of the FFB. While one could construct a model of the velocity structure in the Flin Flon Belt using the results of these velocity measurements, it is likely that this model would not be very representative of the real situation given the range and heterogeneity of elastic properties, densities and velocities within any given suite of rocks (Figure 2.10). That is, it would be difficult

to unambiguously explain the strong seismic reflectivity seen in Figure 2.4 on the basis of the present measurements alone. Indeed, while one may want to make an interpretation that the reflectivity is simply due to impedance contrasts between the plutons and the other metamorphosed rocks, this interpretation is difficult to make given that the elastic properties of the plutons do not noticeably differ from the other rocks (Figure 2.10). The best way to study the reflectivity in detail would be to acquire a continuous section of the rocks by drilling and to carry out wellbore seismic and sonic logging experiments throughout the zone to better understand where exactly the reflections are coming from. The relatively shallow depth of the reflectors beneath the pluton in Figure 2.4 makes this area a good potential target for scientific drilling.

Finally, although the measurements presented are already relatively extensive, the results could be greatly improved by additional off-symmetry axis measurements of P- and S-wave velocities. These would be useful to constrain the behaviour outside of the symmetry planes and to calculate the off-diagonal elastic stiffnesses. Such information may be particularly important for the interpretation and future reprocessing of active source seismic data given that lineations in the region dip at angles near 45°. Future work may involve the ultrasonic array methods developed in *Mah and Schmitt* (2003) to test whether even more complex elastic symmetries than orthorhombic are required to fully describe the elasticity of deformed metamorphic rocks.

Chapter 3

Elasticity of polycrystalline aggregates of orthotropic symmetry: application to olivine texture

[1]

The elasticity of a textured olivine polycrystalline aggregate is investigated on the basis of the Voigt, the Reuss, and the Geometric Mean Averaging (GMA) procedure. To account for the aggregate textural properties the orientation distribution function (ODF) of the hypothetical texture of polycrystalline aggregate of orthotropic symmetry is developed and incorporated into the averaging. The Voigt (upper) and the Reuss (lower) bounds are generally accepted as limits of a range of values for elastic constants of textured aggregate. The Geometric Mean Averaging technique is employed to provide a set of elastic constants that are independent on the initial averaging assumptions. This averaging procedure is applied to the monomineralic olivine aggregate with hypothetical texture of orthotropic symmetry that reflects one of the main types of texture developed in naturally deformed mantle peridotites. The effect of the averaging assumptions on the elastic velocities and anisotropy is discussed. Elastic velocities and intrinsic anisotropy derived from the hypothetical texture are compared to experimental ultrasonic velocities of peridotites reported in the literature.

---

[1]Different parts of this Chapter have been presented at EGS 2001, AGU 2001, 2003 annual meetings, and CGU/AGU/SEG/EEGS 2004 joint assembly.

3.1 Introduction

The investigation of the elasticity of polycrystalline aggregates has a long history. Since the work of Voigt (1928) and Reuss (1929) based on assumptions of uniform strain and stress within the isotropic polycrystalline aggregate, respectively, more sophisticated techniques have emerged. The self-consistent approach of Kröner (1958) and the variational approach of Hashin and Shtrikman (1962a,b) have been incorporated by Zeller and Dederichs (1973) and Kröner (1977) into a generalized effective medium theory and since have been successfully applied mainly to isotropic polycrystalline aggregates composed of weakly anisotropic cubic crystals, usually metals.

If an aggregate is textured its elastic properties will deviate from isotropy. In order to investigate the elasticity of a textured polycrystalline aggregate detailed knowledge of the crystallographic orientation of the constituent minerals relative to a convenient reference frame is necessary. This information can quantitatively be provided by the orientation distribution function (ODF) of Viglin (1960). Roe (1965) and Bunge (1982) described application of the ODF in the Voigt averaging procedure to calculate elastic constants of textured polycrystalline in the stiffness domain. Similarly, results of the Reuss approximation can be produced if the averaging is performed in the compliance domain. Kneer (1965) incorporated the ODF into self-consistent approximation of Kröner (1958). Morris (1970, 1971) further developed this technique and Humbert and Diz (1991) and Diz and Humbert (1992) discussed its applications to the elasticity of polycrystals. It has been mentioned by these authors that specific care has to be taken in this types of calculations to provide convergence of the solution.

An elegant approach to estimate the elastic properties of an aggregate that reduces complicated calculations and the restrictive assumptions has been proposed by Aleksandrov and Aizenberg (1966). They modified the volume weighted averaging procedure of Voigt (Voigt, 1928) or Reuss (Reuss, 1929) to produce a set of elastic constants that is independent of the averaging domain employed, i.e. the same answer is obtained regardless of whether stiffnesses or compliances are averaged. This concept was further developed by Morawiec (1989) and later by Matthies and Humbert (1993) to average physical properties described by a fourth-rank tensor. This technique is referred to as Geometric Mean

Averaging (GMA) (*Matthies and Humbert*, 1993) and is used here for the first time to our knowledge to estimate the elasticity of textured aggregate with defined symmetry, i.e. aggregate of orthotropic symmetry composed of orthorhombic symmetry crystals.

In Geophysics, application of the above mentioned averaging techniques to geomaterials is usually complicated (e.g. *Wenk*, 1985). The difficulty in modelling rocks originates from the complexity of textured multiphase polycrystalline aggregates composed of a variety of low-symmetry minerals. In geosciences the ODF averaging procedure has mainly been mainly applied to monomineralic aggregates, for example *Johnson and Wenk* (1986) and *Wenk et al.* (1988) estimated the elastic properties of an aggregate with orthorhombic symmetry composed of trigonal calcite using the Voigt averaging scheme.

In order to model the elasticity of textured olivine aggregates the Voigt averaging technique has usually been used (e.g. *Crosson and Lin*, 1971; *Christensen*, 1971; *Babuška*, 1972). Application of different averaging techniques to geomaterials is one of the objectives of this study and presently a topic of investigation in Rock Physics (e.g. *Kocks et al.*, 1998). *Mainprice and Humbert* (1994) applied several averaging techniques, including the GMA and the self-consistent approach, to calculate compressional and shear velocities of textured plagioclase feldspar and biotite aggregates. It is unclear from the paper if any assumption on the symmetry of the aggregate' elasticity has been incorporated into the GMA procedure. These authors compared velocities modelled by different techniques with experimental measurements and concluded that the GMA provides the closest results to experimental data among simple averaging techniques.

The fabrics of ultramafic rocks in general, and peridotites in particular, display symmetries that are close to transversely isotropic, orthorhombic or monoclinic (*Babuška and Cara*, 1991). In this Chapter the elasticity of the aggregate expressing orthotropic statistical symmetry is considered. Here the term *orthotropic* instead of *orthorhombic* is used. The term *orthotropy* reflects a statistical sample symmetry consistent with three mutually orthogonal symmetry planes, and three orthotropic two fold rotation axes defined by intersection of three mirror symmetry planes (*Kocks et al.*, 1998). Orthotropic symmetry holds in a statistical sense within the medium, not for every point, and is therefore more suitable for description of overall aggregate symmetry. For orthotropic symmetry the number of the unknown elastic constants is nine (the same as for orthorhombic symmetry). In

practice, the nine independent elastic constants are usually unknown. This complicates a model compared to an isotropic medium with two unknown. The orthotropic medium, however, is still a simplified approximation if compared to twenty-one unknown elastic constants for the most general case of triclinic anisotropy with no symmetry. Seismological observations of elastic anisotropy interpreted using orthotropic approximation may provide a more exact characterization of elastic wave behavior by better fitting data and assisting proper interpretation. Orthotropic symmetry also provides the best characterization of elastic wave behaviour when rocks exhibit foliation and lineation (see Chapter 2 for discussion).

The main purpose of this Chapter is to investigate the effect of different averaging techniques on modelling the elasticity of polycrystalline aggregates of orthotropic symmetry. The polycrystalline aggregate considerate here composed solely of Mg-rich upper mantle olivine, $(Mg_{1-x}Fe_x)_2SiO_4$ where $x \approx 0.1$, which is elastically orthorhombic. The algorithm of averaging orthotropic aggregate composed of orthorhombic crystals based on the standard the Voigt and the Reuss averages is developed following a *Bunge* (1982) style of ODF normalization. Further, to avoid generalizing assumptions of the Voigt or the Reuss averages the GMA has been developed for this orthotropic-orthorhombic case and incorporated into the ODF averaging procedure. Although application of the ODF to model the elasticity of polycrystalline olivine aggregate is not new (the Voigt approximation has been used before, e.g. *Ben Ismail and Mainprice* (1998)), the investigation of the effect of different approximations, particularly development of a GMA solution to this problem, provides new insights.

Earlier studies in which the olivine texture in dunite and peridotites is described are reviewed. On the basis of this information, a hypothetical texture representative of one type of naturally deformed peridotites, is constructed for a olivine aggregate with a strong lattice preferred orientation (LPO) and quantitatively described by the ODF of orthotropic symmetry. The elastic constants and corresponding elastic wave velocities for this olivine texture are calculated and discussed in light of comparison to the laboratory measurements of the elastic velocities of peridotites.

3.2 Elasticity of polycrystalline aggregate: averaging procedure

In order to evaluate the intrinsic elastic properties of the polycrystalline aggregate, knowledge about the single crystal elastic constants, the aggregate density and the distribution of the orientations of the crystals in the aggregate are required. In this Section averaging procedures used to obtain the elasticity of textured polycrystalline aggregate are discussed. Quantitative description of the crystals orientations within the aggregate (i.e. the texture) is provided through the orientation distribution function $f(g)$ (See Appendix D for definitions and details on the ODF). The reader should refer to the monograph by *Bunge* (1982) for extensive and detailed description of the ODF. In the present study, his notation and normalization are adopted directly.

The relationship between stress and strain in the single crystal in the linear regime of small deformations is described through the generalized Hooke's Law and represented by the forth-rank tensor of elastic stiffnesses C_{ijkl}, where $i, j, k, l = 1, 2, 3$. The inverse of the elastic stiffnesses are the elastic compliances S_{ijkl}, where $i, j, k, l = 1, 2, 3$, relate acquired stain to applied stress in the crystal. Naturally, $[C_{ijkl}]^{-1} = [S_{ijkl}]$.

When crystals comprise a polycrystalline aggregate, the stresses applied to the aggregate are related to its strain via the elastic stiffnesses of the aggregate $\tilde{C}_{ijkl}$. Corresponding elastic compliances of the aggregate are $[\tilde{S}_{ijkl}] = [\tilde{C}_{ijkl}]^{-1}$. These values, also knows as the *effective* elastic constants, can in principle be measured experimentally. When averaging procedures are used, the assumption is made that elastic constants of the aggregate are equal to the volume weighted average values of elastic constants of constituent minerals $\tilde{C}_{ijkl} = \overline{C}_{ijkl}$. If the aggregate is textured, the averaged elastic constants are also appropriately weighted by the textural properties, this weighting is quantitatively described by the ODF. In the case of the Voigt assumption of uniform strain throughout the aggregate, the average value of elastic constants is calculated as (e.g. *Kneer*, 1965):

$$\overline{C}_{ijkl}^{V} = \oint C_{ijkl} f(g)\, dg \tag{3.1}$$

where integration is carried out over the orientation domain $g = (\varphi_1, \Phi, \varphi_2)$ composed the three Euler angles (cf. *Morse and Feshbach*, 1953), the ODF is discussed in more detail in Appendix D. The choice of the integration symbol employed here is intended

to provide consistency with notations of *Bunge* (1982). Similarly, to obtain elastic compliances of the aggregate, the compliances of the constituent minerals are averaged in the identical procedure fulfilling the Reuss approximation of uniform stress:

$$\overline{S}^{R}_{ijkl} = \oint S_{ijkl} f(g)\, dg \tag{3.2}$$

In practice, the averaging procedure in equation (3.1) is written as:

$$\overline{C}^{V}_{i} = \sum_{j} \overline{a}^{V}_{ij} C_{j} \tag{3.3}$$

where $\overline{C}^{V}_{i}$, $i = 1, 2, ..., m$ are averaged symmetry-dependent elastic stiffnesses of the aggregate using the Voigt notations (e.g Nye, 1990), the C_{j}, $j = 1, 2, ... n$ are elastic stiffnesses of the single crystal, and the $\overline{a}^{V}_{ij}$ are averaging constants that contain information about statistical symmetry of the aggregate and its textural properties. These $\overline{a}^{V}_{ij}$ are determined from the ODF or theoretically derived for the case of isotropic aggregate (*Voigt*, 1928).

Equation (3.3) can be re-written in a matrix form (See Appendix C for description of an isotropic Voigt and Reuss averaging matrixes):

$$\overline{C}^{V} = \overline{a}^{V} C \tag{3.4}$$

where $\overline{C}^{V}$ is a vector of length $[m]$, composed of the m elastic stiffnesses of the aggregate in the Voigt approximation, C is vector of length $[n]$, corresponding to the n independent elastic stiffnesses of the single crystal, and $\overline{a}^{V}$ is the Voigt $[m \times n]$ averaging matrix. In the present case of orthotropic aggregate composed of orthorhombic crystals $n = m \equiv 9$ and the averaging matrix $\overline{a}^{V}$ is a square matrix of size $[9 \times 9]$.

Corresponding to Equation 3.2, the Reuss assumption (*Reuss*, 1929) of uniform stress is fulfilled if instead the compliances S are averaged:

$$\overline{S}^{R} = \overline{a}^{R} S \tag{3.5}$$

where similarly S is vector of length $[9]$ of independent elastic compliances of the single crystal, $\overline{a}^{R}$ is the Reuss $[9 \times 9]$ averaging matrix, and $\overline{S}^{R}$ is a resulting vector of nine elastic compliances of aggregate in the Reuss approximation.

To compare results of these two averages either the Voigt stiffnesses or the Reuss compliances must be inverted. A complication with the application of either the Voigt or the Reuss averages is that $\overline{C}^R \neq \overline{C}^V$ and $\overline{S}^V \neq \overline{S}^R$. That is, the Voigt and the Reuss averages, generally accepted to provide respectively the upper and lower bounds to the aggregate elastic constants, diverge from one other with an increase in anisotropy of the single crystal. Usually one of the bounding assumption is chosen to be used in the averaging, depending on whether experimental results are presumed to be closer to the Voigt or the Reuss solution. In the absence of the experimental constrains, justification of specific averaging assumption to be used is usually cumbersome (for discussion see *Kumazawa*, 1969).

In order to overcome the difficulty of choosing appropriate averaging assumption *Aleksandrov and Aizenberg* (1966) suggested a modified averaging procedure that in addition to the general averaging assumption $\tilde{C}_{ijkl} = \overline{C}_{ijkl}$, also accommodates the physical requirement of the invertibility of aggregate elastic stiffnesses $\overline{C}_{ijkl}$ into the corresponding elastic compliances $\overline{S}_{ijkl}$, i.e. $[\overline{C}_{ijkl}]^{-1} = [\overline{S}_{ijkl}]$.

The details of *Aleksandrov and Aizenberg* (1966) idea, which underly much of the current averaging techniques but are perhaps not always properly acknowledged, are described here retaining these authors' original notation for consistency. Assume the unknown physical properties of the aggregate are $\overline{R}_i$, $i = 1, 2, ..., N$. The inverse of these properties defined as $\overline{Q}_i$, $i = 1, 2, ..., N$ exist, and $\overline{R}_i^{-1} \equiv \overline{Q}_i$. The averaging operator $\Re_\phi(R_j)$ contains an averaging function $\phi(R_j)$, which has its inverse function ϕ^{-1}, and R_j, $j = 1, 2, ..., N$ are corresponding physical properties of the constituent minerals (their inverse $Q_j = R_j^{-1}$). The averaged physical properties can then be written in the averaging operator form:

$$\overline{R}_i = \Re_\phi(R_j) = \phi^{-1}\left\{\sum_j \overline{a}_{ij}\, \phi(R_j)\right\} \tag{3.6}$$

where $\overline{a}_{ij}$ are averaging constants that contain an information about statistical symmetry of the aggregate and its textural properties. *Aleksandrov and Aizenberg* (1966) proved that the averaging function that allows the assumption $\overline{R}_i^{-1} = \overline{Q}_i$ to be satisfied has a form $\varphi = \alpha \ln R_j + \beta$, for any $\alpha \neq 0$ and β, and the averaging operator can then be

written:

$$\overline{R}_i = \Re_{\phi=\alpha ln R+\beta}(R_j) = \Re_{\phi=ln R}(R_j) = exp\left[\sum_j p_{ij}\,ln(R_j)\right] = \prod_j R_j^{p_{ij}} \qquad (3.7)$$

Aleksandrov and Aizenberg (1966) applied this technique to calculate the bulk and the shear moduli of weakly anisotropic cubic crystals with random orientation distributions. *Morawiec* (1989) and *Matthies and Humbert* (1993) further developed *Aleksandrov and Aizenberg* (1966) idea, and *Matthies and Humbert* (1993) demonstrated its applicability to average physical properties of aggregates described by forth-rank tensors, e.g. elasticity.

In order to model elasticity using GMA, the elastic constants must be re-arranged into a matrix form. The elastic stiffnesses and compliances of the single crystal in the Voigt notation written as a vector in equation (3.4) and (3.5), correspondingly, usually appear in the form of the of [6 × 6] symmetric matrix known as the *elasticity matrix*. This elasticity matrix contains either stiffnesses C_{ij} or compliances S_{ij}, where $i,j = 1,2,....,6$, and correspondence between stiffnesses and compliances in this case is provided by the matrix operation of inversion, $[C_{ij}]^{-1} = [S_{ij}]$.

Matthies and Humbert (1993) demonstrated that *Aleksandrov and Aizenberg* (1966) idea of modification of averaging technique to make results of an averaging operator invertible can be extended to physical properties described by the forth-order tensor (e.g. elasticity tensor). The elasticity tensor should be re-written in matrix form, and the GMA is implemented by diagonalizing elasticity matrix to average modified eigenvalues of elasticity matrix:

$$C_{ij} = U\Lambda^0 U^T \qquad (3.8)$$

where Λ^0 is a diagonal matrix of the eigenvalues of the elasticity matrix C_{ij}, and U is the matrix of its eigenvectors. Equation (3.8) basically describes the operation of single value decomposition (SVD) of elasticity matrix. *Matthies and Humbert* (1993) showed that a proper implementation of the GMA requires conditions of orthogonality of the matrix U and positivity of eigenvalues in Λ^0 to be satisfied. If the matrix U is orthogonal, it satisfies property $U^T = U^{-1}$, and equation (3.8) can also be re-written as eigenvalue

decomposition of the elasticity matrix C_{ij}:

$$C_{ij} = U \Lambda^0 U^{-1}$$

Following averaging operator $\Re_\varphi$ the diagonalized matrix Λ^0 must be modified according to the averaging function φ, i.e. new diagonal matrix $\overline{\overline{\Lambda}} = \exp \Lambda^0$ that contains exponents of eigenvalues of C_{ij} is calculated. The elasticity matrix is now modified:

$$\overline{\overline{C}}_{ij} = U \overline{\overline{\Lambda}} U^{-1} \tag{3.9}$$

and its values can now be used in the averaging procedure similar to equation (3.4):

$$\hat{C} = \bar{a} \overline{\overline{C}} \tag{3.10}$$

where averaging matrix $\bar{a}$ that contains an information on both the symmetry and the texture of the aggregate (detailed description on construction of the averaging matrix for aggregate of orthotropic symmetry from the ODF is presented in Appendix D). Following the averaging operator $\Re_\varphi$ in Equation (3.7), the inverse averaging function φ^{-1} must be applied through the eigenvalue decomposition of matrix $\hat{C}_{ij}$:

$$\hat{C}_{ij} = W \hat{\Lambda} W^{-1} \tag{3.11}$$

and

$$\overline{\Lambda} = \ln \hat{\Lambda} \tag{3.12}$$

where $\overline{\Lambda}$ is a diagonal matrix that contains the logarithms of the eigenvalues of matrix $\hat{C}_{ij}$. Finally, to complete averaging operator $\Re_\varphi$ matrix of elastic constants of the textured aggregate can be obtained by:

$$\overline{C}_{ij} = W \overline{\Lambda} W^{-1} \tag{3.13}$$

$\overline{C}_{ij}$ is a matrix of elastic stiffnesses of textured aggregate averaged by the GMA. If one applies the averaging operator $\Re_\varphi$ to the elastic compliances of the single crystal S_{ij}, the GMA elastic compliances matrix $\overline{S}_{ij}$ would satisfy the condition of invertibility of

the elastic stiffnesses to its elastic compliances, $[\overline{S}_{ij}]^{-1} = [\overline{C}_{ij}]$. In this sense the GMA procedure described by equations (3.8) - (3.13) is *self-consistent*. One also might note, that if the averaging function in the operator $\mathfrak{R}_\varphi$ is chosen to be unity, $\varphi \equiv 1$, the averaging operator reduces to the those used in the Voigt or the Reuss averaging, equations (3.4) and (3.5), respectively.

3.3 Application to an olivine aggregate of orthotropic symmetry

The averaging procedure described in Section 3.2 is general and restricted only by the symmetries of the constituent minerals and the statistical symmetry of the aggregate. It is also intended to model single-phase polycrystalline aggregate and developed to investigate elasticity of orthotropic aggregate of orthorhombic olivine. Olivine is the major constituent of peridotite and as such its properties significantly affect the propagation of seismic waves through the Earth's upper mantle. Many studies of mantle peridotites brought to the surface by different geological processes show peridotites have acquired noticeable texture suggesting these rocks are likely deformed within the Earth.

The mineral phases composing peridotite, olivine particularly, develop a strong texture as a result of plastic deformation and recrystallization. It is the lattice preferred orientation of olivine in textured peridotite rocks that is believed to be primarily responsible for compressional and shear wave anisotropy and shear-wave splitting in the upper mantle (e.g. *Christensen*, 1984; *Nicolas and Christensen*, 1987; *Babuška and Cara*, 1991).

Dunites and peridotites have long been studied by a variety of methodologies. Elastic wave anisotropy was observed by ultrasonic measurements on dunites (e.g. *Christensen*, 1966; *Crosson and Lin*, 1971; *Christensen*, 1971; *Babuška*, 1972; *Kern and Richer*, 1981) and peridotites (e.g. *Peselnick et al.*, 1974; *Peselnick and Nicolas*, 1978; *Kern*, 1978; *Kern et al.*, 1996). The relationship between seismic anisotropy and peridotite fabric was investigated in numerous studies (e.g. *Christensen and Salisbury*, 1979; *Christensen*, 1984; *Nicolas and Christensen*, 1987; *Kern*, 1993b,a; *Mainprice and Silver*, 1993; *Ji et al.*, 1994; *Ben Ismaïl and Mainprice*, 1998; *Weiss et al.*, 1999a; *Soedjatmiko and Christensen*, 2000; *Christensen et al.*, 2001).

Strong *lattice preferred orientation* (LPO's) are observed in naturally deformed peri-

dotites from almost all classic type exposures (e.g. *Mercier*, 1985). In this Chapter a hypothetical olivine texture that is representative of one common type of peridotite is developed for purposes of investigation of effects of averaging assumptions on the elasticity of textured olivine aggregate. This texture is characterized with the crystallographic axes [100], [010] and [001] distributed around the specimen X, Z and Y axes, respectively (Figure 3.1).
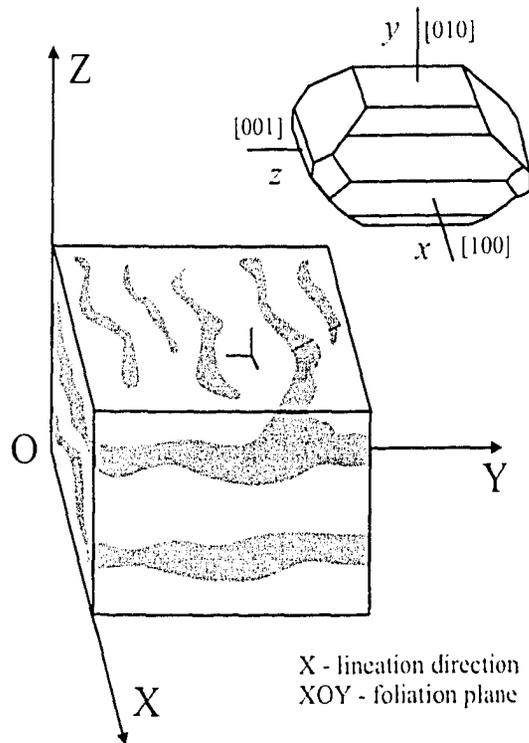
Figure 3.1: Olivine crystallographic axes alignment with respect to the sample coordinate system.

This type of texture is well described in the literature and has been called a (010)[100] or *Type I* olivine pattern (*Ben Ismaïl and Mainprice*, 1998; *Tommasi et al.*, 2000) or a characteristic *Type IV* (*Weiss et al.*, 1999a). The olivine crystallographic axes [100], [010] and [001] are primarily aligned to the specimen *lineation direction* (X) within the *foliation plane* (XOY), the normal (Z) to the foliation plane and the normal ($\overline{Y}$) to the lineation direction within the foliation plane, respectively (Figure 3.1). This *'point maximum'* type of olivine

texture has been observed in dunites (*Crosson and Lin*, 1971; *Christensen*, 1971; *Babuška*, 1972), and almost all types of naturally deformed peridotites including those from Alpine - type massifs (*Nicolas et al.*, 1971, 1973; *Peselnick et al.*, 1974; *Weiss et al.*, 1999a), ophiolitic massifs (*Christensen and Salisbury*, 1979; *Suhr*, 1993; *Ben Ismail and Mainprice*, 1998), xenoliths (*Mercier and Nicolas*, 1975; *Poirier and Nicolas*, 1975; *Ji et al.*, 1994; *Kern et al.*, 1996; *Soedjatmiko and Christensen*, 2000; *Christensen et al.*, 2001), and in kimberlite nodules (*Boullier and Nicolas*, 1975; *Mainprice and Silver*, 1993; *Ben Ismail and Mainprice*, 1998).

During plastic deformation in the lithosphere under high pressure and temperature conditions the olivine within peridotite develops a highly oriented lattice preferred orientation (e.g. *Nicolas and Christensen*, 1987). High temperature further promotes the development of extremely strong fabrics enhanced by diffusion and large grain boundary mobility. The mechanisms of peridotite deformations were extensively studied by numerous workers (e.g. *Poirier and Nicolas*, 1975; *Nicolas et al.*, 1971; *Karato*, 1988) who suggest that combination of several mechanisms including sliding, dislocation gliding and dynamic recrystallization contribute to the plastic deformation. The role of each process on the texture development of an olivine aggregate greatly depends on the pressure and the temperature conditions as well as on the presence of fluid and minor mineral phases during the formation or recrystallization periods.

The development of LPO in olivine aggregates has also been theoretically evaluated with several models based on polycrystalline plasticity theory. Some examples include the *viscoplastic self-consistent* (VPSC) theory (*Wenk et al.*, 1991), the stress equilibrium approach (*Chastel et al.*, 1993), their combination (*Tommasi et al.*, 2000), and the kinematic approach (*Ribe and Yu*, 1991). These models consider the LPO to evolve solely by intracrystalline slip and are able to make predictions about olivine LPO development under pressure-temperature (P-T) conditions where recrystallization may be neglected. However, early experimental results by *Ave'Lallemant and Carter* (1970) and *Nicolas et al.* (1973) indicate that recrystallization also likely plays an important role for LPO development in the high temperature regime.

Most recently, *Zhang and Karato* (1995); *Karato et al.* (1998) and *Zhang et al.* (2000) reported the results of simple shear deformation experiments on olivine synthetic aggregates. These experiments clearly indicate that the olivine crystallographic axes develop

a so-called "point maximums" type of texture, when axes are concentrated in particular directions with close to circular spatial distribution. The degree to which this preferred alignment occurs depends on the shear strain regime and the presence of fluids. *Zhang et al.* (2000) suggested that dynamic recrystallization has a strong effect on both the mechanical behavior and the LPO development.

Recent advances in texture modelling allow for dynamic recrystallization including subgrain rotation and grain-boundary migration (GBM) to be accounted for. *Wenk et al.* (1997) used modified VPSC model to investigate dynamic recrystallization on several mineral aggregates. *Wenk and Tomé* (1999) include processes of boundary migration and nucleation into VPSC plasticity theory to model simple shear experiment results. Most recently, *Kaminski*
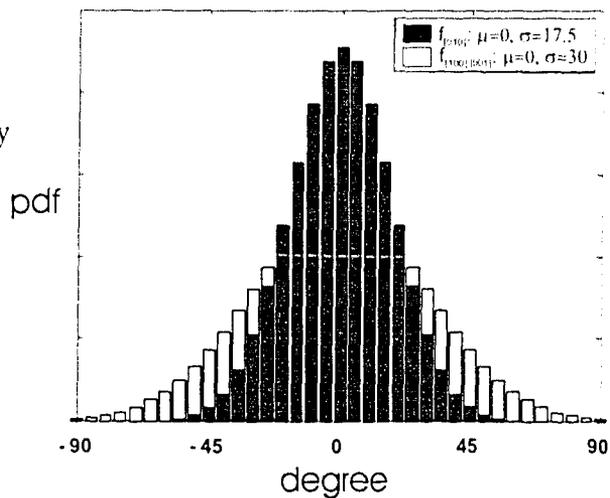
Figure 3.2: Probability density functions (PDF) used in construction of hypothetical olivine texture of orthotropic symmetry.

and Ribe's (2001) kinematic model incorporates dynamic recrystallization and LPO development in olivine aggregates. Reported modelling results compare favorably with the simple shear experiments of *Zhang and Karato* (1995) and *Zhang et al.* (2000). *Kaminski and Ribe* (2001) suggest that the [100] and [010] secondary peaks on pole figures observed during shear deformation experiments correspond to the crystallographic axis of the harder residual olivine grains with low dislocation densities that were not consumed by grain boundary migration. Modelling results indicate that these [100] and [010] secondary peaks tend to disappear at larger strain (*Kaminski and Ribe*, 2001).

Based on the discussed above experimental results, theoretical modelling calculations and observations in natural peridotites, a hypothetical but representative texture of olivine aggregate with characteristic point maximum distributions along the sample

70

symmetry axes was constructed. To create this texture the $[100]$, $[010]$ and $[001]$ olivine' crystal axes were normally distributed with the mean values of distributions centered on the specimen X, Z and $\bar{Y}$ axes, respectively.

Here, the distribution of the olivine crystallographic axes around the specimen symmetry axes are represented by Gaussian distributions with standard deviation σ adjusted to reflect distributions in naturally deformed peridotites of orthotropic symmetry. In order to reflect the observations of usually stronger concentration of the $[010]$ axis within the deformed peridotites, the axis' standard deviation is smaller than for the $[100]$ and $[001]$ axes (Figure 3.2).

Normal distributions of Figure 3.2 were used to construct an orthotropic texture with distribution of olivine crystallographic axes shown in pole figures in the Figure 3.3. Olivine $[100]$ and $[001]$ axes distributions within the foliation plane XOY are identical and more broadly distributed in the foliation plane in comparison to the more centered $[010]$ axis distribution (Figure 3.3). The values are normalized by uniform distribution and shown as *multiples of uniform distribution* or m.u.d. (e.g. *Wenk*, 1985). No secondary $[100]$ or $[010]$ axis peaks were assumed.

3.4 Results and discussion

The Voigt, the Reuss, and the GMA averaging procedures described above were applied to the olivine polycrystalline aggregate with hypothetical texture characterized by equal-area projections of Figure 3.3. The elasticity of the olivine aggregate considered here is bounded by the two extreme orientation distributions: first a perfectly aligned aggregate with the properties similar to those of the single crystal (*quasi* single crystal) and second a randomly distributed aggregate with isotropic properties that may be calculated by the traditional Voigt-Reuss (VR) bounds (Appendix C). The olivine single crystal elastic constants reported by *Webb* (1989) (shown in matrix notation alone with the VR bounds for an isotropic aggregate on Figure 3.4) were used in the calculations. Clearly from Figure 3.4, the isotropic VR bounds are narrow for all elastic constants (with $C_{11}^{V(iso)}$ being 103.6% of $C_{11}^{R(iso)}$). This may explain why experimental results reported in the literature (which have experimental error close to the value of separation of the bounds for this

case) could be close to either the Voigt or the Reuss bound (e.g. for further discussion see *Crosson and Lin*, 1971)

Knowing the full set of elastic constants, compressional and shear-wave velocities can be calculated for any specific direction of wave propagation within the aggregate. By applying the *Christoffel equation* (details on the derivation of the Christoffel equation are available in Appendix B), the elastic velocities of the *quasi*-compressional and the fast and the slow *quasi*-shear waves (denoted as P, S_{fast} and S_{slow} in the following for simplicity) were calculated by assuming equal values of aggregate and single crystal densities. The P-wave velocities, shear wave splitting, $\delta S = (S_{fast} - S_{slow})$, and the S_{fast} polarization directions for an olivine single crystal and for the hypothetical polycrystalline aggregate are presented on an equal-area projections in Figure 3.5.

As expected, the averaging procedure moderates the anisotropic properties of the textured aggregate if compared to the single olivine crystal. The hypothetical LPO considered is relatively strong, and the aggregate's P-wave anisotropy is reduced insignificantly relative to that for the single crystal ($A(V_p) = 24.2\%$, where $A(V_p) = 2(V_{pmax} - V_{pmin})/(V_{pmax} + V_{pmin}) \times 100\%$ (e.g. *Mainprice and Silver*, 1993)). The P-wave anisotropy is insignificantly influenced by the use of either the Voigt or Reuss averaging procedures (varies by 2%).
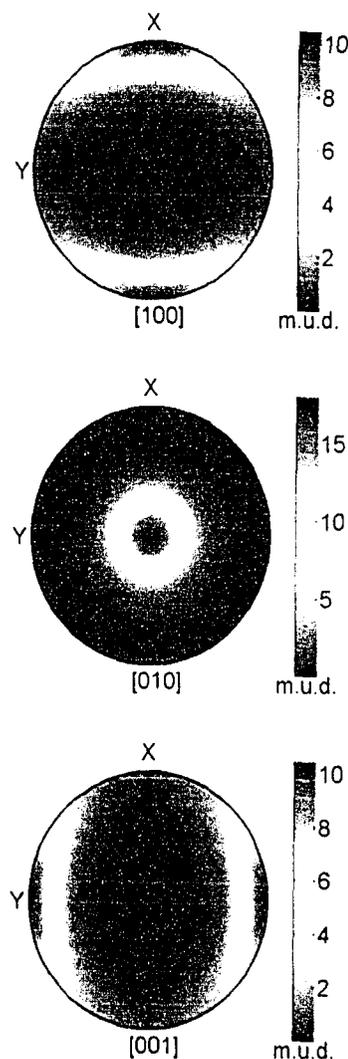
Figure 3.3: Hypothetical orthotropic aggregate: equal-area projections of olivine crystallographic axes.
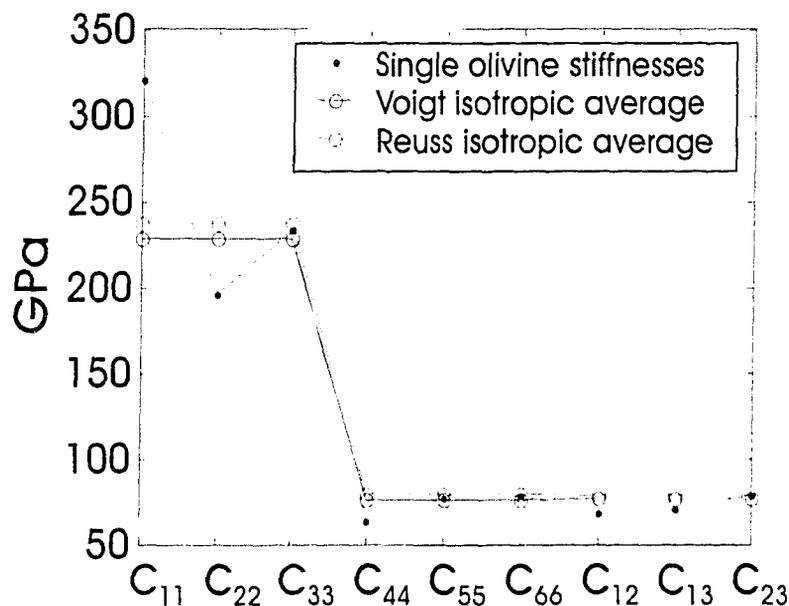
Figure 3.4: Elastic constants of single olivine crystal from Webb (1989), and the isotropic Voigt-Reuss bounds.

However, the spatial distribution of S-wave splitting is more sensitive to the averaging assumptions. The maximum shear wave splitting for the Reuss average is $\delta S = 0.82$ km/sec while the Voigt average gives $\delta S = 0.76$ km/sec. The pattern of the shear wave splitting is sensitive to the elastic constants and therefore affected by the choice of the averaging method used, as seen in Figure 3.5. The various approximations have practically no influence on the S_{fast} polarization directions, although polarization direction differs from the polarization directions of the single crystal in some directions of propagations. The results here indicate that the calculated elasticity of olivine textured polycrystalline aggregate is significantly more influenced by its textural properties rather than the averaging assumption. Variations or errors in estimating the textural coefficients and consequently the ODF would have a profound effect on the estimation of elasticity of the olivine aggregate.

The calculated elastic wave velocities and anisotropy obtained by different averaging techniques are comparable to those reported for naturally deformed dunites and peridotites with similar textures. P-wave elastic anisotropy was measured directly at

Table 3.1: Elastic constants of single olivine crystal from Webb (1989), and the isotropic Voigt-Reuss bounds

Averaging	Elastic constants, GPa								
technique	C_{11}	C_{22}	C_{33}	C_{44}	C_{55}	C_{66}	C_{12}	C_{13}	C_{23}
Single crystal	320.2	195.9	233.8	63.5	76.9	78.1	67.9	70.5	78.5
Voigt	237.2	237.2	237.2	79.2	79.2	79.2	78.7	78.7	78.7
Reuss	228.9	228.9	228.9	76.0	76.0	76.0	76.9	76.9	76.9

ultrasonic frequencies on Twin Sisters dunites by Christensen (1971). His samples TW-2 and TW-4 were characterized by an explicit point maximum texture, although not as strong as hypothetical one developed here, and displayed P-wave anisotropy of 6% and 7.9%, respectively. The lower values of P-wave anisotropy in dunites can partially be attributed to the fact that the pure olivine texture is weaker than the olivine textures in mixed phase rocks (i.e. peridotites) for the same amount of overall shear (Wenk et al., 1991). The stronger LPO of olivine in peridotites reflects the concentration of strain on the plastically weaker olivine, which has more crystallographic slip systems available than the more rigid pyroxene. Ben Ismail and Mainprice (1998) calculated P-wave seismic anisotropies for olivine based on the olivine petrofabric data from a large ensemble of 110 peridotite samples and using Mainprice's (1990) code based on the Voigt assumption. They determined P-wave anisotropies varying from 4% to 21.4% with a mean value of 12.2%. They estimated the P-wave seismic anisotropy for Type 1 (orthorhombic symmetry) olivine aggregates to be 15.3%. Soedjatmiko and Christensen (2000) have calculated the average $A(V_p)$ anisotropy of fifteen harzburgites and lherzolites from Cima volcano field xenoliths to be 6.9%. Samples CX-08-3, CX-17-7 and CX-21-1 that exhibit orthotropic LPO pattern have the P-wave anisotropies of 9.5%, 9.0% and 12.8%, respectively. Tommasi et al. (1999) reported seismic anisotropy of olivine aggregates based on results of LPO development modelling. The authors predicted P-wave anisotropy to be 14.7% in case of deformations by simple shear and 15.4% for pure shear deformations. Zhang and Karato (1995) calculated the seismic anisotropy for experimentally deformed by simple shear olivine aggregate to be 16.6% for case of highly strained aggregate. Another shear deformation experimental results on olivine aggregate (Zhang et al., 2000) allowed $A(V_p)$ to be estimated in the interval of 9-10% for samples with the LPO controlled by the flow geom-

Table 3.2: Elastic constants of single olivine crystal rotated $90°$ around X axis and textured olivine aggregate calculated by the Voigt, the Reuss, and the GMA technique

Averaging technique	Elastic constants, GPa								
	C_{11}	C_{22}	C_{33}	C_{44}	C_{55}	C_{66}	C_{12}	C_{13}	C_{23}
Single crystal	320.2	233.8	195.9	76.9	63.5	78.1	70.5	67.9	78.5
Voigt	289.7	235.7	198.4	77.1	68.4	88.3	103.1	48.9	80.0
Reuss	295.4	216.1	219.7	75.9	67.2	84.9	109.5	47.9	73.6
GMA	289.6	221.8	200.5	75.9	67.1	87.7	103.9	49.3	77.4

etry. All these results suggest that seismic properties of olivine aggregates in the upper mantle peridotites are broadly scattered due to textural variations even within one type of LPO pattern. Further the anisotropy will depend on additional factors such as the degree of recrystallization, the type of deformation, and the origin of the peridotite. The calculation results obtained here are an upper range of possible anisotropy that can be observed in naturally deformed peridotites on the scale of hand specimens.

The hypothetical texture employed here is representative of one of the types of olivine texture widely observed in the naturally deformed peridotites collected worldwide. Consequently, the calculated seismic properties of this hypothetical aggregate may be considered as possible average properties characteristic to the upper mantle region subject to simple shear deformation in which the olivine aggregate may have mostly orthotropic texture. Interpretation of seismologically observed traveltimes anisotropy usually relies on trade-off of the thickness of anisotropic layer (region) and the strength of the anisotropy. Sophisticated full elastic field forward modelling techniques, e.g. anisotropic finite-element code, based on the initial models obtained from anisotropic tomographic inversion and constrained by results of modelled rock properties would aid proper seismological interpretation. Rock physical modelling of elasticity, as presented here, allow estimating variations in initial model parameters and constrain solution. In addition, proper estimation of the upper mantle elasticity should incorporate models that allows for multi-phase polycrystalline composites (see recent paper by Ji et al. (2004) for application of the GMA to multi-phase but isotropic aggregates). In order to incorporate fluid/melt inclusions a combination of the GMA technique with effective medium theories is worth consideration.

The averaging of hypothetical aggregate properties over the upper mantle thickness
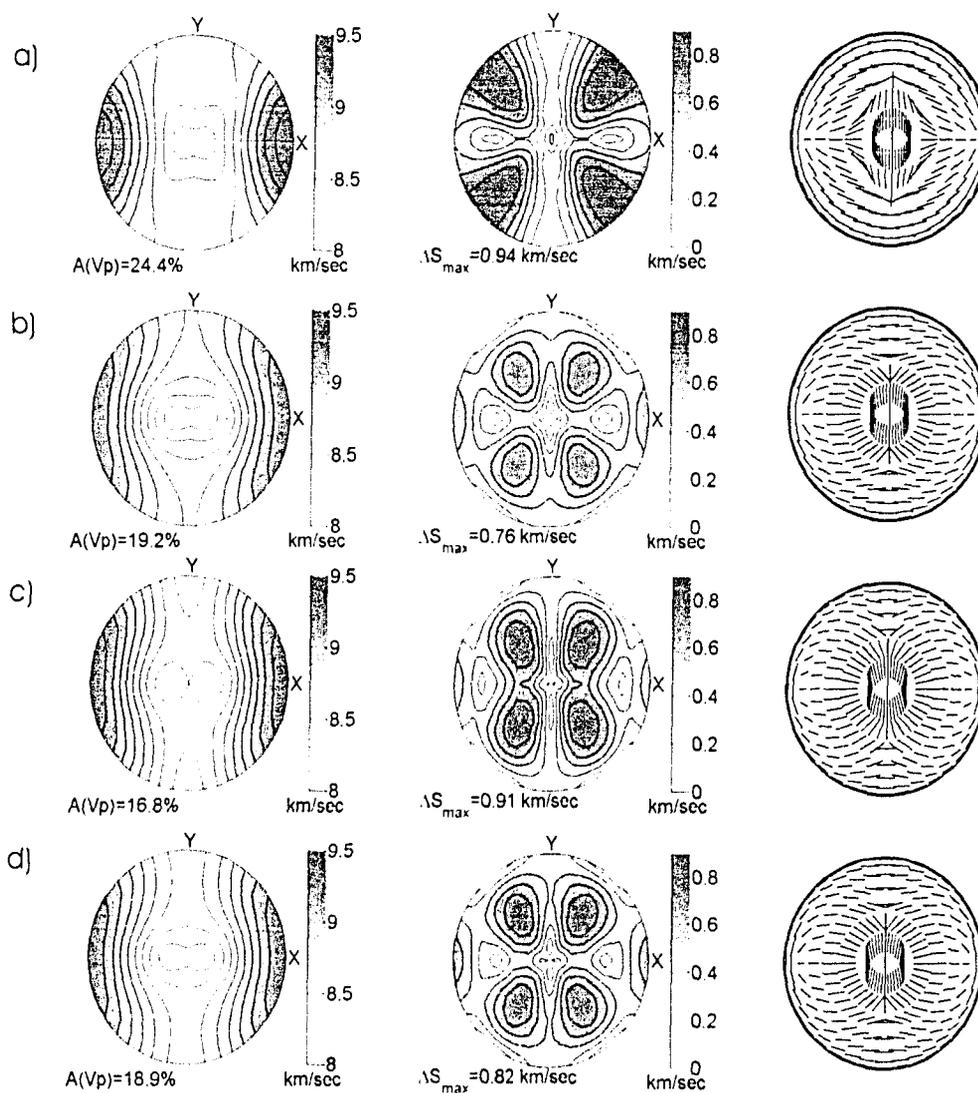
Figure 3.5: Compressional velocities, shear-wave splitting and S_{fast} polarization directions on the equal-area projection: a) single olivine crystal; b) the Voigt average; c) the Reuss average; d) the Geometric Mean Average.

as well as presence of more randomly oriented pyroxenes and accessory minerals in peridotites reduces the anisotropy. The azimuthal distribution patterns of the seismic and elastic properties, however, may still be governed by the olivine LPO (*Peselnick et al.*, 1974; *Peselnick and Nicolas*, 1978; *Weiss et al.*, 1999a). Orthotropic model with nine un-

76

known elastic constants that can be estimated by the GMA technique could be useful for seismological interpretations of P_n anisotropy and SKS shear wave splitting.

3.5 Conclusions

This Chapter discusses application of volume weighted averaging techniques to model the elasticity of an aggregate of orthotropic symmetry composed of olivine with orthorhombic symmetry. Textural properties of the aggregate were incorporated into the algorithm through the analytical derivation of an orthotropic-orthorhombic ODF (Appendix D). The expansion coefficients of the ODF into a series of symmetrical generalized spherical harmonics was included into the averaging procedure following the Voigt and the Reuss assumptions. The averaging technique developed further to incorporate the GMA, i.e. implement an idea of the averaging procedure independent on the averaging domain.

A hypothetical texture was constructed to reflect one type of texture of naturally deformed peridotites with distinctive orthotropic texture. This textural pattern has been widely observed in naturally deformed peridotites and has been reproduced in high strain experimental deformations of synthetic olivine aggregates in simple shear deformation regimes. Several plastic deformation theories including recent dynamic recrystallization models also predict the development of similar LPO patterns. All these results taken together suggest that orthotropic olivine symmetries may be one of the dominant textures within the regions of the upper mantle undergoing simple shear deformation.

An orientation distribution function was applied to model the elastic parameters of the textured olivine aggregate. The ODF coefficients were recalculated from information about the orientations of the individual crystals. Results of the modelling suggest that the aggregates with strong LPO develops spatial distribution of P-wave velocities comparable to velocity distribution of a single crystal. This anisotropy is, however, reduced with respect to single crystal up to 7% depending on the averaging assumption. One of the main objectives of this study was to estimate effect of the averaging techniques on elasticity and intrinsic anisotropy of olivine aggregate of orthotropic symmetry. The application of the different averaging techniques appears to have no crucial effect on the

elasticity of a textured olivine aggregate. While this result may be true for the olivine aggregate, one cannot presume this conclusion is universal as will be demonstrated in the next Chapter.

The textural properties of olivine aggregate, however, have significant effect on the calculated elasticity. Therefore, efforts should be directed to insure not only quality of textural information but also statistical representativeness of this information that reflects purposes of particular investigation. The P-wave anisotropy is relatively insensitive to the averaging procedures employed. The degree of shear wave splitting and especially its spatial distribution is more averaging procedure dependent. Overall, all averaging techniques produce similar results for textured olivine aggregate, however, application of the GMA to the orthotropic texture allows assumptions of the uniform stress or strain to be omitted.

The orthotropic sample approximation makes an averaging result more readily comparable to seismological observations with anisotropic pattern in data, and could be a reasonable approximation of regional elasticity in the upper mantle undergoing simple shear deformation. The results presented here and successful applications of the ODF in several other studies to model elastic properties of different geomaterials clearly indicate that the ODF could be useful not only for quantitative texture analysis but also for modelling textural effects on seismic wave properties of anisotropic aggregates. The possibility of including different sample symmetries into the calculation algorithm makes this modelling technique an important tool to investigate texture dependent seismic velocities and predict reliable symmetry of the upper mantle materials.

Chapter 4

The intrinsic anisotropy of phyllosilicate rich rocks

1

This chapter deals with the modelling of the intrinsic elastic properties of phyllosilicate-rich rocks that occur naturally and are highly anisotropic to seismic waves. The anisotropic properties of such rocks are investigated through the modelling of the intrinsic elasticity of a solid matrix. 'Intrinsic' implies properties of a non-porous and non-fractured solid matrix that can be investigated on the basis of the theory of polycrystalline aggregates. The study is specifically concerned with the investigation of intrinsic elasticity of shales as a function of texture. Modelling of the intrinsic elasticity takes into consideration the textural properties of shales and assumptions about the elasticity of constituent shale minerals (i.e. clays). Elastic constants of solid matrix with developed texture were calculated using volume averaging techniques and widely used Voigt, Reuss and Hill assumptions. Taking into account the plausibility of the significant anisotropy of clay minerals and the resulting wide separation of the Voigt and Reuss (upper and lower) bounds of the textured aggregate, the method of the Geometric Mean Averaging (GMA) was employed to further refine the elasticity. The GMA method employs straightforward physical requirement of the invertibility of the elastic stiffnesses of textured aggregate into its elastic compliances and yields a unique set of elastic constants independent of the averaging domain (either stiffnesses or compliances). The resulting elastic constants are not lim-

---

[1] A version of this Chapter has been published, Cholach and Schmitt (2003), and presented in CSPG/CSEG 2003, SEG 2003, CSEG 2004 annual conventions.

ited by Hill's assumption and can lie either above or below the Hill average, depending on a certain elastic constants and textural properties of the aggregate, and fall predominantly within the Voigt-Reuss bounds. Limits of the seismic anisotropy and anisotropic parameters of the solid monomineralic muscovite matrix have been estimated. It has been shown that despite the strong dependence of absolute values of elastic constants on the averaging assumptions, properties of elastic waves and especially anellipticity of P-wave is practically independent on the averaging procedure.

4.1 Introduction

Shales are elastically anisotropic rocks with complex petrophysical properties. Their abundance in sedimentary basins significantly affects seismic wave propagation. The most direct consequence of this shale induced anisotropy is erroneous determination of the depths of subsurface events (e.g. *Banik*, 1984). Perhaps more importantly, ignoring anisotropy during migration does not provide for proper lateral positioning of seismic reflectors in areas with dipping sedimentary strata (e.g. *Vestrum et al.*, 1999). Consequently, estimating the elastic properties of shales is both an academic and a practical problem.

Since the pioneering work of *Kaarsberg* (1959) shales elastic properties have been extensively investigated both theoretically (*Hornby et al.*, 1994; *Sayers*, 1994; *Schoenberg et al.*, 1996; *Sayers*, 1999; *Jakobsen et al.*, 2003), and experimentally (*Jones and Wang*, 1981; *Vernik and Nur*, 1992; *Johnston and Christensen*, 1995; *Hornby*, 1998; *Jakobsen and Johansen*, 2000; *Wang*, 2002; *Domnesteanu et al.*, 2002). These studies demonstrated that anisotropy is a feature of seismic wave propagation in the majority of shales. The anisotropic behaviour of shales was also observed in a variety of seismic field observations (e.g. *Jolly*, 1956; *White et al.*, 1983; *Winterstein and Paulsson*, 1990; *Miller et al.*, 1994; *Kebaili and Schmitt*, 1996; *Leslie and Lawton*, 1999; *Leaney et al.*, 1999). The significant lithological and compositional variability is responsible for variations in the magnitude of shale anisotropy from almost isotropic to highly anisotropic (*Banik*, 1984; *Jakobsen and Johansen*, 2000; *Wang*, 2002) with the coefficient of anisotropy for compressional wave ($A(V_P) = (V_{Pmax} - V_{Pmin})/V_{Pmean} \times 100\%$) exceeding 40% in some cases (cf. *Johnston and Christensen*, 1995).

80

A number of different modelling techniques have been employed to explain the observations. *Vernik and Nur* (1992) applied the long wavelength theory of *Backus* (1962) to average the properties of a composite medium consisting of layers of isotropic illite and kerogen in an attempt to explain ultrasonic observations of strong anisotropy in source rock shales. *Hornby et al.* (1994) used the combination of *the self-consistent* (SCA) (*Kröner*, 1958) and *the differential effective medium* (DEM) (e.g. *Sheng and Callegari*, 1984) approximations to first provide an estimate of the elasticity of a perfectly aligned clay-fluid composite that was then averaged according to a statistical measure of the relative orientation of clay platelets. The calculated elastic constants of this clay-water composite was almost identical to those obtained from ultrasonic measurements on Cretaceous shales by *Jones and Wang* (1981). *Schoenberg et al.* (1996) invoked a simplified three-parameter transversely isotropic (TI) medium to model shale anisotropy. Their initial model is based on the long wavelength approximation of stiffened media consisting of two interchangeable, infinitely thin isotropic layers (*Schoenberg and Muir*, 1989). Most of the calculated elastic constants of this simplified transversely isotropic medium, with exception of one (C_{33}), are in reasonable agreement with reported elastic constants of shales.

Despite these advances, there remains significant ambiguity in the models with respect to the *in situ* sources of seismic anisotropy. The seismic anisotropy of shales is influenced by several factors, including the preferred orientation (texture) of clay platelets (*Kaarsberg*, 1959; *Tosaya*, 1982; *Sayers*, 1994; *Johnston and Christensen*, 1995), alternation of fluid filled collinear cracks with clay platelets (*Vernik and Nur*, 1992; *Hornby et al.*, 1994), microcracks (*Vernik*, 1993; *Vernik and Liu*, 1997), fine layering (*Schoenberg et al.*, 1996), fluid filled porosity (*Hornby*, 1998), and stress-induced anisotropy (*Sayers*, 1999). A combination of several of these factors (e.g. *Jakobsen et al.*, 2003; *Johansen et al.*, 2004) is required to fully describe shale anisotropy.

In this Chapter the issue of the origin of the seismic anisotropy of shales is partially addressed by modelling of their intrinsic elastic properties. *Intrinsic* implies here the elastic anisotropy due solely to the averaging of the elastic properties of the constituent minerals as controlled by their orientation texture within the aggregate. An example of this texture in a wet shale may be seen in Figure 4.1. That is, this study attempts to provide a measure of the elasticity of a pore free shale solid matrix. In the paper

the Geometric Mean Averaging (GMA) procedure is applied for a first time to a series of monomineralic muscovite aggregates with different degrees of texture. The evolution of the anisotropy with texture provides insight into some of the factors controlling shale anisotropy.

4.2 Averaging the elastic properties of a polycrystalline aggregate

Modelling of the intrinsic anisotropy is based on *the orientation distribution function* (ODF) averaging technique (*Viglin*, 1960; *Roe*, 1965; *Bunge*, 1982) in combination with the concept of the "Geometric mean" (*Aleksandrov and Aizenberg*, 1966; *Morawiec*, 1989; *Matthies and Humbert*, 1993). *The Geometric mean averaging* (GMA) technique aims to show the limits of the possible anisotropy of the solid matrix. The results obtained here are intended to be used as a starting point for more complex models that consider the elasticity of porous and/or fractured shales. ODF averaging has previously been applied to shales by *Sayers* (1993, 1994) to identify the textural parameters responsible for anisotropic velocity variations in shales. *Sayers* (1993, 1994) showed that only two coefficients of the ODF expansion affect the seismic anisotropy of shales with *vertical transversely isotropic* (VTI) symmetry. The Voigt approximation of uniform strain of shale aggregate was used to derive explicit formulae for calculation of averaging elastic constants. By varying the values of texture coefficients Sayers (1994) demonstrated that shales might develop a strong anelliptic anisotropy the degree of which is a function of a single texture parameter, viz. W_{400}.

In order to carry out ODF averaging, one needs knowledge of the volumetric fraction of the constituent mineral phases, their elasticity, and the statistics of the textural orientation distributions. Despite the expectations that clay minerals themselves are highly anisotropic (*Kaarsberg*, 1959; *Tosaya*, 1982), they are often assumed to be isotropic in attempts to estimate some of their elastic characteristics (cf. *Katahara*, 1996; *Wang et al.*, 1998; *Vanorio et al.*, 2003). The absence of reliable data on the elastic stiffnesses of clay minerals remains the most serious obstacle for the proper modelling of the intrinsic elasticity of shales and may be attributed to the difficulty of carrying out experimental mea-

82

surements on the small, typically submicron, size of naturally occurring illite, chlorite, kaolinite and montmorillonite. Wetting effects due to the presence of water is an additional concern of which little is known. To overcome this limitation several assumptions are made here, firstly that shale matrix is composed solely of illite, which is one of the most abundant clay minerals in shales (*Kaarsberg*, 1959) and contributes significantly to their overall elasticity. Due to the fact that elastic stiffnesses of illite are not yet known the second assumption is made that properties of the muscovite mica crystal (chemical formula is $KAl_2(Si_3Al)O_{10}(OH)_2$) are instead taken as representative (*Tosaya*, 1982; *Sayers*, 1994). This assumption is mainly based on the similarity of the structures of both layered silicates with the replacement of some of the K^+ ions in muscovite by H_3O^+ (e.g. *Putnis*, 1992). The anisotropy of a single muscovite crystal is large (compressional wave anisotropy $A_P = (V_{Pmax} - V_{Pmin})/V_{Pmean} \times 100\% = 56.8\%$; Thomsen parameters $\varepsilon = 1.12$; $\delta = -0.27$; $\gamma = 2.28$) and, although while, rigorously, muscovite has monoclinic symmetry, it may be considered to have *quasi*-hexagonal symmetry (*Alexandrov and Ryzhova*, 1961b). Similarly structured illite (the illite group general formula is $K_{1-1.5}Al_4(Si.Al)_8O_{20}(OH)_4$) is also expected to be highly anisotropic. Consequently, results of the modelling under the assumption of 100% clay mineral (illite) composition with exclusion of the silt portion of the matrix can be treated as a major component contributing to the intrinsic anisotropy of shales.

The presence of non-clay phases (silt), particularly quartz, feldspar, calcite and dolomite, in the shale matrix, will affect its overall elasticity and, normally, reduce the anisotropy. The reduction is dependent on the volumetric presence of each of these phases. A substantial volumetric presence of randomly oriented and spatially distributed silt particles in shales also interferes with the alignment of the clay minerals (*Ho et al.*, 1999). The effect of the silt particles on the texture of clay minerals will be discussed below. However, quantitative estimates of the effect of the silt particles *per se* on the shale elasticity are not considered here.

The elasticity of the textured solid matrix may be investigated in the theoretical framework of the elasticity of polycrystals. The prediction of the elasticity of polycrystalline aggregates is a classic problem in solid mechanics and rock physics with the roots of the investigation coming from early in the last century (e.g. *Voigt*, 1928; *Reuss*, 1929; *Hill*,
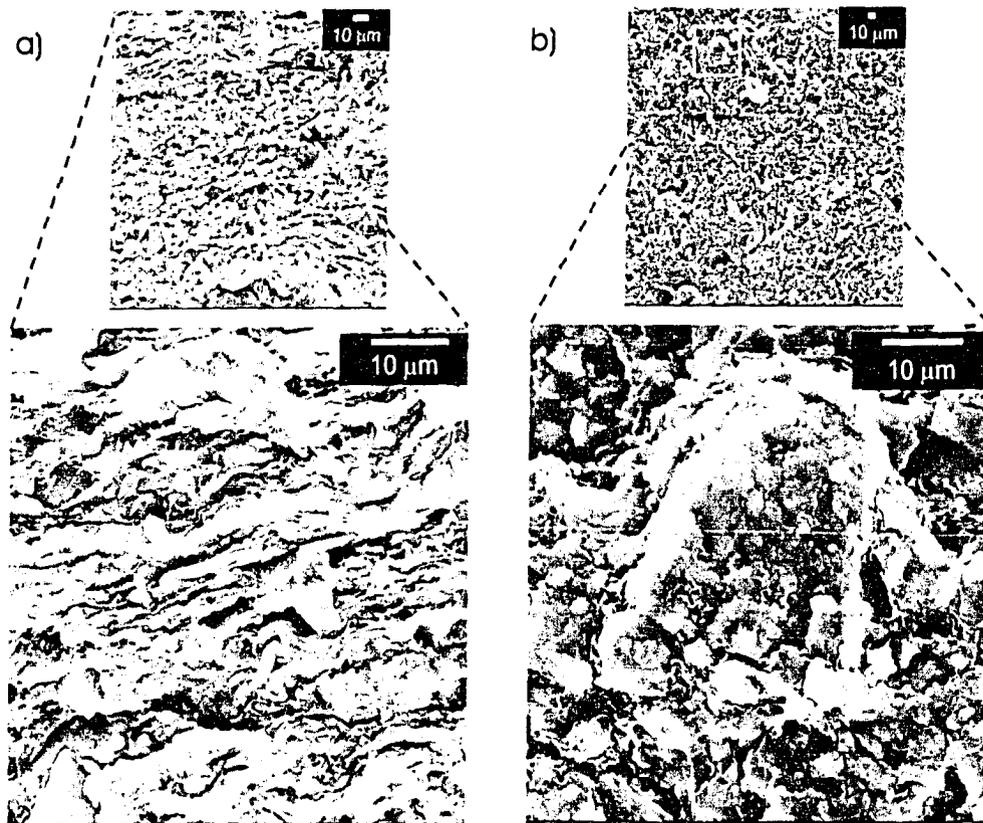
Figure 4.1: SEM images of Colorado Shale from the Cold Lake area of Alberta, Canada: *a)* section perpendicular to the bedding plane; *b)* section parallel to the bedding plane. Observed strong shape preferred orientation of clay particles directly correlates with lattice preferred orientation of clay minerals (see text for details). Average size of clay platelets is several microns and almost order of magnitude smaller then embedded randomly distributed silt (quartz, calcite etc.) particles.

1952; Kröner, 1958; Kumazawa, 1969; Morris, 1970; Thomsen, 1972; Watt et al., 1976; Ono, 1992). In geophysics, the so-called bounding estimates are well established (Watt et al., 1976). The simplest, most universal, and widely applied calculations employ the Voigt (Voigt, 1928) upper and the Reuss (Reuss, 1929) lower bounds that assume either uniform strain or stress within the isotropic aggregate, respectively. The bounds are widely separated for aggregate composed of highly anisotropic crystals such as clays. The degree of texturing of the crystals within the aggregate further influences the separation of the lower and upper bounds. Effective medium schemes, such as the already mentioned

self-consistent approximation (SCA) method (e.g. *Kröner*, 1978), are frequently applied to provide a more constrained solution, which lies within the Voigt-Reuss (VR) bounds. However, despite the fact that the SCA solution is unique and converges within the VR bounds, the initial effective medium developments usually require a perfectly disordered aggregate and an absence of correlation between grains shapes and orientations, these conditions may not always hold for the case of a polycrystalline aggregate (*Ono*, 1992). *Hill* (1952) suggested that the simple arithmetic mean value of the two VR bounds of an isotropic polycrystalline aggregate might be most representative of experimental results (e.g. *Chung and Buessem*, 1967a). The Hill approximation, however, has no solid physical foundation and is applied as rather simple intuitive solution.

Another approach to refine the values of the elastic constants of the aggregate was taken by (*Aleksandrov and Aizenberg*, 1966) who suggested that use of the physically meaningful condition of the invertibility between the elastic stiffnesses and the elastic compliances be a basis for the search for elastic constants. Description of *Aleksandrov and Aizenberg's* (1966) technique is provided in Chapter 3. In this Chapter alternative description of their modification to the averaging procedure is provided. Following these authors notation, if the particular physical property of the crystal can be described by the constants $R_i > 0, i = 1, 2, ... N$ which have it's inverse $Q_i = [R_i]^{-1}$, then the corresponding properties of polycrystalline aggregate composed of these crystals should fulfill $\overline{Q}_i = [\overline{R}_i]^{-1}$, where $\overline{Q}_i$ and $\overline{R}_i$ are values averaged by certain mathematical function. The not yet defined averaging function ϕ has it's inverse function ϕ^{-1} and the averaging operator $\Re_\phi(R_j)$ can be written in the form:

$$\overline{R}_i = \Re_\phi(R_j) = \phi^{-1}\left\{\sum_{j=1}^{N} p_{ij}\, \phi(R_j)\right\}$$

with $p_{ij} \geq 0$ is an orientation distribution, $\sum p_{ij} \equiv 1$, and fulfill conditions:

- $\overline{Q}_i = \Re_\phi(Q_j) = \left[\Re_\phi(R_j)\right]^{-1} = \overline{R}_i^{-1}$

- $\Re_\phi(k R_j) = k\, \Re_\phi(R_j)$

It has been shown that the only averaging function fulfilling these conditions is $\phi(R) =$

85

$a \ln R + b$, for any $a \neq 0$ and b (*Aleksandrov and Aizenberg*, 1966). Therefore, the averaging procedure can be rewritten:

$$\overline{R_i} = \Re_{\phi = \ln R}(R_j) = exp\left[\sum_{j=1}^{N} p_{ij} \ln(R_j)\right] = \prod_j R_j^{p_{ij}}$$

Aleksandrov and Aizenberg (1966) applied this method to find the bulk and the shear moduli of isotropic aggregates composed of cubic crystals. The resulting moduli lie not only within the VR bounds but also within the narrower Hashin - Shtrikman bounds (*Hashin and Shtrikman*, 1963). More recently, *Morawiec* (1989) and *Matthies and Humbert* (1993) further developed this technique to average elastic constants of the textured polycrystalline aggregate and have referred to the technique as the "Geometric mean" method. *Matthies and Humbert* (1993) have calculated the Young's modulus of an hypothetical Zn sample and found good agreement (if compared to experimental accuracy) between the GMA and self-consistent approach. *Mainprice and Humbert* (1994) applied GMA technique to geomaterials. Orientation distributions of biotite grains obtained by optical microscopy were used to calculate elastic constants of aggregates by the Voigt, Reuss, Hill and GMA methods. Elastic constants were also obtained by employing the self-consistent model that assumes spherical shape of aggregate grains. From the elastic constants obtained by these different techniques P- and S-wave velocities have been calculated and compared with experimental velocity measurements. Results show that the GMA is close to the Hill solution for both V_P and V_S values. These authors concluded *"the geometric mean is the best estimate of the seismic properties of the simple averaging methods".* Alternative to Chapter 3 description of the GMA procedure is discussed in detail below.

There are several major factors that influence the intrinsic anisotropy of a solid rock matrix including the elasticity of the constituent minerals, their volumetric fraction and, most importantly, their texture (orientation distribution) within the aggregate. Following *Bunge* (1982) the elastic constants of a non-porous textured monomineralic polycrystalline aggregate may be approximated by the mean value that depends on the elastic constants of the constituent single crystal C_{ijkl} and the orientation distribution function $f(g)$ of the aggregate. Integration of the single crystal elastic constants weighted by the

ODF over all values of the orientation domain g yields elastic constants in the Voigt approximation of uniform strain throughout the aggregate (e.g. *Kneer*, 1965):

$$\overline{C}_{ijkl}^{V} = \oint C_{ijkl} f(g) \, dg \qquad (4.1)$$

where $g = (\varphi_1, \Phi, \varphi_2)$ is the orientation domain that consists of the three Euler angles (cf. *Morse and Feshbach*, 1953). Three consecutive rotations of an initially misaligned single crystal coordinate system x_i $(i = 1, 2, 3)$ by Euler angles $(\varphi_1, \Phi, \varphi_2)$ allow x_i to coincide with the rock (shale) coordinate system X_j $(j = 1, 2, 3)$. The rock coordinate system X_j is defined such that $X_1 X_2$ plane is collinear with the bedding plane of shale and X_3 is normal to the bedding plane (Figure D.1).

The orientation distribution function $f(g)$ is normalized to satisfy:

$$\oint f(g) \, dg \equiv 1, \qquad \text{where } dg = \frac{1}{8\pi} \sin \Phi \, d\Phi \, d\varphi_1 \, d\varphi_2 \qquad (4.2)$$

In the discrete orientation space g (4.1) can be rewritten in the form:

$$C_{ijkl}^{V} = \sum_{n=1}^{N} C_{ijkl} f(g_n) \Delta g_n, \qquad \text{with } \sum_{n=1}^{N} f(g_n) \Delta g_n \equiv 1 \qquad (4.3)$$

Equation (4.3) explicitly defines the elastic constants of polycrystalline aggregate according to the Voigt approximation: an arithmetic mean of the single crystal elastic constants weighted by the ODF. The Reuss approximation of constant stress throughout the textured aggregate can be implemented through the procedure similar to (4.1) and the aggregate elastic constants are obtained if the elastic compliances S_{ijkl} are instead used in the averaging procedure such that:

$$\overline{C}_{ijkl}^{R} = \left[\oint S_{ijkl} f(g) \, dg \right]^{-1} \qquad (4.4)$$

Note that the averaging procedure in (4.4) yields elastic compliances $\overline{S}_{ijkl}^{R}$ that should be inverted into the elastic stiffnesses $\overline{C}_{ijkl}^{R}$. It is particularly important to note that averaging in either the stiffness or the compliance domains (Equations (4.1) and (4.4), respectively) yields different solutions presumably with $\overline{C}_{ijkl}^{V} > \overline{C}_{ijkl} > \overline{C}_{ijkl}^{R}$.

87
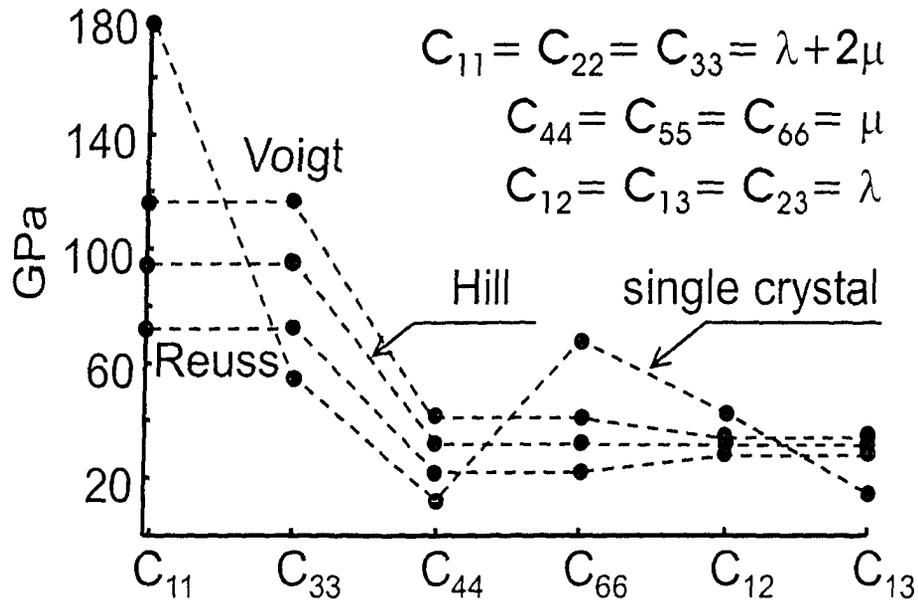
Figure 4.2: Elastic constants of the muscovite single crystal assuming hexagonal symmetry (after *Aleksandrov and Ryzhova* (1961)) and an isotropic polycrystalline aggregate composed of muscovite crystals in the Voigt, the Reuss and the Hill approximations. Elastic constants $C_{11} = C_{33}$ in the Voigt approximation are 160% of those in the Reuss.

Table 4.1: Elastic constants of single muscovite crystal from *Aleksandrov and Ryzhova* (1961), and the isotropic Voigt, Hill and Reuss bounds

Averaging	Elastic constants, GPa					
technique	C_{11}	C_{33}	C_{44}	C_{66}	C_{12}	C_{13}
Single crystal	178.0	54.9	12.2	67.8	42.4	14.5
Voigt	116.3	116.3	41.1	41.1	34.1	34.1
Hill	94.4	94.4	31.6	31.6	31.1	31.1
Reuss	72.5	72.5	22.2	22.2	28.1	28.1

The VR bounds were originally developed for an isotropic medium and generally accepted as the limits to the possible elastic constants to the polycrystalline aggregate (*Hill*, 1952) with the true solution expected at an intermediate value. In the case of the random orientation distribution (i.e. equal probability in all directions) of the constituent anisotropic minerals medium results in an elastically isotropic solid. Perfectly aligned constituent minerals, on the other hand, create a medium with properties the same as the single anisotropic crystal.

Elastically anisotropic shales are usually highly textured (e.g. *Johnston and Christensen*, 1995; *Hornby*, 1998). SEM images of Colorado shale from the Cold Lake region of Alberta (Figure 4.1) show strong clay minerals alignment within the bedding plane. Observed on the SEM images shape orientation distribution provide insight on the lattice preferred orientation for phyllosilicate minerals as the normals to the clay platelets can be considered as a crystallographic normal of basal plane in layer-lattice clay minerals. In such an aggregate both the Voigt and Reuss assumptions of uniform strains and stress, respectively, are violated. Consequently, the elastic properties of textured shales should be unbiased by the VR bounds and lie between the two extreme cases of the single crystal and the isotropic medium. In addition to the broad range of the possible values of elastic constants within the bounds due to presence of texture, there is a large uncertainty in the values of elastic constants even for an isotropic aggregate (Figure 4.2). The separation of the VR bounds at this isotropic limit depends solely on the range of values of the elastic constants of the constituent mineral. For strongly anisotropic single crystals as in the present case of muscovite the isotropic Voigt and Reuss bounds of some of the elastic constants differ substantially. For example, value of isotropic muscovite aggregate $C_{11} = C_{22} = C_{33} = \lambda + 2\mu$ (where λ and μ are *Lamé parameters*) in Figure 4.2 in the Voigt approximation is 160% of those calculated with the Reuss approximation. Therefore, technique of averaging the elastic properties of highly anisotropic solids must be modified to overcome these large uncertainties.

In the Geometric Mean Averaging method a unique solution is obtained independent of whether the averaging is carried out using the stiffnesses or compliances (equations (4.1) and (4.4), respectively). The solution also predominantly lies within the VR bounds. Following *Matthies and Humbert* (1993) the averaged elastic constants of the textured aggregate may be expressed as:

$$\langle \overline{C}_{ij} \rangle = U_{ik}\, exp\,(\mu_k)\, U_{kj} \tag{4.5}$$

where $\langle \overline{C}_{ij} \rangle$ are the Geometric mean averaged elastic constants of the polycrystalline aggregate. The reduced Voigt matrix notation and Einstein summation conventions are assumed here (see *Nye*, 1990). U_{ij} and μ_k are components of two arrays described below. (4.5) may be rewritten in the matrix form:

89

$$\langle \overline{C} \rangle = U \, exp \, (\overline{\Lambda}) \, U^T \qquad (4.6)$$

where U and U^T an orthogonal matrix and its transpose. $\overline{\Lambda}$ is a diagonal matrix composed of the exponents of the eigenvalues μ_k obtained from the eigenvalue decomposition of the matrix $\langle C \rangle$:

$$\langle C \rangle = U \, exp \, (\Lambda) \, U^T \qquad (4.7)$$

where Λ diagonal matrix with the eigenvalues μ_k. Matrix $\langle C \rangle$ results from the ODF averaging procedure:

$$\langle C \rangle = \int W \overline{\Lambda}^0 W^T f(g) \, dg \qquad (4.8)$$

where W and $\overline{\Lambda}^0$ are defined by the eigenvalue decomposition of the elastic constants of the single crystal in the matrix notation C:

$$C = W \Lambda^0 W^T \qquad (4.9)$$

where Λ^0 is diagonal matrix containing eigenvalues μ^0 of the matrix C of the single crystal elastic stiffnesses and W is the orthogonal matrix of eigenvectors. The diagonal matrix $\overline{\Lambda}^0$ used in the averaging procedure in (4.8) is composed of the natural logarithms of the eigenvalues μ^0 of the elastic stiffnesses matrix C that results from (4.9). Equations (4.6)-(4.9) implement *Aleksandrov and Aizenberg's* (1966) concept for an anisotropic solid by averaging the modified eigenvalue functions of the stiffnesses or the compliances rather then directly averaging stiffnesses or compliances. The resulting matrix of elastic constants $\langle \overline{C} \rangle$ in (4.6) is independent of the domain of averaging (i.e. stiffnesses or compliances) and therefore is a unique solution of the ODF averaging procedure.

In order to obtain this unique solution the textural information is incorporated via $f(g)$ (4.8). The ODF $f(g)$ quantitatively describes the texture and may be obtained from the measured pole figures of the distributions of the crystallographic axes of the constituent minerals (*Bunge*, 1982). The number of the pole figures required to fully describe an ODF, in general, depends on both the constituent mineral and the overall rock sample symmetries. Such information is usually obtained from thin-section microscopy or

90

X-ray, neutron diffractions, and *electron back scattering diffraction* (EBSD) techniques (e.g. *Ullemeyer et al.*, 2000). The choice of the texture determination technique depends on the rock type and the purpose of the investigation. *Ullemeyer et al.* (2000) suggested that so-called 'statistical' or 'volume' type texture determination techniques, such as X-ray or neutron diffraction, are most suitable for bulk texture determination and calculations of the elastic properties of rocks.

In shales, a weak bedding-parallel preferred orientation of clay minerals may be developed initially during the depositional process. However, the strong preferred orientation of clay platelets, as can be seen on the SEM images of the Colorado shale (Figure 4.1), most probably develops during the diagenetic transition from smectite to illite (S-I). *Ho et al.* (1999) investigated a depth progression of pelites from the Gulf Coast that were subject to lithostatic stress only. Shallow occurring clay-rich pelites, initially composed of smectite as the predominant authigenic phase, undergo the S-I transition at depth interval of $\sim$ 2100 - 2400m ($\sim T = 83 - 88°$C). A strong bedding normal orientation of packed ($\sim$ 0.1 mm thick) illite minerals develops as a result of this transition. The pore dimensions in the post-transition zone of illite are small (i.e. cannot be observed directly on SEM images) and estimated to be a maximum of a few angstroms from high resolution TEM images. It has to be stressed, however, that the shale sequence investigated by *Ho et al.* (1999) had been removed from their *in situ* fluid rich environment and examined by SEM and TEM, i.e. conditions when pore space would be modified. The main feature of the developed illite texture is strong clay platelets orientation within the bedding plane with normals distributed *quasi*-collinearly to the bedding normal without a specific lateral preferential direction, which is in agreement with the estimates of shale texture by *Hornby et al.* (1994). As such, the orientation distribution $f(g)$ of the constituent clay minerals suggests that the textured clay matrix should statistically have transversely isotropic elastic symmetry.

The ODF $f(g)$ used in the averaging procedure (4.8) carries information about the shale matrix texture and, following *Bunge* (1982), may be expanded into the series of symmetrical generalized spherical harmonics referred to as a *Viglin expansion* (*Viglin*, 1960):

91

$$f(g) = \sum_{l=0}^{\infty} \sum_{m=-l}^{+l} \sum_{n=-l}^{+l} C_l^{mn} T_l^{mn}(g) \tag{4.10}$$

where T_l^{mn} are *generalized spherical harmonics* (GSH) and C_l^{mn} are constants, representing the magnitude of the corresponding harmonic in the expansion. The advantage of the Viglin expansion is that the GSH in (4.10) can be further modified to reflect the specific rock and constituent mineral symmetries via:

$$f_4(g) = \sum_{l=0}^{4} \sum_{\mu=1}^{M(l)} \sum_{\nu=1}^{N(l)} C_l^{\mu\nu} \ddot{T}_l^{\mu\nu}(g) \tag{4.11}$$

where for the case considered in this paper the $\ddot{T}_l^{\mu\nu}$ are *symmetrical generalized spherical harmonics* (SGSH) specially constructed to fulfill both the shales transverse isotropy and the single crystal hexagonal symmetry properties. The $C_l^{\mu\nu}$ are coefficients of the SGSH that carry information about the shale texture and are described below. $M(l)$ is the number of linearly independent spherical harmonics required for a specific symmetry. Note that $f_4(g)$ represents truncation (to the degree $l = 4$) of the infinite expansion series of $f(g)$ (4.10). The maximum degree of the ODF expansion in equation (4.10) corresponds to the order of the tensor that describes the particular physical properties of the rock. The elastic properties of the solid material can be fully described by the 4th order elasticity tensor C_{ijkl} (or S_{ijkl}); consequently the coefficients of the ODF expansion of $l = 4$ are sufficient for the averaging procedure (*Backus*, 1970).

Averaging of the elastic constants by the ODF for transversely isotropic shales with constituent minerals of hexagonal symmetry has been discussed in detail by *Sayers* (1994). He analyzed the anelliptic behaviour of the P-wave slowness surface and showed its dependence on only a single coefficient of the ODF expansion. It must be noted that *Sayers* (1994) development is based on *the Roe formalism* (*Roe*, 1965), which differs from the present development because a different ODF normalization (Equation 4.10) is applied. In addition, in the Roe formalism, the coefficients of the Viglin expansion must be adjusted to accommodate rock and constituent crystal symmetries. In the Bunge formalism (*Bunge*, 1982) adopted here the generalized spherical harmonics reflect both the rock and constituent crystal symmetries (*Ferrari and Johnson*, 1988). For the transversely isotropic

92

aggregate only five coefficients $C_l^{\mu\nu}$ of the expansion (viz. $C_2{}^{11}$, $C_2{}^{21}$, $C_4{}^{11}$, $C_4{}^{21}$, $C_4{}^{31}$) are non-trivial. Furthermore, when the infinite symmetry (i.e. rotational) axis of the TI medium is aligned with the X_3 axis of the right handed $X_1X_2X_3$ shale coordinate system, the coefficients C_2^{21}, C_4^{21} and C_4^{31} vanish (reflecting hexagonal crystal symmetry: $C_l^{\mu\nu} = 0$, if $\mu \geq 1$, Bunge et al. (1981)) and only two coefficients $C_2{}^{11}$ and $C_4{}^{11}$ contribute to the elasticity of the aggregate (cf. with W_{200} and W_{400} in Sayers development). The additional coefficient $C_0{}^{11} \cong 1$ carries an isotropic component in the expansion and must be taken into account.

Following Bunge (1982) the coefficients of the expansion can be written (taking into account the orthonormal properties of the SGSH):

$$C_l^{\mu\nu} = (2l + 1) \int f(g)\, \ddot{T}_l^{*\mu\nu}(g)dg \tag{4.12}$$

In the case of TI - hexagonal symmetries all the SGSH in expansion are real (μ and ν in Equation (4.10) are even) and the complex conjugate symbol '$*$' may be omitted. For aggregates that consist of a single crystal with specific orientation taking into account normalization (4.2) Equation (4.12) can be simplified to:

$$C_l^{\mu\nu} = (2l + 1)\, \ddot{T}_l^{\mu\nu}(g_0) \tag{4.13}$$

where g_0 is an orientation of the aligned single crystal. Calculation of the expansion coefficients $C_l^{\mu\nu}$ can further be simplified if one takes into account that $\ddot{T}_l^{\mu\nu} = P_l^{\mu\nu}$ for $\mu = 1$ and $\nu = 1$, where $P_l^{\mu\nu}(\cos\Phi)$ are the generalized associated Legendre functions (GALF). It should be noted that the GALF are functions of only one Euler angle Φ and the ODF of TI - hexagonal symmetry is independent of the φ_1 and φ_2. Bunge (1982) showed that the GALF can be represented by a Fourier series:

$$P_l^{\mu\nu}(\Phi) = \sum_{s=-l}^{+l} a_l^{\mu\nu s}\, e^{is\Phi} \tag{4.14}$$

where $a_l^{\mu\nu s}$ are Fourier expansion coefficients. For $\mu + \nu$ even (4.14) can be rewritten:

$$P_l^{\mu\nu}(\Phi) = \sum_{s=0}^{+l} a'_l^{\mu\nu s}\, \cos(s\Phi) \tag{4.15}$$

93

coefficients $a'^{\mu\nu s}_l$ were tabulated by *Bunge* (1982) and the coefficients of the SGSH for the ODF consistent of single crystal can finally be written in a simple form of the combination of cosine functions:

$$C_2^{11} = 5(0.25 + 0.75\cos(2\Phi)) \tag{4.16a}$$

$$C_4^{11} = 9(0.140625 + 0.3125\cos(2\Phi) + 0.546875\cos(4\Phi)) \tag{4.16b}$$

4.3 Results and discussion

It has been mentioned above that the elasticity of a solid matrix varies with the texture, and as such one might expect the elasticity to lie between two extreme limiting cases of a perfectly aligned aggregate, which is indistinguishable from the single crystal, and an isotropic aggregate with completely random crystal orientations. The resulting averaged elastic constants are, by definition, dependent on the alignment of the crystalline x_i ($i = 1, 2, 3$) and rock coordinate systems X_j ($j = 1, 2, 3$). For the case of fully aligned crystallites Equation (4.14) describe this dependence and values of the textural coefficients C_2^{11} and C_4^{11} can be directly incorporated into the averaging procedure.

Investigation of the effect of the different averaging procedures on the intrinsic anisotropy of shale as a function of textural strength would provide more insight. If the texture peak of the [001] crystallographic axis of the constituent mineral in aggregate of TI symmetry is aligned with the X_3 axis of the shale coordinate system, then elasticity of such an aggregate will depend only on the elasticity of the single crystal and the strength of the texture. A perfectly aligned aggregate has the elastic properties of a single crystal; all three coefficients of the ODF expansion (viz. C_0^{11}, C_2^{11} and C_4^{11}) are non-zero and contribute to the averaging. The textural peak of the distribution of the [001] crystallographic axis in real shales is not fully aligned but rather distributed around the X_3 bedding normal (*Hornby et al.*, 1994; *Ho et al.*, 1999). This distribution can be approximated by the normal (Gaussian) distribution function characterized by its standard deviations (Figure 4.3). The Gaussian becomes broader as the standard deviation of the normal distribution increases and, eventually, the distribution of the [001] axis can be treated as nearly uniform within the aggregate with no specific preferential orientation and, therefore, re-

94
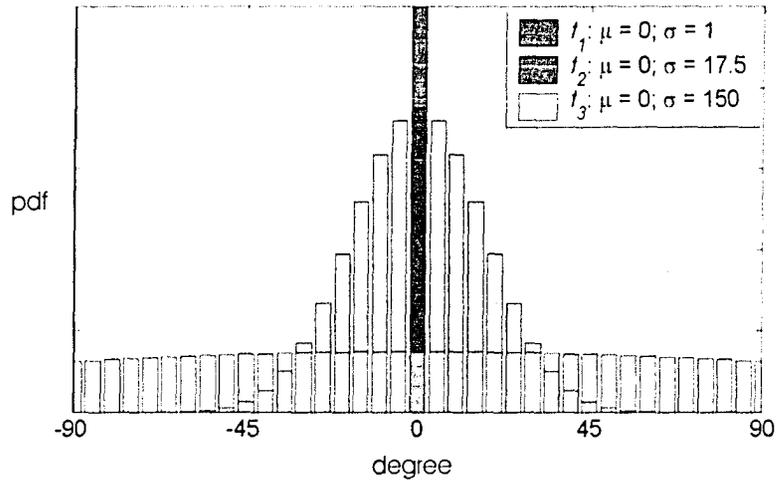
Figure 4.3: Normalized Gaussian distributions with different standard deviations: $\sigma = 1$ represents fully aligned muscovite aggregate with the properties identical to the single crystal; $\sigma = 17.5$ is an intermediate value of standard deviation representative of distribution likely to be observed in textured phyllosilicate aggregate (e.g. clay minerals in shale); and $\sigma = 150$ simulates almost uniform spatial distribution of aggregate with *quasi*-isotropic properties.

semble a random distribution of the crystals. For the random orientation distribution the only non-zero texture coefficient is C_0^{11} (*Bunge*, 1982). By definition $C_0^{11} \equiv 1$ and the averaging of this single coefficient over the elastic stiffnesses yields well-known isotropic solution in the Voigt approximation (e.g. *Simmons and Wang*, 1971). The identical averaging procedure over the elastic compliances yields the isotropic Reuss elastic compliances. Therefore, $C_0^{11} \equiv 1$ can generally be treated as an isotropic part of arbitrary texture that is described by the coefficients C_l^{mn}.

The elastic behaviour of the solid matrix with different degrees of textural alignment is shown in the Figure 4.4. The elastic constants on the left-hand side of the graphs are those for the single crystal limit (marked by XTL) while those on the right-hand side are for an isotropic aggregate (marked by ISO). The Voigt, Reuss, Hill and Geometric Mean Averaging results are all shown for comparison. The Geometric mean averages are close to Hill's, but can lie either above or below it. These results indicate that for an anisotropic solid neither the Voigt, Reuss or Hill approximations uniquely define the elastic proper-
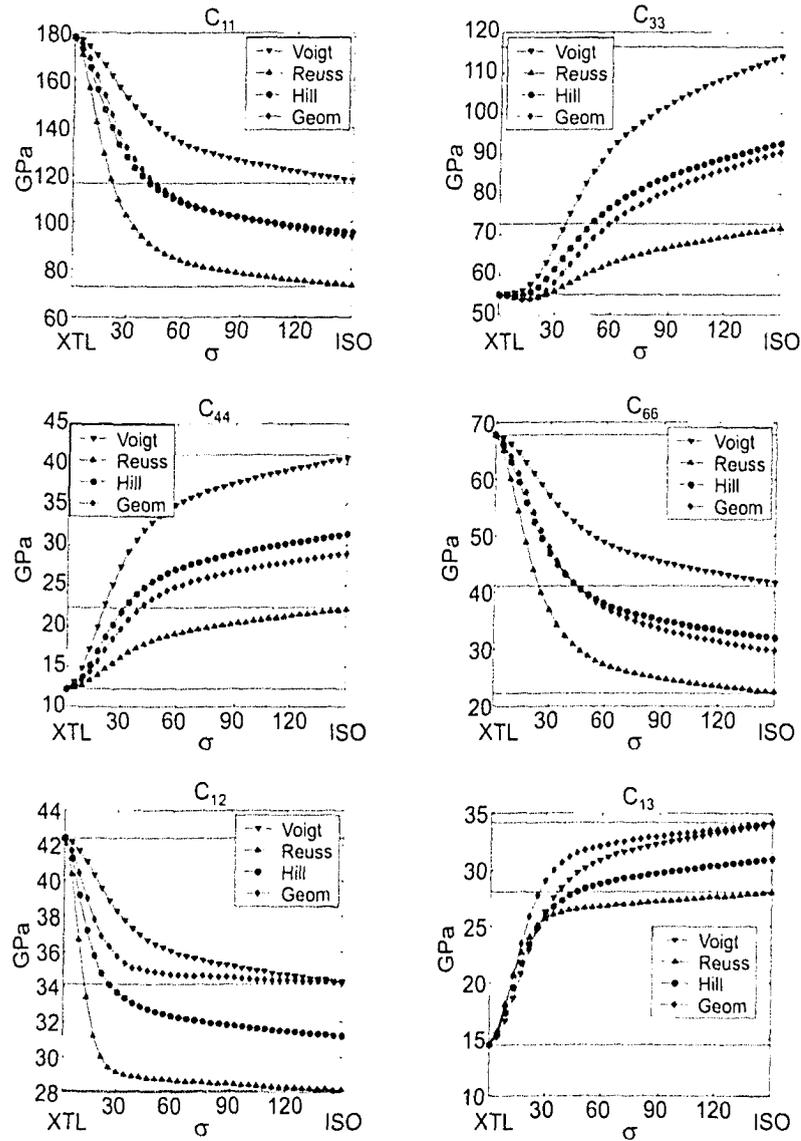
Figure 4.4: Elastic constants of the transversely-isotropic (TI) matrix as a function of textural strength, defined by the standard deviation of the Gaussian distribution σ of clay platelets normals from the shale bedding plane normal (see text for details). Left end of the ordinate axis for each plot represents values of fully aligned polycrystalline with the properties of a single crystal (XTL). Right end represents *quasi* isotropic aggregate (ISO). Solid lines show values of the elastic constants of single crystal and an isotropic Voigt and Reuss solutions.

96

ties of such a medium. The GMA elastic constants of the anisotropic aggregate vary with respect to the VR bounds and may have values close to either upper or lower bound depending on the aggregate strength of texture and the elasticity of the constituent minerals. In other words, if the GMA solution is presumed to provide a more accurate estimate of the polycrystalline aggregate properties, then the elastic constants of textured shale cannot be defined by the values based on the VR assumptions. For instance, elastic constants obtained experimentally from ultrasonic laboratory measurements may be close to either the Voigt, the Reuss or the Hill solutions depending on the particular rock sample texture. To further complicate matters, proximity to either Voigt, Reuss or Hill approximation differs from constant to constant in anisotropic solid. This may be reflected in experiment by values of elastic constants inferred from the ultrasonic measurements of velocity of specific mode of elastic wave in particular direction of propagation to lie either below or above Hill approximation.

The importance of this result is that it shows that the rigid constraints of the Hill approximation with respect to the VR bounds might not be very suitable for accommodating elastic behaviour of such anisotropic solids. Values of the elastic constants (viz. C_{12} and C_{13}) for a particular range of textural strengths do not even necessarily lie within the traditional VR bounds. Notice also that the Voigt and Reuss values even cross for a certain range of σ for C_{13} coefficient (Figure 4.4) and therefore for this case they cannot be treated as bounds *per se*.

The values of elastic constants are fundamental and completely describe a solids' elasticity. Elastic properties of the weakly anisotropic medium, however, can be characterized by anisotropic parameters. In general, parameterizations are designed to simplify the description of complex anisotropic elastic behaviour of materials and reduce the number of initially unknown coefficients responsible for anisotropy. It should, however, be stressed that parameterization of anisotropic medium should not aim to replace more fundamental elastic constants but rather to assist in the description of the elastic wave behaviour for specific cases when it is applicable. For a transversely isotropic medium *Thomsen* (1986) introduced three anisotropic parameters ε, δ and γ to describe the behaviour of P, SV and SH modes of elastic wave. For completeness, these parameters are calculated from the elastic constants of Figure 4.4. and plotted as a function of the
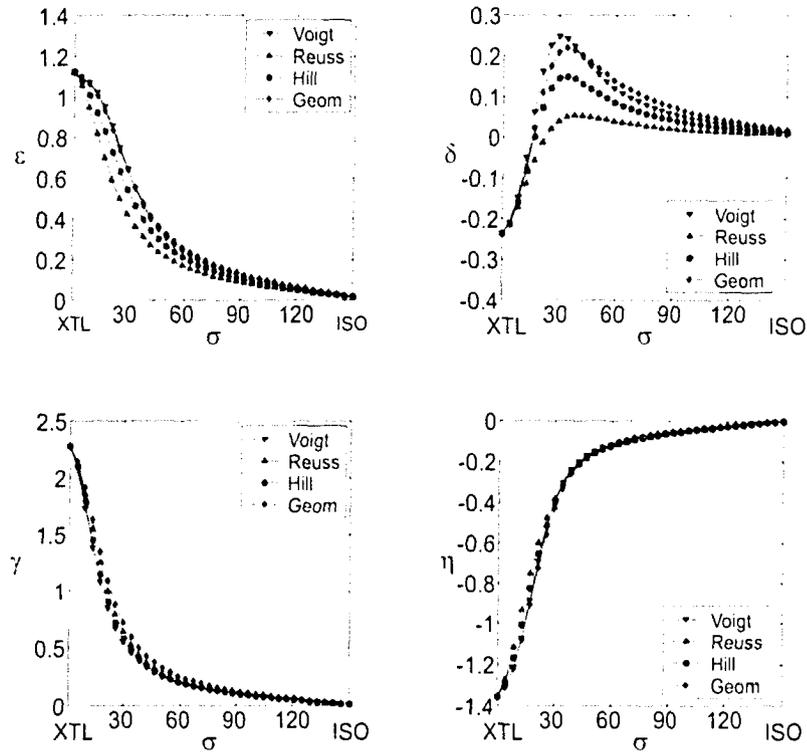
Figure 4.5: Anisotropic parameters for transversely-isotropic (TI) medium as a function of textural strength (same as Figure 4.4). All parameters approach zero for an isotropic aggregate. Notice dependence of ε and, especially, δ on the averaging procedure. Anellipticity (η) values are very close for all approximations.

strength of texture on Figure 4.5. Both, ε and γ behave similarly and decay from the maximum single crystal value to zero for the isotropic aggregate as expected. It is interesting to note that the different averaging approximations insignificantly affect these anisotropic parameters, except for a certain range of values of ε (corresponding to highly textured aggregate).

The parameter δ has rather vague physical meaning but it reflects the P-wave phase velocity dependence on the direction in the vicinity of the vertical incidence angle. It has a more complex behaviour (Figure 4.5) being negative for the single crystal, but increasing to at least the same positive value before eventually decaying towards zero for the quasi-isotropic aggregate. It is interesting to note that for a certain range of textural strengths, δ is sensitive to the averaging method with the Voigt values several times those

98
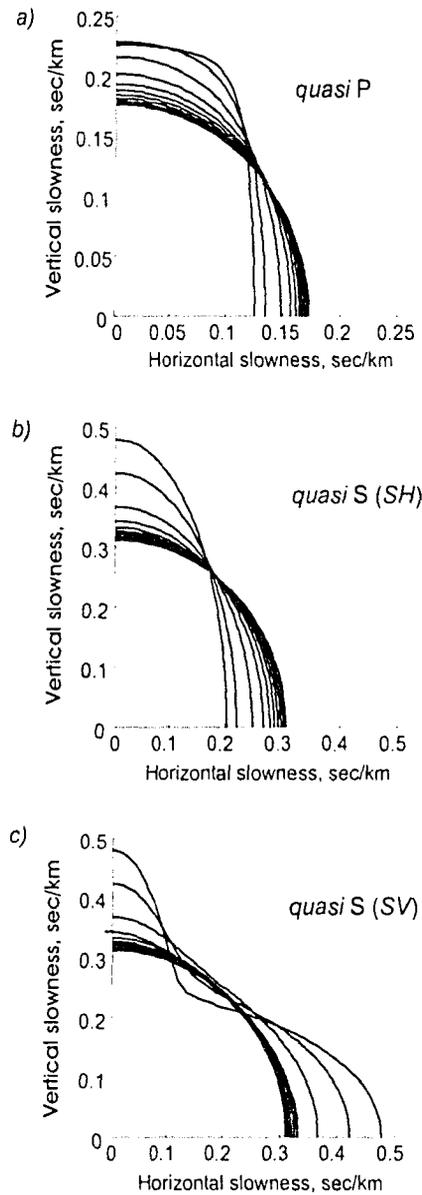
Figure 4.6: Slowness surfaces for qP and qS (SH and SV) waves for intrinsically anisotropic shale of TI symmetry calculated from the elastic constants obtained by the GMA procedure and shown in the Figure 4.4. Slowness surfaces vary from highly anisotropic for a single crystal to almost circular for $quasi$-isotropic aggregate.

99

for the Reuss.

Anellipticity characterizes the deviation of the P-wave slowness surface from elliptical. *Gassmann* (1964) showed that the elliptical behaviour of P-wave slowness surface can be characterized by parameter $A = (C_{13} + C_{44})^2 - (C_{11} - C_{44})(C_{33} - C_{44})$. P-wave slowness surface is elliptical for $A = 0$. This condition occurs in TI medium for $\varepsilon = \delta$ (*Thomsen*, 1986). By defining anellipticity as $\eta = \delta - \varepsilon$ (cf. *Sayers*, 1995; *Alkhalifah and Tsvankin*, 1995), η relates to A as $\eta = A/2C_{33}(C_{33} - C_{44})$ and vanishes for an elliptical slowness surface.

The resulting curves of η for the Voigt, Reuss, Hill, and GMA averages all yield nearly the same value of anellipticity as shown in Figure 4.5. Despite the fact that the various averaging procedures give different absolute values of the elastic constants, the overall behaviour of the elastic waves (especially anellipticity) predicted by these approximations is similar.

Finally, solving the *Christoffel's equation* (e.g. *Musgrave*, 1970) for a set of elastic constants obtained from the GMA procedure elastic wave slowness surfaces has been calculated and plotted on Figure 4.6. The initial highly anisotropic slownesses for the textured aggregates approach circular slowness surfaces for the *quasi*-isotropic aggregate. The P slownesses are generally anelliptic while those of SH mode are always elliptical in a TI medium. The P and S vertical velocities for intrinsically anisotropic shales are always less than those for the corresponding isotropic aggregate.

Phase velocity surfaces resulted from the solution of the Christoffel equation for all wavefront propagation directions within the symmetry planes are shown on Figure 4.7. Phase velocity surfaces are normalized in order to be comparable with those of the Chattanooga Shale (*Johnston and Christensen*, 1995). Chattanooga Shale elastic constants were obtained from the laboratory ultrasonic measurements at a confining pressure of 50 MPa and reflect mainly the intrinsic properties of the shale predominantly composed of il-lite (*Johnston and Christensen*, 1995). The experimentally observed P-wave anisotropy of Chattanooga Shale can be explained on the basis of intrinsic anisotropy and attributed to textural shale properties, which is in agreement with *Johnston and Christensen's* (1995) conclusions. The calculated and measured shear wave surfaces have very similar elastic behaviour with the higher calculated intrinsic anisotropy of shear waves due to relatively

100
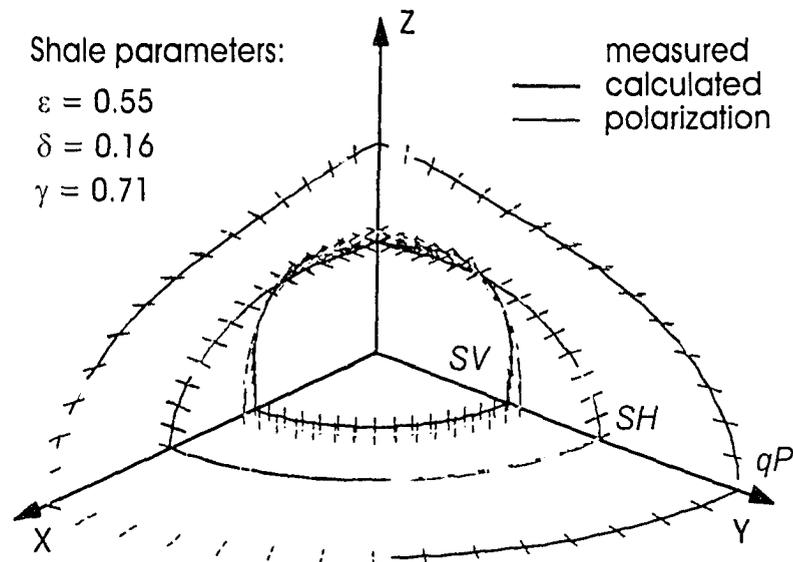
Figure 4.7: Normalized phase velocity surfaces (qP and qS (SH and SV)) and polarization directions of the modelled intrinsically anisotropic shale matrix compared with phase velocity surfaces of the Chattanooga Shale that have been calculated from the elastic constants obtained from the laboratory measurements at confining pressure of 50 MPa (see *Johnston and Christensen* (1995)).

low value of the modelled C_{44} elastic constant.

The modelling presented here is based on several assumptions that include the shales mineralogical composition, the elasticity of the constituent minerals and their orientations. These assumptions may not hold in more realistic shales and the consequences of these approximations must be discussed. First, knowledge about the true elasticity of the constituent clay minerals (i.e. illite, chlorite, kaolinite and montmorillonite) will be essential for proper modelling of the intrinsic elasticity and, subsequently, determining the seismic velocities of shales. Elastic constants of constituent minerals predefine intrinsic elasticity of the highly textured aggregates and influence the absolute values of the elastic constants in *quasi*-isotropic aggregates with randomly oriented minerals. Second, various clay minerals will have different elastic behaviours and levels of anisotropy (cf. differences between the elasticity of the micas biotite and muscovite) and should be treated separately in the calculations. Furthermore, the clay only assumption is violated, as considerable amounts of less anisotropic mineral phases (silt) are present in real

101

shales. Substantial amounts of randomly oriented quartz, calcite or pyrite grains (as can be seen on Figure 4.1b) first affect the clay mineral distribution by interfering with their alignment and second increase the volumetrically weighted isotropic components in the matrix. The presence of additional phases with different physical properties in shales would only enhance fluctuations of both stress and strain within solid making the solution further deviate from either of the VR bounds. The assumptions of either uniform strain or stress are violated in such aggregates and the solutions obtained on their basis are erroneous.

As has been shown the intrinsic elasticity of monomineralic muscovite aggregate is significantly influenced by texture. The degree of the clay platelet alignment (i.e. texture strength) varies substantially in shales and depends on several factors such as the state of compaction (i.e. function of depth) and maturation (e.g. *Vernik and Liu*, 1997; *Hornby*, 1998) and diagenetic processes (*Ho et al.*, 1999). Intrinsic elastic anisotropy may vary from high anisotropy for perfectly aligned clay aggregates to *quasi*-isotropic for the case of almost randomly distributed clay platelets orientation. A further assumption of no lateral preferences in the orientation of normals of the clay platelets is usually made. Under this assumption the matrix composed of hexagonal crystals has TI statistical symmetry. Knowledge about the hexagonal symmetry of the constituent minerals and the TI symmetry of the matrix allows the number of independent coefficients in the ODF expansion to be reduced. The assumption of no preferred lateral orientation may not hold in the presence of additional textural features such as microfolding caused by the tectonic stresses, which may lower the statistical intrinsic elastic symmetry from TI to orthotropic or lower.

Finally, the overall elasticity of shales (especially in the fluid-rich conditions) depends not only on its intrinsic properties but also on the presence of oriented microcracks (e.g. *Vernik*, 1993), the amount of the fluid-filled porosity (e.g. *Hornby*, 1998) and the *in situ* distribution of stresses (*Sayers*, 1999), i.e. factors that may significantly influence anisotropy and cannot be ignored. Models that incorporate these factors would, however, benefit by starting from the intrinsically anisotropic matrix.

4.4 Conclusions

The intrinsic elasticity of shales has been estimated by the Orientation Distribution Function (ODF) averaging of the elastic constants of muscovite, a mica structurally similar to illite. The generally accepted approximations based on the assumptions of uniform strain and stress within the solid matrix yield, correspondingly, the Voigt and the Reuss averaging solutions. The VR bounds are widely separated which allows significant variation in the values of intrinsic elastic constants of shales. To overcome this limitation, *the Geometric Mean Averaging* (GMA) method has been developed and appklied for first time for aggregate of TI-hexagonal symmetry and incorporated into the ODF averaging procedure. The GMA provides a solution fulfilling the requirement of invertibility between aggregate stiffnesses and compliances. This solution lies predominantly relatively close to the Hill average within the VR bounds for the diagonal elastic constants (Figure 4.4). The purpose of implementation of the GMA solution was to examine the effect of the texture strength *per se* on the elasticity of solid matrix. In case of textured muscovite aggregate, the Voigt and Reuss bounds progressively diverge as the crystals become more randomly oriented. The GMA results vary with respect to the VR bounds (cf. the Hill solution). This implies that neither the Voigt, the Reuss or the Hill approximation uniquely define the elasticity of highly anisotropic aggregates; the elastic constants of an anisotropic solid obtained by GMA method may lie close to any of these solutions depending on the values of the elastic constants of the constituent minerals and aggregate texture. The GMA solution is constrained by physically meaningful requirement of the invertibility of stiffnesses to compliances.

Results of different volume averaging techniques (viz. the Voigt, the Reuss, the Hill and the GMA) show that absolute values of elastic constants of textured muscovite aggregate, and, consequently, shales depend on the averaging assumptions. Unexpectedly, however, anisotropic parameters are less influenced by the choice of the averaging technique (Figure 4.5), i.e. GMA solution is close to the VRH results. Consequently, while the choice of the averaging technique is essential for proper estimation of the absolute values of the elastic constants (and, eventually, wave velocities), it is less significant when describing the behaviour of the elastic velocities. Slowness surfaces calculated from the

103

GMA elastic constants show significant anellipticity of P-wave surface for highly textured muscovite aggregate. In addition, it is clear that axial P- and S- velocities of textured aggregate with VTI symmetry are always slower than those of isotropic one.

Chapter 5

Discussion and Conclusions

This thesis deals with elastic properties of different types of intrinsically anisotropic rocks. Both experimental measurements and modelling techniques are considered here. Three Chapters of the thesis consider different types of rocks that exhibit intrinsic anisotropy. Each Chapter has Discussion and Conclusions section that addresses specific issues related to particular rock type. Conclusion sections of each Chapter cover topics of laboratory measurements of intrinsic elastic properties of rocks, modelling elastic constants and anisotropic parameters as a function of rock's texture, and discussion of advantages of application of the geometric mean averaging (GMA) technique, developed in the thesis, for specific rock symmetries.

In this concluding part of the thesis the main implications of the above studies to the understanding of the overall elasticity of intrinsically anisotropic rocks are discussed along with related problems. Conclusions and general outlook on the topic of intrinsic elasticity of rocks with directions for future research are also provided.

5.1   Some aspects of experimental measurements

Results of experimental laboratory measurements of ultrasonic elastic velocities of metamorphosed rocks are discussed in details in Chapter 2. Two collections of rocks from the Flin Flon Belt (FFB) of Trans-Hudson Orogen (THO) were investigated and results of this study are summarized in the Chapter 2. Rocks were selected along two profiles that correspond on the surface to the strong inclined reflections of the LITHOPROBE THO seismic profile 9. Outcrop samples classified as metavolcanics and metasediments, dis-

105

play strong, in most cases visible texture. Samples of plutonic rocks were also selected for this study. Core samples were cut from the hand specimens following their visible textural properties.

Ultrasonic velocity measurements of P- and two S-waves reveal velocity anisotropy and shear-wave splitting. Metasediments and metavolcanics exhibit strong anisotropy (up to 24%) while the plutonic rocks were characterized as *quasi* isotropic.

Implementation of the 'time of flight' type of laboratory velocity measurements (see Appendix A for more details and discussion on different experimental techniques) suffers from the directional dependency of the velocity measurements, and allowed determination of only the diagonal constants of the elasticity matrix. Even though incomplete, this set of elastic constants provide useful insights on the symmetries of investigated rocks. Two anisotropic parameters ε and γ were calculated from the elastic constants and listed for comparison. Based on the values of the obtained elastic constants and the pattern of shear wave splitting, both transversely isotropic and orthorhombic elastic symmetries were identified. Rocks with weak or inconsistent variations in velocities (mainly plutonic rocks) were considered as *quasi* isotropic. In addition to anisotropy, heterogeneity (on the scale of laboratory measurements) was observed.

Ultrasonic velocities were measured for confining pressure of up to 300 MPa. Measured anisotropy was attributed to intrinsic rocks properties, i.e. texture. This conclusion is inferred from the weak and almost linear dependency of measured velocities on confining pressure. At confining pressure exceeding 100 MPa most of the rock's fluid-free cracks and micropore voids were assumed to be closed and have no significant effect on measured velocity values. Observation of weak (if any) changes in anisotropy and shear wave splitting for investigated rocks suggest no strong effect of cracks on measured velocities at higher pressures. Results of this study demonstrate that metamorphosed rocks of the FFB exhibit a strong intrinsic P-wave anisotropy and shear-wave splitting. Whether this anisotropy can be considered in broader content as a source of observed reflectivity in the FFB remains to be seen. Plot of velocity versus density for the investigated rocks suggest some weak separation of impedances for the plutonic rocks and metasediments. However, upscaled seismic experiments (e.g. vertical seismic profiling) are needed to overcome laboratory uncertainties due to heterogeneities and statistical

uncertainties of sample representations.

This study has demonstrated advantages as well as drawbacks of the currently used experimental technique. Robustness and reliability of this type of laboratory measurements allow for high accuracy of the determination of elastic constants to be achieved and infer intrinsic origin of observed anisotropy. The directional dependence of the measurements, however, imposes requirements that a sufficient number of core samples be used to obtain full set of elastic constants.

The advantages and disadvantages of different experimental techniques currently used to obtain full set of elastic constants are discussed in the Appendix A. The choice of suitable experimental technique to study intrinsic elasticity of rocks also depends on the rock type, and the volumetric abundance, the homogeneity and the physical conditions of available specimens.

5.2 Some aspects of modelling techniques

The purpose of the modelling techniques employed in the thesis Chapters 3 and 4 is to investigate elastic properties of selected rocks as a function of texture. In Chapter 3 the Voigt and the Reuss averaging techniques were developed to employ the orientation distribution function (ODF) for specific case of orthotropic-orthorhombic symmetry applied to an olivine aggregate. This new development was further extended to incorporate the GMA method. Chapter 3 deals mainly with the effect of different averaging techniques on elastic properties of textured aggregate with application to olivine aggregates of orthotropic symmetry.

In Chapter 4 the same techniques are employed to phyllosilicate aggregates. Simpler aggregate texture reflected by transversely isotropic elastic symmetry allowed not only investigate effect of the averaging techniques (the Voigt, the Reuss, and the GMA) on values of elastic constants but also fully investigate effect of strength of the aggregate texture on the overall elasticity. This investigation was implemented by developing hypothetical textures and calculating elastic properties of muscovite aggregate from isotropic (randomly oriented) to highly aligned aggregate with the properties of single aggregate. Results of this study were implemented to discuss the effect of intrinsic anisotropy on the

107

elasticity of shales.

In all three studies intrinsic anisotropy plays an essential role in rocks elastic properties. These properties can be estimated by means of forward modelling, i.e. employment of available information on the elasticity of constituent minerals and textural (spatial) distribution of crystals within aggregate to calculate its elastic properties. In order to complete information needed for forward modelling, distribution of stress and strain within the aggregate is also required. It can be obtained with certain level of accuracy by numerical calculations of stresses considering orientations, shapes of grains and boundary conditions. Although applicable for specific cases and geometries, this approach is too computationally expensive for most practical purposes. Alternatively, the state of stress or strain in an aggregate may be assumed, e.g. Voigt's assumption of uniform strain or Reuss's of uniform stress. One of the main objectives of this study was to estimate the effect of these assumptions on results of modelling intrinsic elasticity. It has been shown that in the case of a textured olivine aggregate the averaging assumption has no significant effect on the aggregate elastic constants (variations are within few percent). Textural information *in this case* has a much stronger effect on the calculated aggregate elasticity.

Conversely, in the case of modelling elasticity of phyllosilicate aggregates (Chapter 4) the averaging assumptions have very significant effect on the values of elastic constants. This effect can be as strong as the influence of the texture on the aggregates elasticity. Therefore, special consideration is needed on the choice of assumptions for the averaging techniques to model intrinsic elasticity of a phyllosilicate aggregate. The GMA technique was developed and applied for first time to the rocks with different symmetries. The geometric mean averaging (GMA) is recommended to be used as it does not depend on the assumptions about stress or strain. Instead, in the GMA the averaging operator is modified by mathematical manipulations to reflect essential requirement of invertibility of modelled physical property. Implying elasticity this means that averaging of either stiffnesses or compliances provide identical result.

This improvement achieved in the GMA through the implementation of a more sophisticated averaging operator. Application of the GMA averaging operator, however, has its drawbacks. Most importantly, the averaging operation in the GMA is realized in the logarithmic domain, i.e. the exponents of the eigenvalues of the elasticity matrix are

averaged instead of direct averaging of the elastic constants. This modification, providing an identical solution for both the stiffnesses and the compliances, makes, however, the GMA more sensitive to the values of averaging coefficients obtained in turns from the aggregate textural properties (the ODF). In other words, the accuracy of textural information (obtained experimentally or by modelling) becomes essential for accurate modelling of elastic constants using the GMA.

Comparing application of averaging techniques on investigated two types of rocks it is obvious that the same assumptions have different effect on the rocks elasticity. For the olivine aggregate the different averaging techniques provide similar results, and the elasticity is mainly affected by the textural properties of the aggregate. In contrast, for the phyllosilicate aggregate the different averaging techniques produce distinct results and have a significant effect comparable with textural one. For rocks composed predominantly of phyllosilicate minerals, e.g. shales, justification of appropriate averaging technique become *critically* important in order to obtain reliable modelling accuracy. The GMA technique, independent of the assumptions on the state of stress or strain within aggregate, appears to be preferable in this case as it provides a unique solution.

It has been previously discussed in the thesis that different methodologies can be used to model elasticity of rocks. Techniques based on volume weighted averaging remains the most popular and widely used for practical applications. Besides being straightforward in implementation they generally provide results with the acceptable level of accuracy for the most geophysical cases. This can be due to the rock type, as was discussed in Chapter 3 when textural properties have stronger effect on the elasticity of olivine aggregate than the choice of the averaging technique.

The averaging techniques are widely applied in Geophysics despite criticism with regard to the lack of model complexity and limited flexibility for inputs of model parameters (i.e. lack of considerations for local (on grain scale) stress and strain distributions and absence of explicit implementation of the boundary conditions). One of the reasons for this persistent use of averaging techniques (e.g. the Voigt and the Reuss) in Geophysics might be a limitation of the accuracy of model due to remote nature of geophysical measurements. Even laboratory samples are difficult to properly characterize. Even though the elasticity of rocks is a forward modelling problem with a unique

109

solution that may, in theory, be calculated with any order of accuracy, if necessary detailed description of model is provided (*Kröner*, 1977), it has never been accomplished in reality for complex multiphase textured rocks. Although the desired accuracy of the experimental measurements or forward modelling results may be achieved for a specific rock sample, assumptions usually made on implementations of these results due to the fact that geophysicists deal with complex geological media that are not uniform and homogeneous, and eventually requires some level of generalization (i.e. averaging). An example of complexity of this problem is comparison of laboratory measurements to seismological observation know also as *the scaling problem*. Complications such as statistical representability of laboratory results, seismic wave dispersion and heterogeneities introduce an error much greater than that of averaging results on a sample level. Therefore effort for ultimate accuracy of modelling techniques should also reflect the need for more accurate representation of the complex geological medium. There is no particular reason to believe that calculated high accuracy properties of a rock sample will not reflect a localized effect of the geological medium and lead to erroneous assumption if extended to greater scale without detailed statistical justification. Furthermore, due to band-limited nature of useful signal recovered in seismological studies, the seismic wave itself is sensitive only to the impedance contrast of certain adjacent layers of the medium and resolves specific features depending on predominant frequency. For instance, elastic wave resolution is limited even for high frequency ultrasonic laboratory experiments.

5.3 Directions for future research

The elasticity of solid materials is a mature and well developed area of Solid State Physics and application of its methods in Rock Physics is becoming increasingly popular with the growing demand for accuracy in determining elastic properties of investigated rocks and in better understanding the causes of seismic anisotropy. This demand originates from increasing need for more realistic and accurate description of geological medium as some old assumptions, e.g. isotropy, no longer satisfy these needs. The significant interest in anisotropy of seismic waves is one of many examples of present day efforts to provide more sophisticated descriptions of complex geological media and developed

new methodologies of remote sensing of their physical properties. Dealing with the intrinsic anisotropy of rocks the scope of this thesis covers only a small fraction of the wide range of topics described by the term *elastic waves anisotropy*. Furthermore, there are variety of topics within intrinsic anisotropy that need more detailed investigation in future. The biggest one is an extension of algorithms developed for monomineralic polycrystalline aggregates to multiphase polycrystalline aggregates as more realistic model for a majority of rocks.

Application of similar studies on modelling intrinsic elasticity to wider range of rocks in combination with results of laboratory measurements will provide further insights on complicated and challenging topic of the elasticity of rocks.

Overall, it has been shown that intrinsic anisotropy significantly affects the elastic properties of textured rocks and is a major source of observed velocity anisotropy for the types of rocks investigated in the thesis.

Present day experimental techniques allow determination of the full set of elastic constants. Pressure dependent measurements allow discrimination between different sources of seismic anisotropy, and estimation of the effect of intrinsic anisotropy.

Forward modelling provides insights on elastic behaviour as a function of texture. Complicated justification of the choice of the averaging assumption of particular averaging technique can be avoided by using the GMA. However, further research on extended range of intrinsically anisotropic rocks and experimental confirmations are required to justify its wider application.

Bibliography

Ahrens, T. J., 1995, *Rock Physics & Phase Relations: a handbook of physical properties*, vol. 3 of *AGU Reference Shelf*, AGU, Washington, D.C.

Aki, K., and P. G. Richards, 2002, *Quantitative Seismology*, second ed., University Science Books, Sausalito, California.

Aleksandrov, K., and G. Prodayvoda, 1994, The study of elastic symmetry and anisotropy of elastic body waves in gneiss, *Geophys. J. Int.*, *119*, 715–728.

Aleksandrov, K. S., and L. A. Aizenberg, 1966, Method of calculating physical constants of polycrystalline materials, *Dokl. Akad. Nauk SSSR*, *167*, 1028–1031.

Aleksandrov, K. S., and T. V. Ryzhova, 1961, The elastic properties of crystals, *Sov. Phys. - Cryst.*, *6*, 228–252.

Alexandrov, K. S., and T. V. Ryzhova, 1961a, The elastic properties of rock-forming minerals. Pyroxenes and amphiboles, *Bull. (Izv.) USSR Acad. Sci., Geophys. Ser.*, *9*, 871–875.

Alexandrov, K. S., and T. V. Ryzhova, 1961b, Elastic properties of rock-forming minerals. ii. Layered silicates, *Bull. (Izv.) USSR Acad. Sci., Geophys. Ser.*, *12*, 1165–1168.

Alkhalifah, T., and I. Tsvankin, 1995, Velocity analysis for transversely isotropic media, *Geophysics*, *60*, 1550–1566.

Arts, R. J., P. N. J. Rasolofosaon, and D. E. Zinszner, 1991, Complete inversion of the anisotropic elastic tensor in rocks: experiment versus theory, in *61st annual International Meeting SEG, Expended Abstracts*, pp. 1538–1541.

Arts, R. J., P. N. J. Rasolofosaon, and B. E. Zinszner, 1996, Experimental and theoretical tools for characterizing anisotropy due to mechanical defects in rocks under varying pore and confining pressures, in *Seismic anisotropy*, edited by E. Fjaer, R. M. Holt, and J. S. Rathore, pp. 384–432, SEG, Tulsa.

Ashton, K., K. Wheatley, K. H. Wilcox, D. Paul, D. Moser, and J. de Taube, 1988, Geology, Wildnest Lake area, Saskatchewan, *Geological survey of Canada, Open file*.

Auld, B., 1990, *Acoustic fields and waves in solids*, John Wiley and Sons, Inc., New York.

Ave'Lalliemant, H. G., and N. L. Carter, 1970, Syntectonic recrystallization of olivine and modes of flow in the upper mantle, *Geol. Soc. Am. Bull.*, *81*, 2203–2220.

112

Babuška, V., 1972, Elasticity and anisotropy of dunite and bronzite, *J. Geophys. Res.*, 77, 6955–6965.

Babuška, V., 1981, Anisotropy of V_p and V_s in rock-forming minerals, *J. Geophys.*, 50, 1–6.

Babuška, V., 1984, P-wave velocity anisotropy in crystalline rocks, *Geophys. J. R. astr. Soc.*, 76, 113–119.

Babuška, V., and M. Cara, 1991, *Seismic Anisotropy in the Earth*, vol. 10 of *Modern Approaches in Geophysics*, Kluwer Academic Publishers, Dordrecht/Boston/London.

Babuška, V., and J. Plomerova, 2001, Subcrustal lithosphere around the Saxothuringian-Moldanubian Suture Zone - a model derived from anisotropy of seismic wave velocities, *Tectonophysics*, 332, 185–199.

Babuška, V., and Z. Pros, 1984, Velocity anisotropy an granodiorite and quartzite due to the distribution of microcracks, *Geophys. J. R. astr. Soc.*, 76, 121–127.

Babuška, V., J. Plomerova, and J. Sileny, 1993, Models of seismic anisotropy in the deep continental lithosphere, *Phys. Earth Planet. Inter.*, 78, 167–191.

Babuška, V., J. P. Montagner, J. Plomerova, and N. Girardin, 1998, Age - dependent large - scale fabric of the mantle lithosphere as derived from surface - wave velocity anisotropy, *Pure appl. geophys.*, 151, 257–280.

Backus, G., 1962, Long-wave elastic anisotropy produced by horizontal layering, *J. Geophys. Res.*, 67, 4427–4440.

Backus, G., 1970, A geometrical picture of anisotropic elastic tensors, *Rev. Geoph. Space Phys.*, 8, 633 – 671.

Bamford, D., 1977, P_n velocity anisotropy in a continental upper mantle, *Geophys. J. R. astr. Soc.*, 49, 29–48.

Banik, N., 1984, Velocity anisotropy of shales and depth estimation in the North Sea basin, *Geophysics*, 49, 1411–1420.

Barruol, G., and H. Kern, 1996, Seismic anisotropy and shear-wave splitting in lower-crustal and upper-mantle rocks from the Ivrea Zone - experimental and calculated data, *Phys. Earth Planet. Int.*, 1996, 175–194.

Barruol, G., and D. Mainprice, 1993, A quantitative evaluation of the contribution of the crustal rocks to the shear-wave splitting of the teleseismic SKS waves, *Phys. Earth Planet. Inter.*, 78, 281–300.

Bass, J. D., 1995, Elasticity of Minerals, Glasses, and Melts, in *Mineral Physics and Crystallography: A Handbook of Physical Constants*, vol. 2 of *AGU Reference Shelf*, pp. 45–63, AGU.

Ben Ismaïl, W., and D. Mainprice, 1998, An olivine fabric database: an overview of upper mantle fabric and seismic anisotropy, *Tectonophysics*, 296, 145–157.

Berryman, J. G., 1979, Long-wave elastic anisotropy in transversely isotropic media, *Geophysics*, 44, 896–917.

Berryman, J. G., 1995, Mixture theories for rock properties, in *Rock physics and phase relations: A Handbook for physical constants*, edited by T. J. Ahrens, vol. 3, pp. 205-228, AGU, Washington, D.C.

Birch, F., 1960, The velocity of compressional waves in rocks to 10 kilobars, part 1, *J. Geophys. Res., 65*, 1083-1102.

Boullier, A. M., and A. Nicolas, 1975, Classification of texture and fabrics of peridotite xenoliths from south african kimberlites, *Phys. Chem. Earth, 9*, 467-475.

Brosch, F. J., K. Schachner, M. Blumel, A. Fasching, and H. Fritz, 2000, Preliminary investigation results on fabrics and related physical properties of an anisotropic gneiss, *J. Struct. Geol., 22*, 1773-1787.

Budiansky, B., 1965, On the elastic moduli of some heterogeneous materials, *J. Mech. Phys. Solids, 13*, 223-227.

Budiansky, B., and R. J. O'Connell, Elastic moduli of a cracked solid, *International Journal of Solids and Structures, 12*, 81-97.

Bunge, H. J., 1974, The effective elastic constants of textured polycrystals in second order approximation, *Kristall und Technik, 9*, 413-424.

Bunge, H. J., 1981, Fabric analysis by orientation distribution functions, *Tectonophysics, 78*, 1-21.

Bunge, H.-J., 1982, *Texture analysis in material science*, Butterworths, London.

Bunge, H.-J., C. Esling, and J. Muller, 1981, The influence of crustal and sample symmetries on the orientation distribution function of the crystalline materials, *Acta Crystallogr., A37*, 889-899.

Burke, M. M., and D. M. Fountain, 1990, Seismic properties of rocks from an exposure of extended continental crust - new laboratory measurements from the Ivrea Zone, *Tectonophysics, 182*, 119-146.

Burlini, L., and D. M. Fountain, 1993, Seismic anisotropy of metapelites from the Ivrea - Verbano zone and Serie dei Laghi (northern Italy), *Phys. Earth Planet. Inter., 78*, 301-317.

Burlini, L., and K. Kunze, 2000, Fabric and seismic properties of carrara marble mylonite, *Phys. Chem. Earth (A), 25*, 133-139.

Byun, B. S., 1984, Seismic parameters for transversely isotropic media, *Geophysics, 49*, 1908-1914.

Carter, N. L., D. W. Baker, and R. P. J. George, 1972, Seismic anisotropy, flow, and constitution of the upper mantle, in *Flow and fracture of rocks*, edited by H. C. Heard, I. Y. Borg, N. L. Carter, and C. B. Raleigh, vol. 16 of *Geophysical monograph*, pp. 167-190, AGU, Washington, D. C.

Chastel, Y. B., P. R. Dawson, H. R. Wenk, and K. Bennett, 1993, Anisotropic convection with implementations for the upper mantle, *J. Geophys. Res., 98*, 17,757-17,771.

Cheadle, S. P., R. J. Brown, and D. C. Lawton, 1991, Orthorhombic anisotropy: a physical seismic modeling study, *Geophysics, 56,* 1603–1613.

Cholach, P. Y., and D. R. Schmitt, 2003, Seismic anisotropy of shales, *CSEG Recorder, 28,* 39–43.

Cholach, P. Y., J. B. Molyneux, and D. R. Schmitt, 2004, Flin Flon Belt seismic anisotropy: elastic symmetry, heterogeneity, and shear wave splitting, *Can. J. Earth Sci., accepted for publication,* LITHOPROBE publication number: 1387.

Christensen, N. I., 1966, Elasticity of ultrabasic rocks, *J. Geophys. Res., 71,* 5921–5931.

Christensen, N. I., 1971, Fabric, seismic anisotropy, and tectonic history of the Twin Sisters dunite, Washington, *Geol. Soc. Am. Bull., 82,* 1681–1694.

Christensen, N. I., 1984, The magnitude, symmetry and origin of upper mantle anisotropy based on fabric analyses of ultramafic tectonites, *Geophys. J. R. astr. Soc., 76,* 89–111.

Christensen, N. I., 1989, Reflectivity and seismic properties of deep continental crust, *J. Geophys. Res., 94,* 17,793–17,804.

Christensen, N. I., and R. Crosson, 1968, Seismic anisotropy in the upper mantle, *Tectonophysics, 6,* 63–107.

Christensen, N. I., and M. H. Salisbury, 1979, Seismic anisotropy in the oceanic upper mantle: evidence from the Bay of Islands Ophiolite Complex, *J. Geophys. Res., 84,* 4601–4610.

Christensen, N. I., L. G. Medaris, H. F. Wang, and E. Jelinek, 2001, Depth variation of seismic anisotropy and petrology in central european lithosphere: A tectonothermal synthesis from spinel lherzolite, *J. Geophys. Res., 106,* 645–664.

Chung, D. H., and W. R. Buessem, 1967a, The elastic anisotropy of crystals, *J. Appl. Phys., 38,* 2010–2012.

Chung, D. H., and W. R. Buessem, 1967b, The Voigt-Reuss-Hill approximation and elastic moduli of polycrystalline MgO, CaF_2, $\beta - ZnS$, $ZnSe$, and $CdTe$, *J. Appl. Phys., 38,* 2535–2540.

Crampin, S., 1978, Seismic wave propagation through a cracked solid: polarization as a possible dilatancy diagnostic, *Geophys. J. R. astr. Soc., 53,* 467–496.

Crampin, S., 1981, A review of wave motion in anisotropic and cracked elastic-media, *Wave motion, 3,* 343 – 391.

Crampin, S., 1984, Effective anisotropic elastic constants for wave propagation through cracked solids, *Geophys. J. R. astr. Soc., 76,* 135–145.

Crampin, S., 1985a, Evidence for aligned cracks in the Earth's crust, *First Break, 3,* 12–15.

Crampin, S., 1985b, Evaluation of anisotropy by shear wave splitting, *Geophysics, 50,* 142–152.

115

Crampin, S., 1991, Effects of point singularities on shear wave propagation in sedimentary basins, *Geophys. J. Int.*, 107, 531-543.

Crampin, S., and B. K. Atkinson, 1985, Microcracs in the Earth's crust, *First Break*, 3, 16-20.

Crampin, S., and J. H. Lovell, 1991, A decade of shear wave splitting in the Earth's crust: What does it mean? What use can we make out of it? And what should we do next?, *Geophys. J. Int.*, 107, 387-407.

Crampin, S., and M. Yedlin, 1981, Shear-wave singularities of wave propagation in anisotropic media, *J. Geophys.*, 49, 43-46.

Crosson, R. S., and J.-W. Lin, 1971, Voigt and Reuss prediction of anisotropic elasticity of dunite, *J. Geophys. Res.*, 76, 570-578.

Daley, P. F., and F. Hron, 1977, Reflection and transmission coeffitients for transversely isotropic media, *Bull. Seism. Soc. Am.*, 67, 661-675.

Dellinger, J., and L. Vernik, 1994, Do traveltime in transmission experiments yield anisotropic group or phase velocities?, *Geophysics*, 59, 1774-1779.

Dey-Barsukov, S., H. Durrast, W. Rabbel, S. Siegesmund, and S. Wende, 2000, Aligned fractures in carbonate rocks: laboratory and in situ measurements of seismic anisotropy, *Int. J. Earth Sci.*, 88, 829-839.

Ditri, J., 1994, On the determination of the elastic moduli of anisotropic media from limited acoustical data, *J. acoust. Soc. Am.*, 95, 1761-1767.

Diz, J., and M. Humbert, 1992, Practical aspects of calculating the properties of polycrystals from the texture according to different models, *J. Appl. Cryst.*, 25, 756-760.

Domnesteanu, P., C. McCann, and J. Sothcott, 2002, Velocity anisotropy and attenuation of shale in under- and overpressured conditions, *Geophys. Prosp.*, 50, 487-503.

Eshelby, J. D., 1957, The determination of the elastic field of an ellipsoidal inclusion, and related problems, *Proc. R. Soc. London. Ser. A,*, 241, 376-396.

Every, A. G., and W. Sachse, 1990, Determination of the elastic constants of anisotropic solids from acoustic-wave group-velocity measurements, *Phys. Rev. B*, 42, 8196-8205.

Fedorov, F. I., 1968, *Theory of elastic waves in crystals*, Plenum Press, New York.

Ferrari, M., and G. C. Johnson, 1988, The equalibrium properties of a 6mm polycrystal exhibiting transverse isotropy, *J. Appl. Phys.*, 63, 4460-4468.

Ferry, J., and F. Spear, 1978, Experimental calibration of partitioning of Fe and Mg between biotite and garnet, *Contrib. Mineral. Petrol*, 66, 113-117.

Fuchs, K., 1977, Seismic anisotropy of the subcontinental lithosphere as evidence for dynamic processes in the upper mantle, *Geophys. J. R. astr. Soc.*, 49, 167-179.

Gaiser, J., 1990, Transversely isotropic phase velocity analysis from slowness estimates, *J. Geophys. Res.*, 95, 11 241 - 11 254.

Gassmann, F., 1964, Introduction to seismic travel time methods in anisotropic media, *Pure Appl. Geophys.*, 58, 63–113.

Godfrey, N. J., N. I. Christensen, and D. A. Okaya, 2000, Anisotropy of shists: contribution of crustal anisotropy to active source seismic experiments and shear wave splitting observations, *J. Geophys. Res.*, 105, 27,991–28,007.

Grechka, V., and I. Tsvankin, 1999, 3-d moveout inversion in azimuthally anisotropic media with lateral velocity variation: Theory and a case of study, *Geophysics*, 64, 1202–1218.

Guéguen, Y., and V. Palciauskas, 1994, *Introduction to the physics of rocks*, Princeton University Press, Princeton, N.J.

Hajnal, Z., M. R. Stauffer, M. S. King, P. F. Wallis, H. F. Wang, and L. E. A. Jones, 1983, Seismic characteristics of a Precambrian pluton and its adjacent rocks, *Geophysics*, 48, 569–581.

Hake, H., K. Helbig, and C. Mesdag, 1984, Three-term Taylor series for $t^2 - x^2$ curves of P- and S-waves over layered transversely isotropic ground, *Geoph. Prosp.*, 32, 828–850.

Hashin, Z., and S. Shtrikman, 1962a, On some variational principles in anisotropic and nonhomogeneous elasticity, *J. Mech. Phys. Solids*, 10, 335–342.

Hashin, Z., and S. Shtrikman, 1962b, A variational approach to the theory of the elastic behaviour of polycrystals, *J. Mech. Phys. Solids*, 10, 343–352.

Hashin, Z., and S. Shtrikman, 1963, A variational approach to the theory of elastic behavior of multiphase materials, *J. Mech. Phys. Solids*, 11, 127–140.

Hearn, T., 1999, Uppermost mantle velocities and anisotropy beneath Europe, *J. Geophys. Res.*, 104, 15,123–14,139.

Helbig, K., 1964, Refraction seismic with an anisotropic overburden: a graphical method of interpretation, *Geophys. Prosp.*, 12, 383–396.

Helbig, K., 1981, Systematic classification of layer-induced transverse isotropy, *Geophys. Prosp.*, 29, 550–577.

Helbig, K., 1984a, Transverse isotropy in exploration seismics, *Geophys. J. R. astr. Soc.*, 76, 79–88.

Helbig, K., 1984b, Anisotropy and dispertion in periodically layered media, *Geophysics*, 49, 364–373.

Helbig, K., 1994, *Foundations of anisotropy for exploration seismics*, Handbook of Geophysical Exploration - Section I: Seismic exploration, Elsevier Science Ltd., Oxford.

Helbig, K., and M. Schoenberg, 1987, Anomalous polarization of elastic waves in transversely isotropic media, *J. Acoust. Soc. Am.*, 81, 1235–1245.

Hershey, A., and V. Dahlgren, 1954, The elasticity of an isotropic aggregate of anisotropic cubic crystals, *J. Appl. Mech.*, 21, 236–240.

Hess, H. H., 1964, Seismic anisotropy of the uppermost mantle under oceans, *Nature*, 203, 629–631.

Hill, R., 1952, The elastic behaviour of a crystalline aggregate, *Proc. Phys. Soc.*, 65(A), 349–354.

Hill, R., 1965, A self-consistent mechanics of composite materials, *J. Mech. Phys. Solids*, 13, 213–222.

Ho, N.-C., D. R. Peacor, and B. A. van der Pluijm, 1999, Preferred orientation of phyllosilicates in gulf coast mudstone and relation to the smectite-illite transformation, *Clays and Clay Minerals*, 47, 495–504.

Hoffman, P. F., 1988, United Plates of America, the birth of a craton: Early proterozoic assembly and growth of Laurentia, *Ann. Rev. Earth Planet. Sci.*, 16, 543–603.

Holmes, G. M., S. Crampin, and R. P. Young, 2000, Seismic anisotropy in granite at the Underground Research laboratory, Manitoba, *Geophys. Prosp.*, 48, 415–435.

Hood, J. A., 1991, A simple method for decomposing fracture-induced anisotropy, *Geophysics*, 56, 1275–1279.

Hornby, B. E., 1998, Experimental laboratory determination of the dynamic elastic properties of wet, drained shales, *J. Geophys. Res.*, 103, 29,945–29,964.

Hornby, B. E., L. M. Schwartz, and J. A. Hudson, 1994, Anisotropic effective-medium modeling of the elastic properties of shales, *Geophysics*, 59, 1570–1583.

Hovem, J. M., 1995, Acoustic waves in finely layered media, *Geophysics*, 60, 1217–1221.

Hudson, J. A., 1980, Overall properties of a cracked solid, *Math. Proc. Camb. Phil. Soc.*, 88, 371–384.

Hudson, J. A., 1981, Wave speeds and attenuation of elastic waves in material containing cracks, *Geophys. J. R. astr. Soc.*, 64, 133–150.

Humbert, M., and J. Diz, 1991, Some practical features of calculating the polycrystalline elastic properties from texture, *J. Appl. Cryst.*, 24, 978–981.

Isaak, D. S., J. D. Carnes, O. Anderson, and H. Oda, 1998, Elasticity of fused silica spheres under pressure using resonant ultrasound spectroscopy, *J. Acoust. Soc. Am.*, 104, 2200–2206.

Jakobsen, M., and T. A. Johansen, 2000, Anisotropic approximation for mudrocks: A seismic laboratory study, *Geophysics*, 65, 1711–1725.

Jakobsen, M., J. A. Hudson, and T. A. Johansen, 2003, T-matrix approach to shale acoustics, *Geophys J Int*, 154, 533–558.

Jech, J., 1991, Computation of elastic parameters of anisotropic medium from travel times of quasi-compressional waves, *Phys. Earth Planet. Inter.*, 66, 153–159.

Ji, S., and D. Mainprice, 1988, Natural deformation fabrics of plagioclase: implications for slip systems and seismic anisotropy, *Tectonophysics*, 147, 145–163.

Ji, S., and M. Salisbury, 1993, Shear-wave velocities, anisotropy and splitting in high-grade mylonites, *Tectonophysics*, *221*, 453–473.

Ji, S., M. H. Salisbury, and S. Hanmer, 1993, Petrofabric, P-wave anisotropy and seismic reflectivity of high - grade tectonites, *Tectonophysics*, *222*, 195–226.

Ji, S., X. Zhao, and D. Francis, 1994, Calibration of shear-wave splitting in the subcontinental upper mantle beneath active orogenic belts using ultramafic xenoliths from the Canadian Cordillera and Alaska, *Tectonophysics*, *239*, 1–27.

Ji, S., C. Long, J. Martignole, and M. Salisbury, 1997, Seismic reflectivity of finely layered, granulite-facies ductile shear zone in the southern Grenville Province (Québec), *Tectonophysics*, *279*, 113–133.

Ji, S., Q. Wang, B. Xia, and D. Marcotte, 2004, Mechanical properties of multiphase materials and rocks: a phenomenological approach using generalized means, *Journal of Structural Geology, In Press, Corrected Proof*.

Johansen, T. A., B. Ole Ruud, and M. Jakobsen, 2004, Effect of grain scale alignment on seismic anisotropy and reflectivity of shales, *Geophys. Prospect*, *52*, 133–149.

Johnson, G. C., and H. R. Wenk, 1986, Elastic properties of polycrystals with trigonal crystal and orthorhombic specimen symmetry, *J. Appl. Phys.*, *60*, 3868–3875.

Johnston, J. E., and N. I. Christensen, 1995, Seismic anisotropy of shales, *J. Geophys. Res.*, *100*, 5991–6003.

Jolly, R. N., 1956, Investigation of shear waves, *Geophysics*, *21*, 905–938.

Jones, L. E. A., and H. F. Wang, 1981, Ultrasonic velocities in Cretaceous shales from the Williston basin, *Geophysics*, *46*, 288–297.

Jones, T., and A. Nur, 1982, Seismic velocity and anisotropy in mylonites and the reflectivity of deep crustal fault zones, *Geology*, *10*, 260–263.

Kaarsberg, E. A., 1959, Introductory studies of natural and artificial argillaceous aggregates by sound-propagation and x-ray diffraction methods, *J. Geol.*, *67*, 447–472.

Kaminski, E., and N. M. Ribe, 2001, A kinematic model for recrystallization and texture development in olivine polycrystals, *Earth Planet. Sci. Lett.*, *189*, 253–267.

Karato, S., S. Zhang, M. E. Zimmerman, M. J. Daines, and D. L. Kohlstedt, 1998, Experimental studies of shear deformation of mantle materials: Towards structural geology of the mantle, *Pure appl. Geophys.*, *151*, 589–603.

Karato, S.-i., 1987, Seismic anisotropy due to lattice preferred orientation of minerals: kinematic or dynamic?, in *High pressure research in mineral physics*, edited by M. H. Manghnani and Y. Syono, pp. 455–471, AGU, Washington, D. C.

Karato, S. i., 1988, The role of recrystallization in the preferred orientation of olivine, *Phys. Earth Planet. Inter.*, *51*, 107–122.

Karato, S.-i., 1998, Seismic anisotropy in the deep mantle, boundary layers and the geometry of the mantle convection, *Pure appl. Geophys.*, *151*, 565–587.

119

Katahara, K. W., 1996, Clay mineral elastic properties, in *SEG International Exposition and 66th Annual Meeting*, vol. 2 of *Expanded abstracts*, p. 1691, SEG, Denver, Colorado.

Kebaili, A., and D. R. Schmitt, 1996, Velocity anisotropy observed in wellbore seismic arrivals: combined effect of intrinsic properties and layering, *Geophysics, 61,* 12–20.

Kebaili, A., and D. R. Schmitt, 1997, Ultrasonic anisotropy phase velocity determination with the Radon transformation, *J. Acoust. Soc. Am., 101,* 3278–3286.

Kern, H., 1978, The effects of high pressure on compressional wave velocities in quartz-bearing and quartz-free igneous and metamorphic rocks, *Tectonophysics, 44,* 185–203.

Kern, H., 1993a, P- and S-wave anisoropy and shear-wave splitting at pressure and temperature in possible mantle rocks and their relation to the rock fabric, *Phys. Earth Planet. Inter., 78,* 245–256.

Kern, H., and M. Fakhimi, 1975, Effect of fabric anisotropy on compressional-wave propagation in various metamorphic rocks for the range 20-700° C at 2 kbar, *Tectonophysics, 28,* 227–244.

Kern, H., and A. Richer, 1981, Temperature derivatives of compressional and shear waves velocities in crustal and mantle rocks at 6 kbar confining pressure, *J. Geophys., 49,* 47–56.

Kern, H., and H.-R. Wenk, 1990, Fabric-related velocity anisotropy and shear wave splitting in rocks from the Santa Rosa mylonite zone, California, *J. Geophys. Res., 95,* 11,213–11,223.

Kern, H., L. Burlini, and I. V. Ashchepkov, 1996, Fabric-related seismic anisotropy in the upper-mantle xenoliths: evidence from measurements and calculations, *Phys. Earth Planet. Inter., 95,* 195–209.

Kern, H. M., 1993b, Physical properties of crustal and upper mantle rocks with regards to lithosphere dynamics and high pressure mineralogy, *Phys. Earth Planet. Inter., 79,* 113–136.

Khazanehdari, J., E. H. Rutter, M. Casey, and L. Burlini, 1998, The role of crystallographic fabric in the generation of seismic anisotropy and reflectivity of high strain zones in calcite rocks, *J. Struct. Geol., 20,* 293–299.

Kneer, V. G., 1965, Uber die Berechnung der Elastizitätsmoduln vielkristalliner Aggregate mit Textur, *phys. stat. sol. (b), 9,* 825–838.

Kocks, U. F., C. N. Tome, and H.-R. Wenk, 1998, *Texture and anisotropy. Preferred orientations in polycrystals and their effect on materials properties*, Cambridge University Press.

Krey, T., and K. Helbig, 1956, A theorem concerning anisotropy of stratified media and its significance for reflection seismics, *Geophys. Prosp., 4,* 294–302.

Kröner, E., 1958, Berechnung der elastischen Konstanten des Vielkristalls aus den Konstanten des Einkristalls, *Z. Physik, 151,* 504–518.

Kröner, E., 1967, Elastic moduli of perfectly disoriented composite materials, *J. Mech. Phys. Solids, 15,* 319–329.

Kröner, E., 1977, Bounds for effective elastic moduli of disordered materials, *Journal of the Mechanics and Physics of Solids*, 25, 137–155.

Kröner, E., 1978, Self-consistent scheme and gradient disorder in polycrystal elasticity, *J. Phys. F*, 8, 2261–2267.

Kumazawa, M., 1969, The elastic constant of polycrystalline rocks and nonelastic behavior inherent to them, *J. Geophys. Res.*, 74, 5311–5320.

Lay, T., and T. C. Wallace, 1995, *Modern Global Seismology*, vol. 58 of *International Geophysical Series*, first ed., Academic Press, San Diego.

Leaney, W. S., C. M. Sayers, and D. E. Miller, 1999, Analysis of multiazimuthal VSP data for anisotropy and AVO, *Geophysics*, 64, 1172–1180.

Leary, P. C., S. Crampin, and T. V. McEvilly, 1990, Seismic fracture anisotropy in the Earth's crust: An overview, *J. Geophys. Res.*, 95, 11,105–11,114.

Leiss, B., K. Ullemeyer, K. Weber, H. G. Brokmeier, H. J. Bunge, M. Drury, U. Faul, F. Fueten, A. Frischbutter, H. Klein, W. Kuhs, P. Launeau, G. E. Lloyd, D. J. Prior, C. Scheffzük, T. Weiss, K. Walther, and H. R. Wenk, 2000, Recent developments and goals in texture research of geological materials, *J Struct. Geol.*, 22, 1531 – 1540.

Leisure, R. G., and F. A. Willis, 1997, Resonant ultrasound spectroscopy, *J. Phys.: Condens. Matter*, 9, 6001–6029.

Leslie, J. M., and D. C. Lawton, 1999, A refraction-seismic field study to determine the anisotropic parameters of shales, *Geophysics*, 64, 1247–1252.

Levin, F. K., 1979, Seismic velocities in transversely isotropic media, *Geophysics*, 44, 918–936.

Lewry, J. F., and M. R. Stauffer, 1990, The early Proterozoic Trans-Hudson Orogen of North America, *The Geological Association of Canada, Special paper, 37*.

Lewry, J. F., Z. Hajnal, A. Green, S. B. Lucas, D. White, M. R. Stauffer, K. E. Ashton, W. Weber, and R. Clowes, 1994, Structure of a Paleoproterozoic continent - continent collision zone: a LITHOPROBE seismic reflection profile across the Trans-Hudson Orogen, Canada, *Tectonophysics*, 232, 143–160.

Lifshitz, I. M., and L. Rozenzweig, 1946, On the theory of the elasticity of polycrystals, *Zh. eksp. teor. Fiz.*, 16, 967–980.

Liu, E., S. Crampin, J. H. Queen, and W. D. Rizer, 1993, Velocity and attenuation anisotropy caused by microcracks and microfractures in a multiazimuthal reverse VSP, *Can. J. Expl. Geophys.*, 29, 177–188.

Liu, Y., and D. R. Schmitt, 2003, Amplitude and avo responses of a single thin bed, *Geophysics*, 68, 1161–1168, tY - JOUR.

Love, A. E. H., 1920, *A treatise on the mathematical theory of elasticity*, Cambridge University Press.

Lucas, S., A. Green, Z. Hajnal, D. White, J. Lewry, K. Ashton, W. Weber, and R. Clowes, 1993, Deep seismic profile across a proterozoic collision zone: surprises at depth, Nature, 363, 339–342.

Lucas, S., R. Stern, E. Syme, B. Reilly, and D. Thomas, 1996, Intraoceanic tectonics and the development of continental crust: 1.92-1.84 Ga evolution of the Flin Flon Belt, Canada, Geol. Soc. Am. Bulletin, 108, 602–629.

Lucas, S., E. Syme, and K. Ashton, 1999a, New perspectives on the Flin Flon Belt, Trans-Hudson Orogen, Manitoba and Saskatchewan: an introduction to the special issue on the NATMAP Shield Margin Project, Part 1, Can. J. Earth Sci., 36, 135–140.

Lucas, S. B., E. C. Syme, and K. E. Ashton, 1999b, Introduction to Special Issue on the NATMAP Shield margin Project: The Flin Flon Belt, Trans-Hudson Orogen, Manitoba and Saskatchewan, Can. J. Earth Sci., 36, 1763–1765.

Lynn, H. B., and L. Thomsen, 1990, Reflection shear-wave data collected near the principal axes of azimuthal anisotropy, Geophysics, 55, 147–156.

Mah, M., and D. R. Schmitt, 2001a, Near point-source longitudinal and transverse mode ultrasonic arrays for material characterization, IEEE Trans. Ustrason. Ferroelect. Freq. Contr., 48, 691–698.

Mah, M., and D. R. Schmitt, 2001b, Experimental determination of the elastic coefficients of an orthorhombic material, Geophysics, 66, 1217–1225.

Mah, M., and D. R. Schmitt, 2003, Determination of the complete elastic stiffnesses from ultrasonic phase velocity measurements, J.Geophys.Res., 108(B1), 10.1029/2001JB001,586.

Mainprice, D., 1990, A Fortran program to calculate seismic anisotropy from the lattice preferred orientation of minerals, Computers & Geosciences, 16, 385–393.

Mainprice, D., and M. Humbert, 1994, Methods of calculating petrophysical properties from lattice preferred orientation data, Surv. Geophys., 15, 575–592.

Mainprice, D., and A. Nicolas, 1989, Development of shear and lattice preferred orientatons: application to the seismic anisotropy of the lower crust, Jour. Struct. Geology, 11, 175–189.

Mainprice, D., and P. G. Silver, 1993, Interpretation of SKS-waves using samples from the subcontinental lithosphere, Phys. Earth Planet. Int., 78, 257–280.

Mainprice, D., M. Humbert, and F. Wagner, 1990, Phase transformations and inherented lattice preferred orientations: implications for seismic properties, Tectonophysics, 180, 213–228.

Matthies, S., and M. Humbert, 1993, The realization of the concept of a geometric mean for calculating physical constants of polycrystalline materials, phys. stat. sol. (b), 177, K47–K50.

Mavko, G., T. Mukerji, and N. Godfrey, 1995, Predicting stress-induced velocity anisotropy in rocks, Geophysics, 60, 1081–1087.

Maynard, J., 1996, Resonant ultrasound spectroscopy, *Physics Today, January*, 26–31.

McCaffree, C., and N. I. Christensen, 1993, Shear wave properties and seismic imaging of mylonite zones, *J. Geophys. Res., 98*, 4423–4435.

Melia, P. J., and R. L. Carlson, 1984, An experimental test of P-wave anisotropy in stratified media, *Geophysics, 49*, 374–378.

Meltzer, A., and N. Christensen, 2001, Nanga Parbat crustal anisotropy: implications for interpretation of crustyal velocity structure and shear-wave splitting, *Geophys. Res. Lett., 28*, 2129–2132.

Mercier, J.-C. C., 1985, Olivine and pyroxenes, in *Preferred orientation in deformed metals and rocks: an introduction to modern texture analysis*, edited by H.-R. Wenk, pp. 407–430, Academic Press Inc., Orlando.

Mercier, J.-C. C., and A. Nicolas, 1975, Textures and fabrics of upper - mantle peridotites as illustrated by xenoliths from basalts, *J. Petrol., 16*, 454–487.

Migliori, A., and Z. Fisk, 1993, Crystals and ultrasounds, *Los Alamos Science, 21*, 182–194.

Migliori, A., and J. L. Sarrao, 1997, *Resonant Ultrasound Spectroscopy. Applications to physics, material measurements, and nondestructive evaluation*, John Wiley & Sons, New - York.

Miller, D. E., S. Leaney, and W. H. Borland, 1994, An in situ estimation of anisotropic elastic moduli for a submarine shale, *J. Geophys. Res., 99*, 21,659–21,665.

Molyneux, J. B., and D. R. Schmitt, 1999, First-break timing: Arrival onset times by direct correletion, *Geophysics, 64*, 1492–1501.

Molyneux, J. B., and D. R. Schmitt, 2000, Compressional-wave velocities in attenuating media: A laboratory physical modeling study, *Geophysics, 65*, 1162–1167.

Montagner, J.-P., 1986, Regional three-dimentional structures using long-period surface waves, *Ann. Geophys., 4*, 283–294.

Montagner, J.-P., 1998, Where can seismic anisotropy be detected in the earth's mantle? In boundary layers..., *Pure Appl. Geophys., 151*, 223–256.

Montagner, J.-P., and H.-C. Nataf, 1986, A simple method for inverting the azimuthal anisotropy of surface waves, *J. Geophys. Res., 91*, 511–520.

Morawiec, A., 1989, Calculation of polycrystal elastic constants from single-crystal data, *phys. stat. sol. (b), 154*, 535–541.

Morris, P. R., 1969, Averaging fourth-rank tensors with weight functions, *J. Appl. Phys., 40*, 447–448.

Morris, P. R., 1970, Elastic constants of polycrystals, *Int. J. Engng. Sci., 8*, 49–61.

Morris, P. R., 1971, Iterative scheme for calculating polycrystal elastic constants, *Int. J. Engng. Sci., 9*, 917–920.

Morris, P. R., and A. J. Heckler, 1967, Crystallite orientation analysis for rolled cubic materials, in *Sixteenth Annual Conference on Applications of X-Ray Analysis*, edited by J. B. Newkirk, G. R. Mallett, and H. G. Pfeiffer, vol. 11 of *Advances in X-Ray Analysis*, pp. 454–472, Plenum Press, New York, Denver Research Insitute, University of Denver, Colorado, USA.

Morse, P. M., and H. Feshbach, 1953, *Methods of theoretical physics*, McGraw-Hill, New York.

Musgrave, M. J. P., 1970, *Crystal acoustics. Introduction to the study of elastic wave and vibrations in crystals.*, Holden-Day series in mathematical physics, Holden-Day, San Francisco, Cambridge, London, Amsterdam.

Nadeau, J. C., and M. Ferrari, 2001, On optimal zeroth-order bounds with application to Hashin-Shtrikman bounds and anisotropy parameters, *International Journal of Solids and Structures*, 38, 7945–7965.

Neighbours, J. R., 1954, An approximation method for the determination of the elastic constants of single crystals, *J. Acoust. Soc. Am.*, 26, 865–869.

Neighbours, J. R., and G. E. Schacher, 1967, Determination of elastic constants from sound-velocity measurements in crystals of general symmetry, *J. appl. Phys.*, 38, 5366–5375.

Nicolas, A., and N. I. Christensen, 1987, Formation of anisotropy in upper mantle peridotites - a review, in *Composition, structure and dynamics of the lithosphere -asthenosphere system*, edited by K. Fuchs and C. Froidevaux, vol. 16 of *Geodyn. Ser.*, pp. 111–123, AGU, Washington, D. C.

Nicolas, A., J. L. Bouchez, F. Boudier, and J. C. Mercier, 1971, Textures, structures and fabrics due to solid state flow in some European lherzolites, *Tectonophysics*, 12, 55–86.

Nicolas, A., F. Boudier, and A. M. Boullier, 1973, Mechanisms of flow in naturally and experimentally deformed peridotites, *Am. J. Sci.*, 273, 853 – 870.

Nye, J. F., 1990, *Physical properties of crystals*, Oxford University Press, Oxford.

O'Connell, R., and B. Budiansky, 1974, Seismic velocities in dry and saturated cracked solids, *J. Geophys. Res.*, 79, 5412–5426.

Okaya, D., and N. Christensen, 2002, Anisotropic effects of non-axial seismic wave propagation in foliated crustal rocks, *Geophys. Res. Letts.*, 29, 10.1029/ 2001GL014,285.

Ono, N., 1992, Physical relevance of physical elasticity theories, *Scripta Metall. et Mat.*, 27, 1379–1384.

Park, J., and V. Levin, 2002, Seismic anisotropy: tracing plate dynamics in the mantle, *Science*, 296, 485–489.

Peselnick, L., and A. Nicolas, 1978, Seismic anisotropy in an ophiolite peridotite: application to oceanic upper mantle, *J. Geophys. Res.*, 83, 1227–1235.

Peselnick, L., A. Nicolas, and P. R. Stevenson, 1974, Velocity anisotropy in a mantle peridotite from the Ivrea zone: Application to upper mantle anisotropy, *J. Geophys. Res.*, 79, 1175–1182.

Plomerova, J., J. Sileny, and V. Babuška, 1996, Joint interpretation of upper-mantle anisotropy based on teleseismic P-travel time delays and inversion of shear-wave splitting parameters, *Phys. Earth Planet. Inter., 95*, 293–309.

Plomerova, J., V. Babuška, J. Sileny, and J. Horalek, 1998, Seismic anisotropy and velocity variations in the mantle beneath the Saxothuringicum-Moldanubicum Contact in the central Europe, *Pure appl. Geophys., 151*, 365–394.

Poirier, J. P., and A. Nicolas, 1975, Deformation - induced recrystallization due to progressive misorientation of subgrains, with special reference to mantle peridotites, *J. Geol., 83*, 707 - 720.

Postma, G. W., 1955, Wave propagation in a stratified medium, *Geophysics, 20*, 780–806.

Prodayvoda, G. T., 1995, Determination of the distribution function for the orientation of olivine and the symmetry of dunite, *Izv. Acad. Sci. USSR, Phys. Solid Earth, 30*, 416–427.

Pros, V. Z., and V. Babuška, 1967, A method for investigating the elastic anisotropy on spherical rock samples, *J. Geophys., 33*, 288–291.

Pros, Z., T. Lokajicek, and K. Klima, 1998a, Laboratory approach to the study of elastic anisotropy on rock samples, *Pure appl. Geophys., 151*, 619–629.

Pros, Z., T. Lokajicek, R. Prikryl, A. Spicak, V. Vajdova, and K. Klima, 1998b, Elastic parameters of west Bohemian granites under hydrostatic pressure, *Pure appl. Geophys., 151*, 631–646.

Putnis, A., 1992, *Introduction to mineral sciences*, Cambridge University Press.

Rasolofosaon, P. N. J., W. Rabbel, S. Siegesmund, and A. Vollbrecht, 2000, Characterization of crack distribution: fabric analysis versus ultrasonic inversion, *Geophys. J. Int., 141*, 413–424.

Reuss, A., 1929, Berechnung der Fliess grenze von Mischkristallen aufgrund der Plastizitätsbedingung für Einkristalle, *Z. Angew. Math. Mech., 9*, 49–58.

Ribe, N. M., and Y. Yu, 1991, A theory for plastic deformation and textural evolution of olivine polycrystals, *J. Geophys. Res., 96*, 8325–8335.

Riznichenko, Y. W., 1949, On seismic quasi-anisotropy, *Izv. Akad. Naud. Nauk SSSR, Ser. Geograf. i Geof., 13*, 518–540.

Roe, R.-J., 1965, Description of crystallite orientation in polycrystalline materials. iii. General solution to pole inversion, *J. Appl. Phys., 36*, 2024–2031.

Roe, R. J., 1966, Inversion of pole figures for materials having cubic crystal symmetry, *J. Appl. Phys., 37*, 2069–2072.

Rytov, S., 1956, Acoustic properties of a thinly laminated medium, *Sov. Phys. Acous., 2*, 68–80.

Sano, O., Y. Kudo, and Y. Mizuta, 1992, Experimental determination of elastic constants of Oshima granite, Barre granite, and Chelmsford granite, *J. Geophys. Res., 97*, 3367–3379.

125

Savage, M. K., 1999, Seismic anisotropy and mantle deformation: what have we learned from shear wave splitting?, *Rev. Geophys.*, 37, 65–106.

Sayers, C. M., 1986, Angular dependent ultrasonic wave velocities in aggregates of hexagonal crystals, *Ultrasonics*, 24, 289–292.

Sayers, C. M., 1987, The elastic anisotropy of polycrystalline aggregates of zirconium and its alloys, *J. Nucl. Mater.*, 144, 211–213.

Sayers, C. M., 1993, Anelliptic approximations for shales, *J. Seism. Expl.*, 2, 319–331.

Sayers, C. M., 1994, P-wave propagation in weakly anisotropic media, *Geophys. J. Int.*, 116, 799–805.

Sayers, C. M., 1995, Simplified anisotropy parameters for transversely isotropic sedimetary rocks, *Geophysics*, 60, 1933–1935.

Sayers, C. M., 1999, Stress-dependent seismic anisotropy of shales, *Geophysics*, 64, 93–98.

Schoenberg, M., and J. Costa, 1991, The insensitivity of reflected SH waves to anisotropy in an underlying layered medium, *Geophys. Prosp.*, 39, 985–1003.

Schoenberg, M., and F. Muir, 1989, A calculus for finely layered anisotropic media, *Geophysics*, 54, 581–589.

Schoenberg, M., and C. M. Sayers, 1995, Seismic anisotropy of fractured rock, *Geophysics*, 60, 204–211.

Schoenberg, M., F. Muir, and C. Sayers, 1996, Introducing ANNIE: a simple three-parameter anisotropic velocity model for shales, *J. Seis. Expl.*, 5, 35–49.

Schreiber, E., O. L. Anderson, and N. Soga, 1973, *Elastic constants and their measurement*, McGraw-Hill, New York.

Seront, B., D. Mainprice, and N. I. Christensen, 1993, A determination of the three-dimentional seismic properties of anorthosite: Comparison between values calculated from the petrofabric and direct laboratory measurements, *J. Geophys. Res.*, 98, 2209–2221.

Shareef, S., and D. R. Schmitt, 2004, Point load determination of static elastic moduli using laser speckle interferometry, *Optics and Lasers in Engineering*.

Sheng, P., and A. J. Callegari, 1984, Differential effective medium theory of sedimentary rocks, *Appl. Phys. Lett.*, 44, 738–740.

Siegesmund, S., and H. Kern, 1990, Velocity anisotropy and shear-wave splitting in rocks from the mylonite belt along the Insubric Line (Ivrea Zone, Italy), *Earth Planet. Sci. Lett.*, 99, 29–47.

Siegesmund, S., T. Takeshita, and H. Kern, 1989, Anisotropy of v_p and v_s in an amphibolite of the deeper crust and its relationship to the mineralogical, microstructural and textural characteristics of the rock, *Tectonophysics*, 157, 251–238.

Silver, P. G., 1996, Seismic anisotropy beneath the continents: Probing the depth of geology, *Annu. Rev. Earth Planet. Sci.*, 24.

126

Simmons, G., and H. Wang, 1971, *Single crystal elastic constants and calculated aggregate properties: A Handbook*, second ed., MIT Press, Cambridge, Massachusetts, London, England.

Smith, M. L., and F. A. Dahlen, 1973, The dependence of Love and Rayleigh wave propagation in a slightly anisotropic medium, *J. Geophys. Res.*, 78, 3321–3333.

Soedjatmiko, B., and N. I. Christensen, 2000, Seismic anisotropy under extended crust: evidence from upper mantle xenoliths, Cima Volcanic Field, California, *Tectonophysics*, 321, 279–296.

Suhr, G., 1993, Evaluation of upper mantle microstructures in the Table Mountain massif (Bay of Islands ophiolite), *J. Struct. Geol.*, 15, 1273–1292.

Takanashi, M., O. Nishizawa, K. Kanagawa, and K. Yasunaga, 2001, Laboratory measurements of elastic anisotropy parameters for the exposed crustal rocks from the Hidaka Metamorphic Belt, Central Hokkaido, Japan, *Geophys. J. Int.*, 145, 33–47.

Thompson, R. B., S. S. Lee, and Y. Li, 1994, Ultrasonic and neutron diffraction characterization of texture in an inhomogeneously rolled titanium plate, *Material Science and Engineering*, A177, 261–267.

Thomsen, L., 1972, Elasticity of polycrystals and rocks, *J. Geophys. Res.*, 77, 315–327.

Thomsen, L., 1986, Weak elastic anisotropy, *Geophysics*, 51, 1954–1966.

Thomsen, L., 1988, Reflection seismology over azimuthally anisotropic media, *Geophysics*, 53, 304–313.

Thomsen, L., I. Tsvankin, and M. Mueller, 1999, Coarse-layer stripping of vertically variable azimuthal anisotropy from shear-wave data, *Geophysics*, 64, 1129–1138.

Tommasi, A., 1998, Forward modeling of the development of seismic anisotropy in the upper mantle, *Earth Planet. Sci. Lett.*, 160, 1–13.

Tommasi, A., B. Tikoff, and A. Vauchez, 1999, Upper mantle tectonics: three-dimentional deformation, olivine crystallographic fabrics and seismic properties, *Earth Planet. Sci. Lett.*, 168, 173–186.

Tommasi, A., D. Mainprice, G. Canova, and Y. Chastel, 2000, Viscoplastic self-consistent and equilibrium-based modeling of olivine lattice preferred orientations: Implications for the upper mantle seismic anisotropy, *J. Geophys. Res.*, 105, 7893–7908.

Tosaya, C. A., 1982, Acoustic properties of clay-bearing rocks, Ph.D. thesis, Stanford University.

Tsvankin, I., 1997, Anisotropic parameters and P-wave velocity for orthorhombic media, *Geophysics*, 62, 1292–1309.

Tsvankin, I., 2001, *Seismic signatures and analysis of reflection data in anisotropic media*, vol. 29 of *Handbook of geophysical exploration*, Pergamon, Amsterdam.

Ullemeyer, K., G. Braun, M. Dahms, J. H. Kruhl, N. O. Olesen, and S. Siegesmund, 2000, Texture analysis of a muscovite-bearing quartzite: a comparison of some currently used techniques, *Journal of Structural Geology*, 22, 1541–1557.

127

Van Buskirk, W. C., S. C. Cowin, and R. Carter Jr, 1986, A theory of acoustic measurements of the elastic constants of a general anisotropic solid, *J. Mater. Sci.*, *21*, 2759–2762.

Van Houtte, P., E. Aernoudt, and K. Sekine, 1981, Orientation distribution function measurements of copper and brass torsion texture, in *Proc. 6th Int. Conf. Textures of Materials*, edited by S. Nagashima, vol. 1, pp. 337–346, The iron and steel Ins. Japan, Tokyo.

Vanorio, T., M. Prasad, and A. Nur, 2003, Elastic properties of dry clay mineral aggregates, suspensions and sandstones, *Geophys. J. Int*, *155*, 319–326.

Vauchez, A., and G. Barruol, 1996, Shear-wave splitting in the Appalachians and the Pyrenees: importance of the inherited tectonic fabric of the lithosphere, *Phys. Earth Planet. Int.*, *95*, 127–138.

Vauchez, A., A. Tommasi, and G. Barruol, 1998, Rheological heterogeneity, mechanical anisotropy and deformation of the continental lithosphere, *Tectonophysics*, *296*, 61–86.

Vauchez, A., A. Tommasi, G. Barruol, and J. Maumus, 2000, Upper mantle deformation and seismic anisotropy in continental rifts, *Phys. Chem. Earth (A)*, *25*, 111–117.

Vavryčuk, V., 2001, Ray tracing in anisotropic media with singularities, *Geophys. J. Int.*, *145*, 265–276.

Vernik, L., 1993, Microcrack-induced versus intrinsic elastic anisotropy in mature HC-source shales, *Geophysics*, *58*, 1703–1706.

Vernik, L., and X. Liu, 1997, Velocity anisotropy in shales: A petrophysical study, *Geophysics*, *62*, 521–532.

Vernik, L., and A. Nur, 1992, Ultrasonic velocity and anisotropy of hydrocarbon source rocks, *Geophysics*, *57*, 727–735.

Vestrum, R. W., 1994, Group- and phase-velocity inversions for the general anisotropic stiffness tensor, Master of Science Thesis, The University of Calgary.

Vestrum, R. W., D. C. Lawton, and R. Schmid, 1999, Imaging structures below dipping TI media, *Geophysics*, *64*, 1239–1246.

Viglin, A. S., 1960, A quantitative measure of the texture of a polycrystalline material - texture function, *Soviet Phys., Solid State*, *2*, 2195–2207.

Voigt, W., 1928, *Lehrbuch der Kristallphysik*, Teubner-Verlag, Leipzig.

Wagner, F., H. R. Wenk, C. Esling, and H. J. Bunge, 1981, Importance of odd coefficients in texture calculations for trigonal -triclinic symmetries, *Phys. Stat. Sol.*, *67*, 269–285.

Wang, C.-Y., D. A. Okaya, C. Ruppert, G. A. Davis, T. S. Guo, Z. Q. Zhong, and H. R. Weng, 1989, Seismic reflectivity of the Whipple mountain shear zone in southern California, *J. Geophys. Res.*, *94*, 2989–3005.

Wang, Z., 2002, Seismic anisotropy in sedimentary rocks, part 2: laboratory data, *Geophysics*, *67*, 1423–1440.

Wang, Z. Z., H. Wang, and M. E. Cates, 1998, Elastic properties of solid clays, in *SEG International Exposition and 68th Annual Meeting*, SEG, New Orleans, Louisiana.

Watt, J. P., 1979, Hashin-Shtrikman bounds on the effective elastic moduli of polycrystals with orthorhombic symmetry, *Journal of Applied Physics, 50*, 6290–6295.

Watt, J. P., 1980, Hashin-Shtrikman bounds on the effective elastic moduli of polycrystals with monoclinic symmetry, *Journal of Applied Physics, 51*, 1520–1524.

Watt, J. P., 1986, Hashin-Shtrikman bounds on the effective elastic moduli of polycrystals with trigonal (3,$\bar{3}$) and tetragonal (4,$\bar{4}$,4m) symmetry, *Journal of Applied Physics, 60*, 3120–3124.

Watt, J. P., and L. Peselnick, 1980, Clarification of the Hashin-Shtrikman bounds on the effective elastic moduli of polycrystals with hexagonal, trigonal, and tetragonal symmetries, *Journal of Applied Physics, 51*, 1525–1531.

Watt, P. J., 1987, POLYXSTAL: A FORTRAN program to calculate average elastic properties of minerals from single-crystal elasticity data, *Computers & Geosciences, 13*, 441–462.

Watt, P. J., 1988, Elastic properties of polycrystalline minerals: comparison of theory and experiment, *Phys Chem Minerals, 15*, 579–587.

Watt, P. J., G. F. Davies, and R. J. O'Connell, 1976, The elastic properties of composite materials, *Rev. Geophys., 14*, 541–563.

Webb, S. L., 1989, The elasticity of the upper mantle orthosilicates olivine and garnet to 3 GPa, *Phys Chem Minerals, 16*, 684–692.

Weiss, T., S. Siegesmund, and T. Bohlen, 1999a, Seismic, structural and petrological model of the subcrustal lithosphere in southern Germany: A quantitative re-evaluation, *Pure appl. Geophys., 156*, 53–81.

Weiss, T., S. Siegesmund, W. Rabbel, T. Bohlen, and M. Pohl, 1999b, Seismic velocities and anisotropy of the lower continental crust: a review, *Pure appl. Geophys., 156*, 97–122.

Wenk, H.-R., 1985, *Preferred orientation in deformed metals and rocks: an introduction to modern texture analysis*, Academic Press, Inc.

Wenk, H. R., and C. N. Tome, 1999, Modeling dynamic recrystallization of olivine aggregates deformed in simple shear, *J. Geophys. Res., 104*, 25,513–25,527.

Wenk, H. R., G. Johnson, and S. Matthies, 1988, Direct determination of physical properties from continuous orientation distributions, *J. Appl. Phys., 63*, 2876–2879.

Wenk, H.-R., K. Bennett, G. R. Canova, and M. A., 1991, Modelling plastic deformation of peridotite with self-consistent theory, *J. Geophys. Res., 96*, 8337–8349.

Wenk, H.-R., G. Canova, Y. Brechet, and L. Flandin, 1997, A deformation - based model for recrystallization of anisotropic material, *Acta mater., 45*, 3283 – 3296.

Werner, U., and S. A. Shapiro, 1998, Intrinsic anisotropy and thin multilayering - two anisotropy effects combined, *Geophys. J. Int., 132*, 363–373.

Werner, U., and S. A. Shapiro, 1999, Frequency-dependent shear-wave splitting in thinly layered media with intrinsic anisotropy, *Geophysics*, *64*, 604–608.

White, J. E., 1983, *Underground sound: application of seismic waves*, Elsevier, Amsterdam, New York.

White, J. E., L. Martineau-Nicoletis, and C. Monash, 1983, Measured anisotropy in Pierre shale, *Geophys. Prosp.*, *31*, 709–725.

Willis, J. R., 1981, Variational and related methods for the overall properties of composites, *Adv. Appl. Mech.*, *21*, 1–78.

Winterstein, D. F., and B. N. P. Paulsson, 1990, Velocity anisotropy in shale determined from crosshole seismic and vertical seismic profile data, *Geophysics*, *55*, 470–479.

Yardley, B. W. D., 1989, *An introduction to metamorphic petrology*, Longman Scientific & Technical, New-York.

Yardley, G. S., and S. Crampin, 1991, Extensive-dilatancy anisotropy: relative information in VSPs and reflection surveys, *Geophys. Prosp.*, *39*, 337–355.

Zappone, A., M. Fernandez, V. Garcia-Duenas, and L. Burlini, 2000, Laboratory measurements of seismic P-wave velocities on rocks from the Betic chain (Southern Iberian Penninsula), *Tectonophysics*, *317*, 259–272.

Zeller, R., and P. Dederichs, 1973, Elastic constants of polycrystals, *phys. stat. sol. (b)*, *55*, 831–842.

Zhang, S., and S.-i. Karato, 1995, Lattice preferred orientation of olivine aggregate deformed in simple shear, *Nature*, *375*, 774–777.

Zhang, S., S.-i. Karato, J. F. Gerald, U. H. Faul, and Y. Zhou, 2000, Simple shear deformation of olivine aggregates, *Tectonophysics*, *316*, 133–152.

Zismann, W. A., 1933, Compressibility and anisotropy of rocks at and near the Earths surface, *Proceedings of National Academy of Sciences*, *19*, 667–679.

Appendix A

Experimental techniques of measuring elastic constants and anisotropy

Several techniques are currently in use for the experimental determination of the elastic constants of the solid materials. Some have a long history as, for example, *static techniques*, which have been known for several hundred years. The simplest 1D implementation is known as the determination of the single elastic constant k of a spring in Hooke's Law, $F = -k.r$. This requires measurement of the displacement as a linear response to applied force. Using present-day technology, the method of *speckle interferometry* (e.g. *Shareef and Schmitt*, 2004) may be applied to precisely determine the surface displacement of the block of solid material. By inverting observed interferometric fringes, the elastic moduli of the investigated material may be obtained.

One method to determine the full set of the elastic constants is based on detection of the natural resonant frequencies of sample with known dimensions. The methos is called *resonant ultrasound spectroscopy* (RUS). RUS has emerged during the last few decades as a powerful tool to study the elasticity of solid materials (*Maynard*, 1996; *Migliori and Sarrao*, 1997; *Leisure and Willis*, 1997). The full set of the elastic moduli may be obtained from a single scan through various frequencies in order to find a number of the sample's normal modes. The main advantage of this technique is the ability to measure elastic constants of samples as small as few millimeters in dimension (*Migliori and Fisk*, 1993). The measurements can be repeated for different pressure and temperature (P-T) conditions to

131

investigate pressure and temperature derivatives of the elastic moduli (e.g. *Migliori and Fisk*, 1993; *Isaak et al.*, 1998). The dissipation of the resonant energy, however, increases linearly with pressure because of impedance and viscous effects at the boundary between the sample and pressurizing medium (Zhang et al., 1998; Sorbello et al., 2000). This is the main obstacle to this technique at even modest pressure let alone at the high-pressure regime of crucial importance in investigations of elastic properties of the Earth's interior. RUS was initially considered to be applied for the investigation of anisotropy of rocks in this study but eventually was abandoned due to resonant frequency energy dissipation at higher pressure.

The most popular and widely used technique in geophysics is based on the elastic vibrations of a solid. Simple ultrasonic measurement of elastic wave transit times through the sample are accomplished by variations known as either *time-of-flight* or *pulse-echo* techniques. It has been important in studies of rocks elasticity (Schreiber et al., 1973) and was employed in Chapter 2 to obtain partial set of elastic constants. In fact, almost all existing full sets of elastic constants for crystals and rocks were obtained by using such methods. Among notable examples are *Alexandrov and Ryzhova* (1961a,b), and compilation by *Simmons and Wang* (1971) The published results of time-of-flight measurements are used as a primary reference source in geophysical investigations. The time-of-flight yield the most accurate characterizations of solid elasticity but suffer several problems including transducer coupling, directional dependency, and scale dispersion.

Experimental techniques based on the ultrasonic measurement of elastic wave propagation yield a set of measured wave traveltimes with different polarizations and directions of propagation. Velocities calculated from traveltimes must, therefore, be inverted for elastic moduli (*Neighbours*, 1954; *Neighbours and Schacher*, 1967). *Mah and Schmitt* (2001b, 2003) provided a review of these methods. To obtain the full set of elastic constants of linearly elastic anisotropic solid (i.e. twenty one for the most general case of triclinic symmetry) both the velocity and the polarization orientation should be measured in at least 6 different directions (*Van Buskirk et al.*, 1986). *Ditri* (1994) has shown that up to 15 elastic constants can be uniquely determined if a series of measurements are taken in different direction within a single plane. Additional 5 elastic constants (making it 20 out of 21) can be determined if measurements are taken within two planes. For instance,

132

measurements within the single X_1X_2 plane of the $X_1X_2X_3$ cartesian coordinate system assigned to the sample allow determination of the following 15 elastic constants:

$$C_{ij} = \begin{pmatrix} C_{11} & C_{12} & - & C_{14} & C_{15} & C_{16} \\ & C_{22} & - & C_{24} & C_{25} & C_{26} \\ & & - & - & - & - \\ & & & C_{44} & C_{45} & C_{46} \\ & & & & C_{55} & C_{56} \\ & & & & & C_{66} \end{pmatrix} \qquad (A.1)$$

It is easy to note that none of elastic constants with an index '3' can be retrieved from the data acquired solely in the X_1X_2 plane. Here, it should also be noted that any number of direction of measurements can be taken, and all three modes of elastic wave, compressional and two shear waves must be considerate (see Appendix B for details on elastic wave velocities in anisotropic solid). A severe limitation of Ditri's analysis is that the polarization need to be found. While this can be done approximately (see *Mah and Schmitt*, 2001a, 2003), it is very difficult to do in practice.

The time-of-flight method, constrained by directionality, usually makes measurements on cylindrical samples (e.g. technique discussed in details in Chapter 2) and requires a number of core samples be cut in different directions from the hand specimen (*Birch*, 1960). Providing high accuracy of velocity measurements and absence of practical limitations on investigation of pressure and temperature dependencies within the scope of geophysical interest, this technique suffer from ambiguity imposed by variation in mineralogy and textural properties from core to core even within one specimen. Furthermore, the physical dimensions of hand specimen should, naturally, be adequate to core the necessary number of samples.

Pros and Babuška (1967) and *Pros et al.* (1998a) introduced a method of measurement of elastic constants on spherical rock samples. Providing sufficient capability on the choice of measurement direction (velocities in 132 independent directions per sample have been reported) this technique allows the velocity anisotropy and pole figures of velocity distribution to be directly plotted from the experimental results. The method may be applied to investigate pressure dependence of elastic velocities up to 400MPa and show direct correlation of observed velocity distribution pattern with the textural properties of constituent minerals and oriented microcracks (*Pros et al.*, 1998b). Drawback of measure-

133

ments on spherical samples is that the group, not the phase velocity, is usually measured (see *Vestrum*, 1994). For details on difference between the phase and the group velocities in anisotropic medium refer to Appendix B. Group velocity surfaces are more complex (i.e. may contain singularities) and, in general, no analytical solution is provided to calculate elastic constants directly from ultrasonic measurements. Elaborate inversion techniques such as one presented by *Every and Sachse* (1990) for materials of cubic symmetry are needed to retrieve elastic constants. Group velocity inversion algorithms, in addition, must deal with instabilities that originate in directions of group velocity singularities for shear waves (*Jech*, 1991; *Vestrum*, 1994). The problem of numerical stability in the forward modelling (raytracing) in the vicinity of singular direction in an anisotropic medium has been recently addressed by *Vavryčuk* (2001).

For composite material of orthorhombic symmetry the full set of elastic constants was calculated from the measured elastic velocities in 6 predefined directions on specially shaped sample by *Cheadle et al.* (1991). Measurements were taken along three principal directions of symmetry inferred from the shear wave behavior and the visible textural features of composite, and three directions at 45° to the principal directions within the symmetry planes. Assuming orthorhombic symmetry analytical expressions have been derived to invert observed velocities for elastic constants. *Arts et al.* (1991, 1996) introduced a method which yields a full set of elastic constants for material of arbitrary elastic symmetry. In this technique, measurements along 9 independent directions on a faceted sample shaped as truncated cube with 18 faces are needed. The inversion of the experimentally measured velocities allows all 21 elastic constants of investigated material to be obtained without prior knowledge of its symmetry. *Aleksandrov and Prodayvoda* (1994) and *Prodayvoda* (1995) reported full sets of elastic constants of anisotropic rocks with different symmetries by employing a similar technique.

Most recently, *Mah and Schmitt* (2001b, 2003) reported method of the determination of full set of elastic constants. A block of a composite material of rectangular shape was used in these investigations. Observed P- and S-wave traveltimes obtained from arrays of sources and receivers were inverted by employing *plain wave decomposition* (also known as $\tau - p$ transformation, e.g. *Kebaili and Schmitt*, 1996) to obtain the elastic constants.

134

Appendix B

The Christoffel equation and elastic velocities of anisotropic solids

The review of elastic wave propagation through anisotropic media presented here follows mainly the development in *Musgrave* (1970).

During seismic wave propagation a solid body changes its shape as a result of applied stress. To the extent that a strained body stays within the elastic limit, the strain is recoverable and the body returns to its original shape. The homogeneous stress and strain are specified as a second-rank tensors σ_{ij} and ε_{kl}, respectively. The magnitude of the strain is proportional to the applied stress. In cases where elastic limit condition holds, linear to first order relation between the six component of *the stress tensor* σ_{ij} and the six component of *the strain tensor* ε_{kl} known as *the generalized Hooke's Law* may be written in the form:

$$\sigma_{ij} = C_{ijkl}\,\varepsilon_{kl} \tag{B.1}$$

where C_{ijkl} is a fourth-order tensor having 81 elements known as *elastic stiffnesses*. Tensor C_{ijkl} fully describes elastic properties of anisotropic crystals or solids. Fortunately, this tensor has symmetry (the symmetry of stress and strain tensors imply that there are six independent choices for the pair of suffixes ij and kl):

$$C_{ijkl} = C_{jikl} = C_{jilk} = C_{ijlk}$$

which reduces the number of independent elements to, at most, 36. Moreover, the

135

condition that the strain energy $\Delta\Phi$, where Φ is a potential energy function, must always be positive (i.e. work must be done to impose strain) leads to additional symmetry of elastic tensor such that:

$$C_{ijkl} = C_{klij}$$

and further reduces the number of independent constants to 21. The number of independent elastic constants depends on the elastic symmetry of investigated material and may vary between one elastic constant (usually defined as bulk modulus K) for fluids, two elastic constants (*Lamé parameters*, λ and μ) for isotropic solids and up to twenty one independent elastic constants for most general case of triclinic symmetry. Knowledge of the elastic constants plays an essential role in the calculation of longitudinal P and two shear waves S_1 and S_2 velocities of elastic wave propagating in anisotropic solids.

Following *Musgrave* (1970) *the equation of motion* (EOM) for a unit volume element of solid has the form:

$$\frac{\partial\sigma_{ij}}{\partial x_j} + \rho X_j = \rho\frac{\partial^2 u_i}{\partial t^2} \tag{B.2}$$

where u_i - is the linear particles displacement, ρ - the density of material, and the t - time. Employing the conventional *Einstein suffix notation* (*Nye*, 1990), EOM may be written:

$$\sigma_{ij,j} + \rho X_j = \rho\ddot{u}_i \tag{B.3}$$

where a comma represents partial differentiation and a dot denotes a derivative with respect to time. If body forces, represented by term ρX_i, are excluded, the equation of motion reduces to form:

$$\sigma_{ij,j} = \rho\ddot{u}_i \tag{B.4}$$

Equation (B.4) is the general constitutive equation for a linear elastic anisotropic medium. The relationship between the strain and displacement in elastic medium has form:

$$\varepsilon_{ij} = \frac{1}{2}(u_{i,j} + u_{j,i}) \tag{B.5}$$

136

Combination of equations (B.1), (B.4) and (B.5) enables one to write:

$$\sigma_{ij} = C_{ijkl}\, u_{k,l} \tag{B.6}$$

Expression (B.6) may be rewritten in a form of linear partial differential equation of the second order:

$$C_{ijkl}\, u_{k,jl} - \rho\, \ddot{u}_i = 0 \tag{B.7}$$

The equation of the particle displacement u for elastic wave propagating in the direction of a wave normal defined by the unit vector $\bar{n} = \bar{n}_1 i + \bar{n}_2 j + \bar{n}_3 k$ has the form:

$$u(x_i, t) = a_0\, e^{i(\omega t - k_i x_i)} \tag{B.8}$$

where a_0 is the maximum amplitude of particle oscillation, x_i are components of the particle position, k_i are components of a wave vector $\mathbf{k}$ which has magnitude $k = 2\pi/\lambda$ known also as a *wave number*, λ - wavelength, and ω - angular frequency, $\omega = 2\pi f$. For the monochromatic monotropic wave *the phase velocity* can be introduced in the form $v = \omega/k$ (this relationship between the wave number and the angular frequency is also known as the *dispersion relation*) and equation (B.8) can be rewritten:

$$u(x_i, t) = a_0\, e^{i \frac{2\pi}{\lambda(n_i)} (v(n_i)t - n_i x_i)} \tag{B.9}$$

where v is the phase velocity along the real vector $\bar{n}$ of the complex wave normal, $n_i = k_i/\omega$, ($i = 1, 2, 3$) are components of the vector which is an inverse of the phase velocity and known as *slowness*. The plane wave assumption of constant phase factor $\phi = (\omega t - k_i x_i) = const$ (i.e. constant amplitude) and substitution of equation (B.9) into equation (B.7) leads to an equation:

$$(C_{ijkl}n_j n_l - \rho v^2 \delta_{ik})u_k = 0 \tag{B.10}$$

where δ_{ij} is *the Kronecker delta (Nye, 1990)*. The nonzero value of displacement u_i are obtained as characteristic (*eigen*) vectors corresponding to the characteristic (*eigen*) values of velocities v^2 which are the roots of the standard *eigenvector-eigenvalue problem*:

$$det \mid C_{ijkl}n_j n_l - \rho v^2 \delta_{ik} \mid = 0 \qquad (B.11)$$

Solution of equation (B.11) in all directions represents the velocity surface of an infinite number of plane waves. It is convenient to rewrite equation (B.11) by introducing the notation

$$\Gamma_{ik} = C_{ijkl}n_j n_l \qquad (B.12)$$

where Γ_{ik} is the symmetric *Christoffel matrix* [1]. Then equation (B.11) becomes:

$$(\Gamma_{ik} - \rho v^2 \delta_{ik})u_k = 0 \qquad (B.13)$$

Equation (B.11) well known as *Christoffel equation* and the standard eigenvalue-eigenvector problem may be now rewritten in the form:

$$det \mid \Gamma_{ik} - \rho v^2 \delta_{ik} \mid = 0 \qquad (B.14)$$

The solution of the cubic equation (B.14) for any specific slowness direction $\bar{n}$ yields three positive eigenvalues of the squared phase velocity v^2, which correspond to a P-wave and two S-waves (strictly, the *"quasi-P"* wave and *"quasi-S"* wave). Two *quasi*-shear waves usually distinguished by their magnitude as *fast* or S_1 and *slow* or S_2 shear wave. The difference $S_1 - S_2 = \delta S$ is known in the geophysical literature as *shear-wave splitting* (*Crampin*, 1981). The eigenvectors corresponding to three eigenvalues are the polarization directions of the three modes. The polarization directions are always orthogonal to one other in an anisotropic medium, but none is necessarily parallel or perpendicular to phase velocity front normal $\bar{n}$ as is seen for isotropic case where pure P-mode is always polarized parallel to $\bar{n}$ and two coinciding pure S-modes transverse to $\bar{n}$.

An additional complication of wave propagation in anisotropic media is the discrepancy between the phase (normal or plane wave) and the group (also known as ray or wave) velocities (*Musgrave*, 1970; *Auld*, 1990; *Helbig*, 1994). *Helbig* (1984b) demonstrates that, in the non-dispersive anisotropic medium, phase velocity vector **v** is independent

---

[1] named after the German mathematician *Elwin Bruno Christoffel* (1829-1900), a student of *Dirichlet*, who contributed significantly to the development of the numerical integration, conformal mappings, the theory of invariants and the tensor calculus

138

of magnitude of the wave vector k but depends on its direction (anisotropy). Following *Helbig* (1994), the phase velocity v is the velocity of propagation of the front of constant phase, i.e. the velocity of the carrier wave, and defined as a vector in the general dispersion relation:

$$v = \frac{\omega}{(k \cdot k)} k$$

with components:

$$v_i = \frac{\omega k_i}{k_j k_j}$$

Velocity of amplitude factor, i.e. the velocity of energy transport, in anisotropic non-dispersive medium is called group velocity g and is defined as:

$$g = \text{grad}_k \omega$$

with components:

$$g_i = \frac{\partial \omega}{\partial k_i}$$

Knowing that $\omega = k_i v_i$ the relationship between phase and group velocities can be written as:

$$g = v + k \, \text{grad}_k \, v$$

The *phase* (velocity) *surface* can be defined as the surface that connects the end points of the infinite number of phase velocity vectors v that originate from a single point and pointing in all directions. The surface connecting the end points of group velocity vectors g is known as *wave* (velocity) *surface*. The geometrical relationship between the phase and the wave surfaces is discussed in detail by *Musgrave* (1970); *Helbig* (1994). Here, for purpose of illustration, the vertical section through the phase and the group (wave) surfaces of *quasi* S - wave of highly anisotropic hexagonal muscovite crystal is plotted on Figure B.1 (a). The cusps on the group velocity surface (i.e. sharp discontinuous end points) are a distinctive feature of *quasi* shear wave propagation in highly anisotropic materials. On

139

Figure B.1 (b) a single direction has been chosen to demonstrate relationship between the phase velocity vector **v** and the group velocity vector **g**. The phase velocity angle β is defined as an angle from the vertical direction to phase velocity vector. Corresponding to this phase velocity group velocity vector is defined by group angle γ. If angles α and γ are known then simple geometrical relationship allows one to calculate group velocity from the phase velocity and vice versa:

$$\mathbf{v}(\beta) = \mathbf{g}(\gamma) \cos(\gamma - \beta) = \mathbf{g}(\gamma) \cos(\alpha)$$

In non-dispersive anisotropic media, the group velocities are always larger than or equal to the corresponding phase velocity (*Helbig*, 1994).
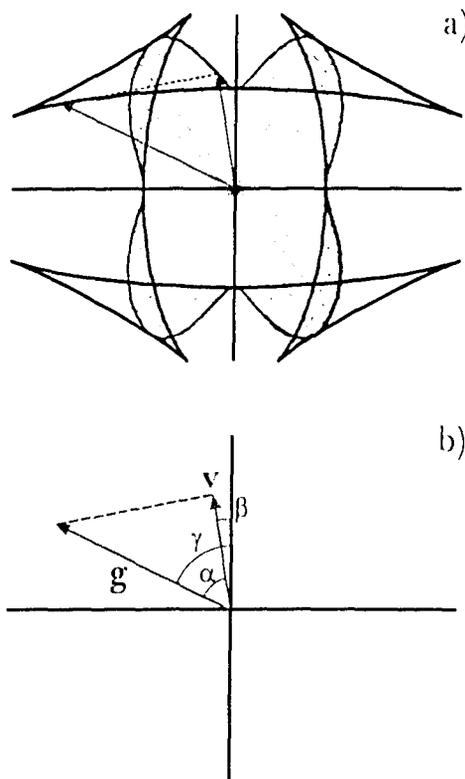
Figure B.1: Relationship between the phase and the group velocity surfaces.

Appendix C

Voigt and Reuss averaging

The theoretical developments describing the elasticity of a polycrystalline aggregate have a long history (see Chapter 1). The original idea of averaging the elastic properties of constituent minerals to obtain the elastic properties of their polycrystalline aggregate was introduced in the beginning of the XX century by *Voigt* (1928) and *Reuss* (1929). Despite their respectful age, the Voigt and the Reuss averages are today the most frequently applied averaging techniques in geophysics. In this Appendix some aspects of the Voigt and the Reuss averaging are presented.

The elastic constants of isotropic (randomly oriented) aggregate in the Voigt approximation of constant strain can be calculated by formulas (e.g. *Simmons and Wang*, 1971):

$$K_V = (A + 2B)/3 \tag{C.1a}$$

$$G_V = (A - B + 3C)/5 \tag{C.1b}$$

where K_V is *the bulk modulus* and G_V is *the shear modulus* of an isotropic aggregate, and

$$3A = C_{11} + C_{22} + C_{33} \tag{C.2a}$$

$$3B = C_{12} + C_{13} + C_{23} \tag{C.2b}$$

$$3C = C_{44} + C_{55} + C_{66} \tag{C.2c}$$

where the C_{11}, C_{22}, C_{33}, C_{44}, C_{55}, C_{66}, C_{12}, C_{13}, C_{23} are elastic stiffnesses of the constituent mineral in *Voigt notation* (see Section 2.2 for more details). Note that only nine

elastic constants are incorporated into the Voigt averaging procedure. This implies that for constituent minerals with symmetry as high as orthorhombic all the elastic constants are required by the averaging procedure. For lower symmetry crystals (monoclinic and triclinic) only the above mentioned elastic stiffnesses contribute to elastic properties of isotropic aggregate according to the above formulation.

Similarly, the Reuss approximation of constant stress leads to the set of equations:

$$K_R = \frac{1}{(3a + 6b)} \tag{C.3a}$$

$$G_R = \frac{5}{(4a - 4b + 3c)} \tag{C.3b}$$

where

$$3a = S_{11} + S_{22} + S_{33} \tag{C.4a}$$

$$3b = S_{12} + S_{13} + S_{23} \tag{C.4b}$$

$$3c = S_{44} + S_{55} + S_{66} \tag{C.4c}$$

where S_{11}, S_{22}, S_{33}, S_{44}, S_{55}, S_{66}, S_{12}, S_{13}, S_{23} are elastic compliances of the constituent mineral. It has been shown in Section 2.2 that properties of isotropic aggregate can be described by *Lamé parameters* λ and μ ($\lambda + 2\mu = C_{11} = C_{22} = C_{33}$, $\mu = C_{44} = C_{55} = C_{66}$, and $\lambda = C_{12} = C_{13} = C_{23}$):

$$\begin{pmatrix} \lambda + 2\mu & \lambda & \lambda & 0 & 0 & 0 \\ & \lambda + 2\mu & \lambda & 0 & 0 & 0 \\ & & \lambda + 2\mu & 0 & 0 & 0 \\ & & & \mu & 0 & 0 \\ & & & & \mu & 0 \\ & & & & & \mu \end{pmatrix}$$

Taking into account relationship between Lamé parameters and bulk and shear modulus:

$$K_V = \lambda + \tfrac{2}{3}\mu$$
$$G_V = \mu$$

averaging procedure (C.1)–(C.2) can be rewritten in the matrix form:

142

$$
\begin{bmatrix}
\overline{C}_{11} \\
\overline{C}_{22} \\
\overline{C}_{33} \\
\overline{C}_{44} \\
\overline{C}_{55} \\
\overline{C}_{66} \\
\overline{C}_{12} \\
\overline{C}_{13} \\
\overline{C}_{23}
\end{bmatrix}
=
\begin{bmatrix}
3/15 & 3/15 & 3/15 & 4/15 & 4/15 & 4/15 & 2/15 & 2/15 & 2/15 \\
3/15 & 3/15 & 3/15 & 4/15 & 4/15 & 4/15 & 2/15 & 2/15 & 2/15 \\
3/15 & 3/15 & 3/15 & 4/15 & 4/15 & 4/15 & 2/15 & 2/15 & 2/15 \\
1/15 & 1/15 & 1/15 & 3/15 & 3/15 & 3/15 & -1/15 & -1/15 & -1/15 \\
1/15 & 1/15 & 1/15 & 3/15 & 3/15 & 3/15 & -1/15 & -1/15 & -1/15 \\
1/15 & 1/15 & 1/15 & 3/15 & 3/15 & 3/15 & -1/15 & -1/15 & -1/15 \\
1/15 & 1/15 & 1/15 & -2/15 & -2/15 & -2/15 & 4/15 & 4/15 & 4/15 \\
1/15 & 1/15 & 1/15 & -2/15 & -2/15 & -2/15 & 4/15 & 4/15 & 4/15 \\
1/15 & 1/15 & 1/15 & -2/15 & -2/15 & -2/15 & 4/15 & 4/15 & 4/15
\end{bmatrix}
\begin{bmatrix}
C_{11} \\
C_{22} \\
C_{33} \\
C_{44} \\
C_{55} \\
C_{66} \\
C_{12} \\
C_{13} \\
C_{23}
\end{bmatrix}
\tag{C.5}
$$

Equation (C.5) now can be written in matrix notation:

$$\overline{C}^{V} = \overline{a}^{V} C \tag{C.6}$$

where C is [9 × 1] vector composed of independent elastic constants of the single crystal, $\overline{a}^{V}$ is the Voigt averaging matrix and $\overline{C}^{V}$ is the resulting [9×1] vector composed of the elastic constants of the aggregate in the Voigt approximation. Similarly, the procedure can be repeated to represent the Reuss averaging:

$$
\begin{bmatrix}
\overline{S}_{11} \\
\overline{S}_{22} \\
\overline{S}_{33} \\
\overline{S}_{44} \\
\overline{S}_{55} \\
\overline{S}_{66} \\
\overline{S}_{12} \\
\overline{S}_{13} \\
\overline{S}_{23}
\end{bmatrix}
=
\begin{bmatrix}
3/15 & 3/15 & 3/15 & 1/15 & 1/15 & 1/15 & 2/15 & 2/15 & 2/15 \\
3/15 & 3/15 & 3/15 & 1/15 & 1/15 & 1/15 & 2/15 & 2/15 & 2/15 \\
3/15 & 3/15 & 3/15 & 1/15 & 1/15 & 1/15 & 2/15 & 2/15 & 2/15 \\
4/15 & 4/15 & 4/15 & 3/15 & 3/15 & 3/15 & -4/15 & -4/15 & -4/15 \\
4/15 & 4/15 & 4/15 & 3/15 & 3/15 & 3/15 & -4/15 & -4/15 & -4/15 \\
4/15 & 4/15 & 4/15 & 3/15 & 3/15 & 3/15 & -4/15 & -4/15 & -4/15 \\
1/15 & 1/15 & 1/15 & -1/30 & -1/30 & -1/30 & 4/15 & 4/15 & 4/15 \\
1/15 & 1/15 & 1/15 & -1/30 & -1/30 & -1/30 & 4/15 & 4/15 & 4/15 \\
1/15 & 1/15 & 1/15 & -1/30 & -1/30 & -1/30 & 4/15 & 4/15 & 4/15
\end{bmatrix}
\begin{bmatrix}
S_{11} \\
S_{22} \\
S_{33} \\
S_{44} \\
S_{55} \\
S_{66} \\
S_{12} \\
S_{13} \\
S_{23}
\end{bmatrix}
\tag{C.7}
$$

and

$$\overline{S}^{R} = \overline{a}^{R} S \tag{C.8}$$

where S is [9 × 1] vector composed of independent elastic compliances of a single crystal, $\overline{a}^{R}$ is the Reuss averaging matrix and $\overline{S}^{R}$ is [9 × 1] vector composed of elastic compliances of aggregate in the Reuss approximation. The apparent difference in an averaging matrix in (C.5) and (C.7) is attributed to the difference in the definition of

143

the Voigt notation for stiffnesses and compliances (see Nye, 1990). One can employ a transformation matrix T to obtain the Reuss averaging matrix from the Voigt averaging matrix:

$$\bar{a}^{R} = T * \bar{a}^{V}$$ (C.9)

where

$$T = \begin{bmatrix}
1 & 1 & 1 & 1/4 & 1/4 & 1/4 & 1 & 1 & 1 \\
1 & 1 & 1 & 1/4 & 1/4 & 1/4 & 1 & 1 & 1 \\
1 & 1 & 1 & 1/4 & 1/4 & 1/4 & 1 & 1 & 1 \\
4 & 4 & 4 & 1 & 1 & 1 & 4 & 4 & 4 \\
4 & 4 & 4 & 1 & 1 & 1 & 4 & 4 & 4 \\
4 & 4 & 4 & 1 & 1 & 1 & 4 & 4 & 4 \\
1 & 1 & 1 & 1/4 & 1/4 & 1/4 & 1 & 1 & 1 \\
1 & 1 & 1 & 1/4 & 1/4 & 1/4 & 1 & 1 & 1 \\
1 & 1 & 1 & 1/4 & 1/4 & 1/4 & 1 & 1 & 1
\end{bmatrix}$$

In equation (C.9) '*' stands for array multiplication (element by element) not for matrix multiplication. Note that to compare the averaging results either the Voigt stiffnesses or the Reuss compliances in the matrix form have to be inverted, e.g. $\bar{C}_{m}^{R} = (\bar{S}^{R})_{m}^{-1}$.

It has been noted by Hill (1952) that neither the Voigt nor the Reuss approach can strictly be accepted as solution for elastic properties of isotropic polycrystalline aggregate. According to Hill, a true solution lies between: $\bar{C}^{V} > \bar{C} > \bar{C}^{R}$. Hill suggested the simple arithmetical average of the Voigt and the Reuss elastic constants provided a more accurate representation of elastic properties of isotropic aggregate $(\bar{C}^{H} = (\bar{C}^{V} + \bar{C}^{R})/2)$. See Section 4.2 for discussion on the limitations of Hill's approach and averaging procedure called 'Geometric Mean Averaging' (GMA) that allows more physically meaningful solution to be introduced.

Solutions (C.5) and (C.7) are special cases of more general approach that incorporates textural properties of the aggregate and described in Appendix D. If a polycrystalline aggregate has a random orientation distribution then it is elastically isotropic and the generalized case of Appendix D reduce to the Voigt and the Reuss solutions presented here.

144

Appendix D

Quantitative texture description: ODF of orthotropic symmetry

In this Section, the derivation of the orientation distribution function (ODF) of orthotropic-orthorhombic symmetry is described. Additional objective of this Appendix is to provide all necessary details for calculation of the aggregate elasticity employing the ODF. This information is usually incomplete in the literature produced over the last two decades and requires researcher go back to the original sources for understanding.

In order to derive the ODF two frames of references must be introduced. The first corresponds to the crystal symmetry (xyz). The second relates to the symmetry of the aggregate specimen (XYZ). The first order elastic properties of an anisotropic crystal in a reference crystal coordinate system xyz can fully be described by the forth-order tensor C_{ijkl} (e.g. Nye, 1990). In the specimen coordinate system XYZ crystal elastic properties are obtained when the xyz crystal reference frame is rotated to coincide with the specimen coordinate system XYZ. This may be accomplished by a series of consecutive rotations through the Euler angles $\varphi_1, \Phi, \varphi_2$ (e.g. Morse and Feshbach, 1953) as defined in Figure D.1. The reorientation of the crystal coordinate system xyz into the sample coordinate system XYZ can then be unambiguously defined when the three Euler angles are combined into an orientation domain $g = \{\varphi_1, \Phi, \varphi_2\}$. In the constrained three dimensional $\varphi_1 - \Phi - \varphi_2$ Euler space ($0 \leq \varphi_1 \leq 2\pi, 0 \leq \Phi \leq \pi, 0 \leq \varphi_2 \leq 2\pi$) a single orientation g is represented by a point as shown in Figure D.2.

In order to quantitatively describe the orientations of the constituent minerals in textured rock the orientation distribution function (ODF) $f(g)$ may be employed (e.g. Bunge,

145

1982). $f(g)$ is probabilistic function defined by the volume fraction of crystals having orientation g within a certain infinitesimal orientation range dg:

$$\frac{dV}{V} = f(g)dg \qquad (D.1)$$

where dV is volume of crystalline with orientation g and V - total volume of the nonporous aggregate. By employing a harmonic method, this ODF can be expanded into a series of generalized spherical harmonics, also known as a *Viglin expansion* (*Viglin,* 1960):

$$f(g) = \sum_{l=0}^{\infty} \sum_{m=-l}^{+l} \sum_{n=-l}^{+l} C_l^{mn} T_l^{mn}(g) \qquad (D.2)$$

where $T_l^{mn}(g)$ are the *generalized spherical harmonics* (GSH) and C_l^{mn} are coefficients, representing the portion of the corresponding harmonics in the expansion and reflecting the textural properties of the particular ODF.

Due to the symmetrical properties of the forth-rank elastic stiffnesses tensor C_{ijkl} (see Section 2.2 and Appendix B for more details on symmetry of C_{ijkl}) only the even parts of the ODF expansion to the maximum degree $l = 4$ is required in the averaging procedure (*Backus,* 1970) as will be described below in details. This implies, that only the "long wavelength" components of the ODF that reflect the strongest trend and smooth textural features contributes to the averaging of the elastic properties of the textured aggregate (e.g. *Diz and Humbert,* 1992).

The generalized spherical harmonics T_l^{mn} are defined through *the generalization of the associated Legendre functions* (GALF) P_l^{mn} (see *Bunge,* 1982):

$$T_l^{mn}(\varphi_1, \Phi, \varphi_2) = e^{im\varphi_2} P_l^{mn}(\cos \Phi) e^{in\varphi_1} \qquad (D.3)$$

where

$$P_l^{mn}(\cos \Phi) = P_l^{mn}(x) = \frac{(-1)^{l-m} i^{n-m}}{2^l (l-m)!} \left[\frac{(l-m)!(l+n)!}{(l+m)!(l-n)!} \right]^{1/2} \times$$
$$\times (1-x)^{-\frac{n-m}{2}} (1+x)^{-\frac{n+m}{2}} \frac{d^{l-n}}{dx^{l-n}} \left[(1-x)^{l-m} (1+x)^{l+m} \right]$$

146
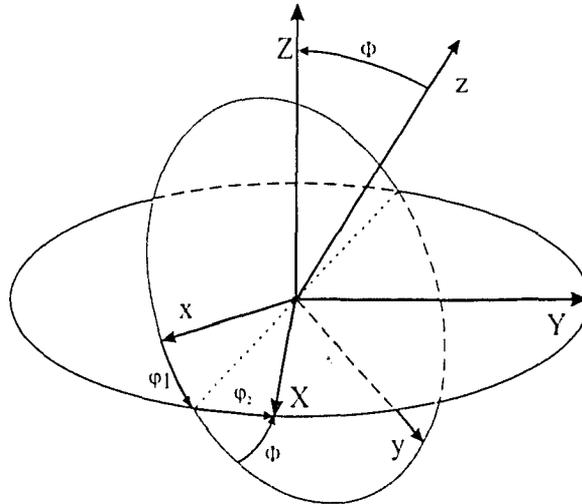
Figure D.1: Definition of the Euler angles (after *Bunge*, 1981).

For the ODF expansion to maximum degree $l = 4$, there are 165 GALFs (85 pure real and 80 pure imaginary functions). Due to the fact that the P_l^{mn} are symmetrical only 55 of these 165 functions are truly independent.
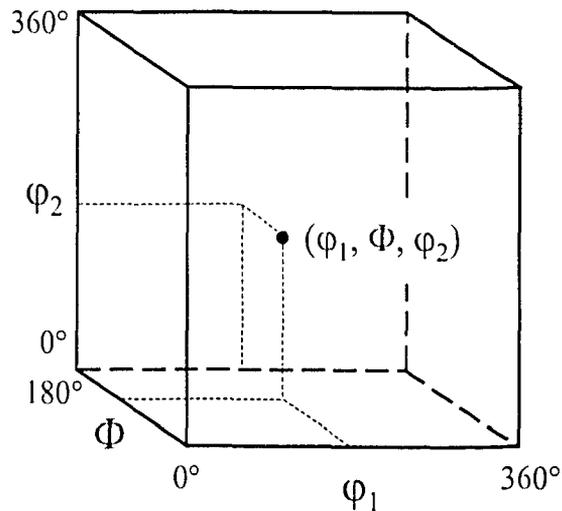
Figure D.2: Representation of the single orientation in the Euler space (after *Bunge*, 1981).

One important advantage of the harmonic method, frequently exploited in textural analysis, is that it is possible to introduce a set of functions $\dot{T}_l^{mv}$ and $\dot{T}_l^{mn}$ that account

147

separately for the specimen and the crystal coordinate systems symmetries, respectively:

$$\dot{T}_l^{m\nu}(g) = \sum_{n=-l}^{+l} \dot{A}_l^{n\nu} T_l^{mn}(g) \tag{D.4a}$$

$$\dot{T}_l^{\mu n}(g) = \sum_{m=-l}^{+l} \dot{A}_l^{m\mu} T_l^{mn}(g) \tag{D.4b}$$

where $\dot{A}_l^{n\nu}$, $\dot{A}_l^{m\mu}$ are the coefficients of symmetry that reflect the specimen and crystal symmetries, respectively, derived to incorporate symmetrical properties. Consequently, the *symmetric generalized spherical harmonics* (SGSH) $\ddot{T}_l^{\mu\nu}(g)$ can be constructed from the GSH, as follows:

$$\ddot{T}_l^{\mu\nu}(g) = \sum_{m=-l}^{+l} \sum_{n=-l}^{+l} \dot{A}_l^{m\mu} \dot{A}_l^{n\nu} T_l^{mn}(g) \tag{D.5}$$

For the case of a textured specimen of orthorhombic symmetry composed solely of orthorhombic olivine crystals the SGSH reflects both the orthorhombic olivine crystal symmetry and the orthorhombic specimen symmetry. *Bunge* (1982) shows that number of independent SGSH required to describe aggregate texture is a function of the symmetries of the crystal and aggregate, and the ODF expansion degree l. For orthorhombic symmetry this dependence has a form $M(l) = l/2 + 1$. Application of 'selection rules' ensures proper definition of new indexes ν and μ which enumerate the number of linearly independent spherical harmonics for specimen and crystal symmetry, respectively. For orthorhombic-orthorhombic symmetry considered in this appendix the Viglin expansion (equation D.2) can be re-written:

$$f_4(g) = \sum_{l=0}^{4} \sum_{\mu=1}^{M(l)} \sum_{\nu=1}^{N(l)} C_l^{\mu\nu} \ddot{T}_l^{\mu\nu}(g) \tag{D.6}$$

Note that $f_4(g)$ is a truncated part of an infinite expansion series (equation D.2. The SGSH, $\ddot{T}_l^{\mu\nu}(g)$, in this case exhibit symmetry with respect to all three Euler angles. Construction of functions with such properties can be accomplished by summation over certain GSHs by the formulas derived here and listed in Table D.2. Symmetrical generalized spherical harmonics for orthorhombic specimen symmetry and orthorhombic

148

Table D.1: Orthorhombic symmetrical generalized spherical harmonics

$\bar{T}_l^{\mu\nu}(g)$			ν	
l	μ	1	2	3
0	1	$T_0^{00} \equiv 1$		
2	1	T_2^{00}	$\frac{\sqrt{2}}{2}(T_2^{02} + T_2^{0-2})$	
	2	$\frac{\sqrt{2}}{2}(T_2^{20} + T_2^{-20})$	$T_2^{22} + T_2^{-22}$	
4	1	T_4^{00}	$\frac{\sqrt{2}}{2}(T_4^{02} + T_4^{0-2})$	$\frac{\sqrt{2}}{2}(T_4^{04} + T_4^{0-4})$
	2	$\frac{\sqrt{2}}{2}(T_4^{20} + T_4^{-20})$	$T_4^{22} + T_4^{-22}$	$T_4^{24} + T_4^{-24}$
	3	$\frac{\sqrt{2}}{2}(T_4^{40} + T_4^{-40})$	$T_4^{42} + T_4^{-42}$	$T_4^{44} + T_4^{-44}$

olivine crystal symmetry with even l degree ($0 \leq l \leq 4$) were calculated using formulas from Table D.1 and the resulting SGSH of the order $l = 2$ and 4 are represented by the volume isosurfaces in Euler space (Fig. D.3).

The coefficients $C_l^{\mu\nu}$ of the symmetric generalized spherical harmonics in equation (D.6) carry information on texture and are essential for calculation of elastic constants of a textured aggregate. In texture analysis techniques, these coefficients may be calculated from the intensity of the pole figures of crystallographic axes of constituent minerals resulted from X-ray, neutron diffractions, and electron back scattering diffraction (EBSD) techniques (e.g. Ullemeyer et al., 2000). If the individual orientation of each mineral are known then the $C_l^{\mu\nu}$ may be obtained from the formula for individual orientations (e.g. Wagner et al., 1981). When texture consists of many crystals of different orientation g_i and volume V_i, then the coefficients $C_l^{\mu\nu}$ may be calculated as volume weighted averages:

$$C_l^{\mu\nu} = (2l + 1)\frac{\sum_i V_i \bar{T}_l^{\cdot\mu\nu}(g_i)}{\sum_i V_i} \tag{D.7}$$

In the current development all the SGSH in our expansion are real and the complex conjugate symbol '*' may be omitted. The coefficients $C_l^{\mu\nu}$ obtained from equation (D.7) are used in the averaging procedure described below.

The problem of determination of the elastic stiffnesses $\tilde{C}_{ijkl}$ of textured polycrystalline aggregates is discussed in details in sections 4.2 and 4.2. The purpose of this appendix is to more fully describe the techniques and the assumptions behind an averaging approximation. If the elastic constants C_{ijkl} of the single crystal are known, then the $\tilde{C}_{ijkl}$ can be approximated by mean value $\overline{C}_{ijkl}$. For the Voigt constant strain assump-

149
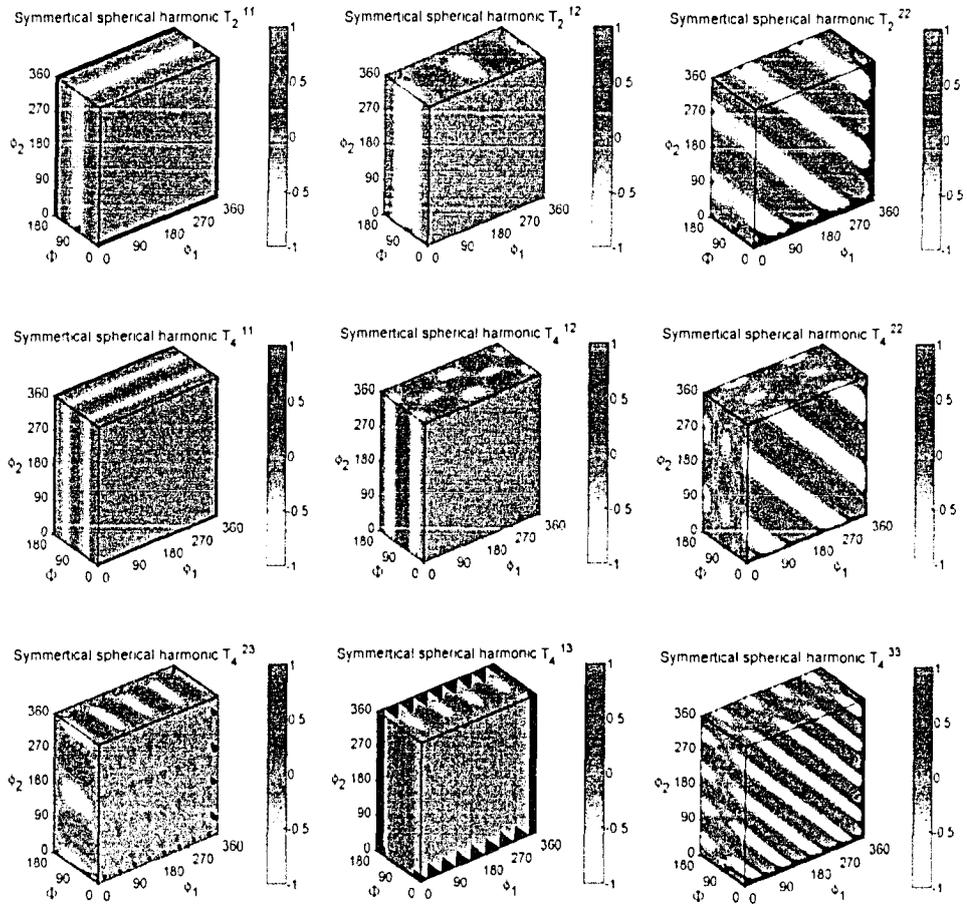
Figure D.3: Symmetric generalized spherical harmonics of order $l = 2$ and 4 represented by volume isosurfaces in the Euler $\varphi_1 - \Phi - \varphi_2$ space.

tion (see appendix C for more details on the Voigt approximation) the elastic constants of the textured aggregate are calculated by integration of the ODF over all possible orientations g (e.g. *Mainprice and Humbert*, 1994):

$$\overline{C}^{V}_{ijkl} = \oint C_{ijkl} f(g)\, dg \tag{D.8}$$

The ODF $f(g)$ in equation (D.8) is a weighting function. In a similar fashion one could perform the averaging procedure with the elastic compliances tensor S_{ijkl}. The resulting elastic compliances $\overline{S}_{ijkl}$ would satisfy the requirement of the Reuss assumption of constant stress throughout the textured aggregate.

150

The fourth order elastic tensor of single crystal C_{mnpq} can be transformed from the crystal coordinate system xyz into sample coordinate system XYZ using the tensor transformation law (e.g. Nye, 1990):

$$C'_{ijkl} = a_{im}\, a_{jn}\, a_{kp}\, a_{lq}\, C_{mnpq} \tag{D.9}$$

where the $a_{im},\, a_{jn},\, a_{kp},\, a_{lq}$ are components of the transformation matrix that contains directional cosines. The signs of the four summations over indexes m, n, p and q are omitted as *the Einstein summation convention* is employed (e.g. Nye, 1990). The product of directional cosines can also be expressed as a series of generalized spherical harmonics (*Bunge*, 1982) according to:

$$a_{im}\, a_{jn}\, a_{kp}\, a_{lq} = \sum_{l=0}^{4} \sum_{m=-l}^{+l} \sum_{n=-l}^{+l} a_l^{mn}(ijkl;mnpq)\, T_l^{mn}(g) \tag{D.10}$$

where the a_l^{mn} are constants that depend on the crystal and sample symmetry. Substituting the directional cosines in (D.9) by expansion (D.10), the elastic stiffnesses of the single crystal in the sample coordinate system XYZ may then be obtained by the formula:

$$C'_{ijkl} = \sum_{l=0}^{4} \sum_{m=-l}^{+l} \sum_{n=-l}^{+l} a_l^{mn}(ijkl;mnpq)\, T_l^{*mn}(g)\, C_{mnpq} \tag{D.11}$$

where '*', in general, indicates the complex conjugate of T_l^{mn}.

Averaging the elastic coefficients C'_{ijkl} in equation (D.11) over all orientations g in the sample coordinate system XYZ as defined by equation (D.8), leads to the elastic properties of the polycrystalline aggregate in the Voigt approximation:

$$\overline{C}^V_{ijkl} = \bar{a}(ijkl;mnpq)\, C_{mnpq} \tag{D.12}$$

where $\bar{a}(ijkl;mnpq)$ are coefficients defined by equation:

$$\bar{a}(ijkl;mnpq) = \sum_{l=0}^{4} \sum_{\mu=1}^{M(l)} \sum_{\nu=1}^{N(l)} \bar{a}_l^{\mu\nu}(ijkl;mnpq)\, C_l^{\mu\nu} \tag{D.13}$$

151
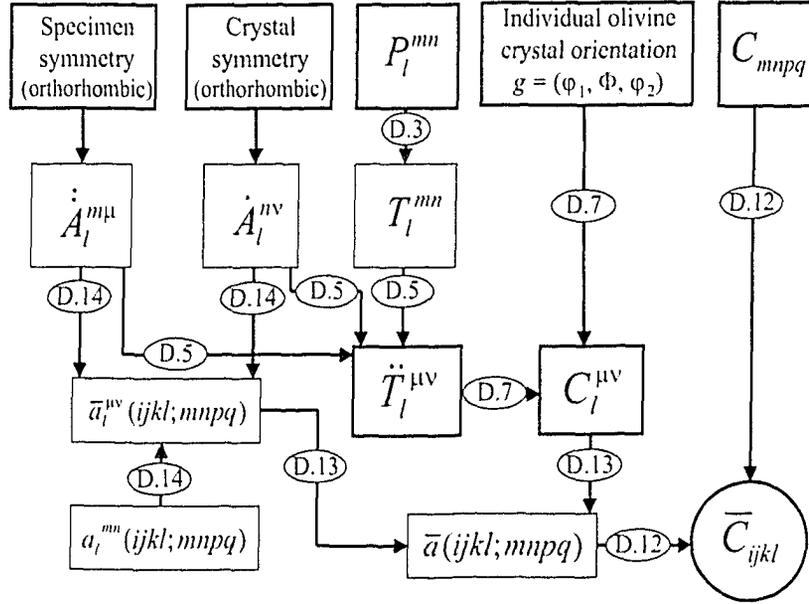
Figure D.4: Flow chart of the calculation of the elastic constants $\overline{C}_{ijkl}$ of the polycrystalline aggregate

The coefficients $C_l^{\mu\nu}$ contain the textural information required for the averaging. The coefficients $\bar{a}_l^{\mu\nu}(ijkl;mnpq)$ are mathematical quantities, defined as:

$$\bar{a}_l^{\mu\nu}(ijkl;mnpq) = \sum_{m=-l}^{+l} \sum_{n=-l}^{+l} a_l^{mn}(ijkl;mnpq) \cdot \dot{A}_l^{m\mu} \cdot \dot{A}_l^{n\nu} \qquad (D.14)$$

The coefficients $\bar{a}_l^{\mu\nu}(ijkl;mnpq)$ incorporate information about both the specimen and the crystal symmetries. The set of coefficients $\bar{a}_l^{\mu\nu}(ijkl;mnpq)$ defined in (D.14) for symmetries up to orthorhombic was calculated and published by Morris (1969), and has been employed here. With the help of (D.13) the coefficients $\bar{a}(ijkl;mnpq)$ can be calculated for the case of orthorhombic crystal and orthorhombic sample symmetry. The coefficients $\bar{a}(ijkl;mnpq)$ for this case may be represented as 9×9 matrix. The consequent substitution of these coefficients into equation (D.12) allows calculation of the elastic constants of an olivine aggregate under the Voigt assumption. The flow chart of the calculations of the elastic constants of the aggregate in the Voigt approximation is shown on Figure D.4.

The elastic properties of an orthotropic material (or medium) are fully described by 9 independent elastic constants (see Section 2.2 and equation (2.4)). In the Voigt notation these constants are:

$$
\begin{pmatrix}
C_{11} & C_{12} & C_{13} & 0 & 0 & 0 \\
 & C_{22} & C_{23} & 0 & 0 & 0 \\
 & & C_{33} & 0 & 0 & 0 \\
 & & & C_{44} & 0 & 0 \\
 & & & & C_{55} & 0 \\
 & & & & & C_{66}
\end{pmatrix}
$$

The assumption of orthotropic symmetry allows equation (D.12), which is written for the most general case, to be rewritten more explicitly in matrix form:

$$
\overline{C}^V = \overline{a}^V C \tag{D.15}
$$

where $\overline{a}^V$ is $[9 \times 9]$ averaging matrix composed of coefficients $a(ijkl:mnpq)$, C is $[9 \times 1]$ vector composed of the independent elastic constants of a single olivine crystal, and $\overline{C}^V$ is $[9 \times 1]$ vector composed of the elastic constants of the aggregate in the Voigt approximation. If the olivine aggregate has a random orientation distribution then the only non-trivial $C_I^{\mu\nu}$ coefficient is $C_0^{11} \equiv 1$. In this case the averaging matrix $\overline{a}^V$ is reduced to the Voigt solution discussed in Appendix C (equation (C.5)).

153